Università degli Studi di Padova

Dipartimento di Biologia

Corso di Laurea Magistrale in Biotecnologie Industriali

Sviluppo di un dispositivo medico basato su Next Generation Sequencing per determinare l'Homologous Recombination Deficiency in tumori all'ovaio

Relatore: Prof. Stefano Cagnin

Dipartimento di Biologia

Correlatore: Dr. Dino Paladin

AB ANALITICA S.R.L.

Controrelatore: Prof. Chiara Romualdi

Dipartimento di Biologia

Laureando: Nicola Marconato

Anno Accademico 2023/2024

To everyone who holds me in their hearth
and to everyone who helped me

Abstract

This thesis is centered around the development of a medical device based on Next Generation Sequencing (NGS) to determine Homologous Recombination Deficiency (HRD) in ovarian tumors. HRD is a condition characterized by the malfunction of the Homologous Recombination Repair (HRR) system, a critical mechanism for repairing double-strand breaks in DNA. This condition is prevalent in several types of cancers, including High-Grade Serous Ovarian Cancer (HGSOC), Triple-Negative Breast Cancer (TNBC), Pancreatic Ductal Adenocarcinoma (PDAC), and prostate cancer. The HRD phenotype in these cancers correlates with an increased sensitivity to Poly (ADP-ribose) polymerase inhibitors (PARPi), making HRD testing crucial for identifying patients who may benefit from PARP inhibitor therapies.

Current HRD detection kits and tests are expensive and much research focus is on developing kits at a more accessible price. However, HRD detection kits require ovarian cancer biopsy which is invasive for the patient. Thus, a kit for HRD detection based on the analysis of cell-free DNA (cfDNA), is of great interest to improve the accessibility of the diagnosis and for monitoring patients' health status.

In this respect, the thesis presents contributions for two HRD detection kits, one based on tumor tissue analysis and one based on cfDNA analysis. This thesis primarily aims to: (i) provide a comprehensive review of existing research on HRD and cfDNA, detailing the characteristics of existing diagnostic tests, and (ii) evaluate the extraction efficiency of various commercial cfDNA kits to identify the most effective one. The majority of the research was conducted at AB ANALITICA S.R.L., contributing to a project focused on creating an early diagnosis kit for hepatocarcinoma using cfDNA analysis. Our results served as a preliminary, but promising, research to develop an efficient kit for HRD diagnosis through DNA from tumor tissues and from liquid biopsies.

Contents

List of Figures

List of Acronyms

BC Breast Cancer

BRCA1 Breast and Ovarian Cancer Susceptibility Protein 1

BRCA2 Breast and Ovarian Cancer Susceptibility Protein 2

cfDNA cell-free DNA

CNA Copy Number Alteration

CNV Copy Number Variation

CO Crossover

ctDNA circulating tumor DNA

DDR DNA Damage Repair

dHJ double Holliday Junction

DSB Double Strand Break

dsDNA double strand DNA

ESMO European Society for Medical Oncology

GIS Genomic Instability Score

HGSOC High Grade Serous Ovarian Cancer

HRD Homologous Recombination Deficiency

HRR Homologous Recombination Repair

LOH Loss of Heterozigosity

LST Large Scale Transition

mBC metastatic Breast Cancer

NGS Next Generation Sequencing

NHEJ Non-Homologous End Joining

OC Ovarian Cancer

PARP Poly (ADP) ribose polymerase

PARPi Poly (ADP) ribose polymerase inihibitor

PC Prostate Cancer

PDAC Pacreatic Duct AdenoCarcinoma

SDSA Synthesis Dependent Strand Annealing

SNP Single Nucleotide Polymorphism

ssDNA single strand DNA

sWGS shallow Whole Genome Sequencing

TAI Telomeric Allelic Imbalances

TNBC Triple-Negative Breast Cancer

UMI Unique Molecular Identifier

VAF Variant Allele Frequency

WGS Whole Genome Sequencing

WES Whole Exome Sequencing

1 Introduction

Homologous Recombination Deficiency (HRD) is a condition of non-functiona- lity of the Homologous Recombination Repair (HRR), a high-fidelity repair system for double-strand breaks in DNA [30, 29]. This condition is caused in cancers where the HRR genes are non-functional and it is particularly common in ovarian tumors (particularly in High Grade Serous Ovarian Cancer, HGSOC), breast tumors (particularly in Triple-Negative Breast Cancer, TNBC), pancreatic tumors (particularly in Pancreatic Ductal Adenocarcinoma, PDAC), and prostate tumors. [81][39]

The HRD condition is correlated with a sensitivity of the tumor to Poly (ADP) ribose polymerase (PARP) inhibitors, PARP is a protein involved in the repairing single-strand breaks. HRD-positive cells treated with PARP inhibitors (PARPi) undergo an accumulation of double-strand breaks due to PARPs being blocked at single-strand break sites. Double-strand breaks are repaired by an error-prone system, such as Non-Homologous End Joining (NHEJ). The accumulation of double-strand breaks and the collapse of replication forks, when they encounter single-strand break sites with blocked PARP, cause cell death through synthetic lethality induced by the HRD condition and PARPi. [97]

HRR is a complex high-fidelity repair system for double-strand breaks that uses the sister chromatid to maintain cell heterozygosity and is thus available only in the S and G2 phases. The main players in HRR are BRCA1 and BRCA2:

- BRCA1 is a tumor suppressor gene mainly responsible for DNA damage repair, cell cycle regulation, and maintaining genomic stability. It primarily protects nascent DNA strands from degradation by stabilizing RAD51 nucleofilaments. [30][37]

- BRCA2 binds RAD51 and promotes the displacement of RPA from ssDNA and the nucleation of RAD51 on single-strand DNA (ssDNA). [30][29]

Deleterious mutations in BRCA1 and BRCA2 are highly correlated with the HRD condition, often present in tumors at the germline or somatic level. Deleterious mutations in other HRR genes such as RAD51 and PALB2 are weakly correlated with the HRD phenotype, but they can give a phenotype similar to the loss of BRCA1 and BRCA2. [92]

The HRD genotype is characterized by the accumulation of characteristic genomic scars due to DNA repair errors. These scars can be macroscopic and are of three types:

- Loss of Heterozygosity (LOH): an allele is lost, making the cell hemizygous for a given gene.
- Telomeric Allelic Imbalances (TAI): the alleles at the end of the chromosome are not equal between the two homologous chromosomes, indicating that one of the chromosomes has lost alleles.
- Large-Scale Transitions (LST): these are chromosomal breaks that generate fragments of size greater than or equal to 10 Mbp, creating discrepancies in the chromosomes, resulting from translocations, deletions, and inversions. [58]

HRD, in addition to causing macroscopic scars in the genome, also causes smaller alterations such as Copy Number Variations (CNVs) and patterns of point mutations, known as mutational signatures, such as mutational signature 3. [25] Developing kits for HRD diagnosis is an open research venue, nowadays, the technologies that calculate the HRD score to determine if a cancer is HRD positive are effective but expensive due to the high amount of DNA that needs to be sequenced, and usually, they executed in a central laboratory which increases the turn-around-time [61][65].

Based on this, it is compelling to develop a new HRD diagnosis kit for ovarian tumors, that will allow to carry out the entire process within a single analysis laboratory, comprehending DNA extraction and result interpretation. Due to the limited information that a panel containing all HRR genes provides and due to the cost of more fine-grained analyses, the kit will sequence only the BRCA1 and BRCA2 genes and perform a low-depth Whole Genome Sequencing (shallow Whole Genome Sequencing). This can be done by leveraging bioinformatic algorithms (like SeqOne HRD, a proprietary algorithm of SeqOne) to compute the HRD status based on mutations in BRCA1 and BRCA2, and the HRD score calculated through sWGS analysis.

One promising route to develop new kits for HRD diagnosis is by analyzing cell-free DNA (cfDNA). cfDNA is free circulating DNA in the bloodstream, primarily originating from necrotic cells. In conditions such as cancer, a significant increase in cfDNA is observed. cfDNA has an average size of 150-200 bp, approximately the DNA wrapped around the nucleosome, and has a very low half-life, around 8 - 16 hours. cfDNA can be isolated and analyzed to interrogate the tumor fraction of cfDNA, known as circulating tumor DNA (ctDNA). ctDNA provides real-time information about the tumor genome and its heterogeneity. [54] [98]

AB ANALITICA is developing this HRD analysis kit for ovarian tumors as part of the DECIDER project. DECIDER is a European project aimed at gaining more knowledge about the mechanisms inducing chemoresistance in patients with HGSOC, creating tools for personalized treatments for HGSOC patients, and commercializing predictive kits and software for patient treatment responses. The University of Helsinki and the University of Turku, which participate in DECIDER, are responsible for providing clinical samples, clinical data, and sequencing data to AB ANALITICA for developing the HRD status diagnosis kit. [24] AB ANALITICA is also involved in the ONCOFLUID project, which aims to develop a kit for the early diagnosis of hepatocarcinoma through the sequencing of cell-free DNA (cfDNA). [66] In the ONCOFLUID project, we outlined that:

- cfDNA analysis is a promising technology for developing a future HRD diagnosis kit for ovarian tumors where a biopsy is not possible.
- cfDNA analysis during therapy allows monitoring of the tumor's response to therapy and identifying particular clones that have developed resistance to PARPi therapy. [10][43]

During the ONCOFLUID project participation, I highlighted several points that need to be taken into consideration to create an efficient kit for the early diagnosis of hepatocarcinoma (and subsequently for HRD diagnosis from cfDNA) as indicated by current research. First, to create a hepatocarcinoma diagnosis kit from cfDNA, it is important to find the most suitable tubes for whole blood preservation. From the current state-of-the-art, one of the best methods for short-term preservation (within 48 hours) is with tubes containing cell stabilizers like Cell-Free DNA BCT tubes (Streck), instead of those containing EDTA which do not stabilize nucleated cells. [33][54] Second, for separating plasma from blood the most efficient methods [60][84] indicate proceeding by first an initial centrifugation at 800-1000g at 4°C for 10 minutes, followed by a second centrifugation at 16000g at 4°C for 10 minutes.

Third, of the main technologies used by commercial cfDNA extraction kits, it emerged that the one most easily automatable by the largest number of automatic extraction robots is the technology that uses paramagnetic beads. Whereas the kits that use silica-based technologies for cfNDA extraction are not easily automated [72, 70, 55]. Finally, by comparing the performance of commercial extraction kits based on the current research and on a commercial analysis accounting for the costs and company reliability, I identified and successively tested commercial kits for cfDNA extraction from plasma.

The results presented here were obtained from extraction kits tested using 3 mL of plasma (or the closest possible volume). The plasma used in these tests was taken from healthy patients or patients with hepatic cirrhosis. To compare the extraction efficiency of the kits tested on plasma from patients with different health statuses, Promega Maxwell RSC LV ccfDNA plasma kit was used as the standard for comparison. [70] The choice of the extraction kit to be used in the diagnosis kits is still open, but the Vazyme: VAHTS Serum/Plasma Circulating DNA Kit was revealed to be the most promising one.[93]

The analysis of cfDNA concentration and fragment size distribution was performed using ThermoFisher Scientific Qubit 3 and Agilent TapeStation 4150 instruments, which according to the current state-of-the-art are the best methods for rapid and reliable determination of cfDNA concentration and its distribution. [2][78]

ctDNA analysis requires the creation of sequencing libraries that allow the observation of mutant alleles at low percentages (low Variant Allele Fraction (VAF)). Untargeted sequencing methods like WGS, WES, and sWGS tend to have a sensitivity of around 5-10% VAF, compared to the 0.1% VAF of some targeted methods. To exponentially increase sensitivity, we have decided that our libraries will contain Unique Molecular Identifiers (UMI), which brings the sensitivity to around 0.1% VAF [83, 86, 12]. All the results point towards the feasibility of creating a diagnosis kit based on cfDNA that requires a low amount of plasma, around 3 mL, which will allow the reduction of all the costs correlated to cfDNA extraction, and will allow it to be minimally invasive and uncomfortable to the patient.

Structure of the thesis. The thesis presents both (i) an in-depth bibliographic research on issues like HRD-positive cancers, HRD, and cell-free DNA and (ii) methodological contributions to the development of an HRD detection kit based on FFPE DNA from ovarian cancer and the assessment

and testing of the preanalytical technologies for cell-free DNA extraction.

In chapter 2, a detailed analysis of HRD-affected cancers, HRD, and cell-free DNA will be presented. This chapter includes information about HRD-positive cancers, the functioning of the HRR system, the role of HRR main proteins, the HRD genotype, and the methods to identify it through genome analysis. Then, the cell-free DNA, and how it can be used to detect HRD in cancers will be discussed. Finally, there will be a discussion about the technologies to extract cfDNA from plasma, the methods to create a sequencing library from cfDNA, and the two main projects in which I participated. In chapter 3 the preliminary steps taken to develop the HRD diagnostic kit based on DNA from FFPE ovarian cancer samples will be introduced. Then, the functioning of the two main bioinformatic tools that we plan to use for HRD diagnosis, and the sequencing panel we will adopt for HRD detection, will be presented.

In chapter 4, the recommended methods to store whole blood, to purify plasma from whole blood, and to conserve plasma, will be argued. Eventually, the cell-free DNA extraction methods from plasma and how to quantify the concentration of cfDNA extracted, will be presented.

In chapter 5 the cfDNA extraction kits that have been tested, the technology used, and the results obtained through Qubit and TapeStation Analysis of the extracted cfDNA, will be discussed.

In chapter 6 the results of cfDNA extraction kits will be presented and which kits on average extracted a higher quantity of cfDNA will be determined.

Finally, in chapter 7 the final conclusions and future perspectives involving creating new detection kits will be outlined.

2

State of the Art

2.1 Ovarian Cancer

Ovarian Cancer is the most common cause of death in women diagnosed with gynecological cancers and it's the fifth cause of death for women in general. It's usually diagnosed in later stages giving low results in disease treatment. The general line for the treatment of this cancer is through the usage of surgery and chemotherapy based on platinum salts. In the last period, patients are treated with the anti-angiogenic antibody Bevacizumab (anti-Vascular Endothelial Growth Factor (VEGF)) and Poly(ADP-ribose) polymerase inhibitors (PARPi). These cancers have a high rate of recurrence after an initial treatment. Many of these relapsed cases are less curable and known to have an increased incidence of treatment failures. Hence, the prevention, detection strategies, and new therapeutic strategies are highly researched. [8]

2.1.1 Etiology

There are many risk factors associated with ovarian cancer, the most impactful ones are advanced age, genetic predispositions, and a family history of cancer. These factors are related to continuous ovulation, hormonal changes, cumulative genetic damage, and chronic inflammation. Reproductive factors that increase ovarian cancer predispositions are early menarche, late menopause onset, long-term hormone replacement therapy, and nulliparity. The risk of ovarian cancer rises significantly with age and menopause, it's usually diagnosed between 50 and 70 years. Other important risk factors

are lifestyle-related factors such as diet, tobacco use, high body mass index, and alcohol use. Ovarian cancer can be inherited, its most common causing mutations are in the BRCA1 and BRCA2, which genomic mutations are significantly associated with a hereditary breast and ovarian cancer syndrome. [90]

2.1.2 Epidemiology

In 2020, there are approximately 21,750 new ovarian cancer cases, which comprises 1.2% of all cancer cases. The estimated number of deaths related to it is 13,940. The 5-year relative survival rate is expected to be 48.6%. Around 15.7% of ovarian cancer cases are diagnosed at the local stage, and about 58% at the metastasized stage. The survival rate greatly depends on which stage the cancer is found, the 5-year survival rate of ovarian cancer diagnosed in an early stage is about 92.6%, while, the survival rate in later stages is about 30.2%. Ninety percent of ovarian cancers are epithelial, with the serous subtype being the most common. [8]

2.1.3 Histopathology

The four most common histological types of epithelial ovarian cancer are serous, endometrioid, clear cell, and mucinous tumor. The one most commonly HRD-positive is High Grade Serous Ovarian cancer. Ovarian cancer can be further classified into two subtypes- Type I or Type II tumors, Type II is a more fatal variant, thought to be caused by continuous ovarian cycles leading to inflammation and endometriosis. Type I tumors mostly arise from atypical proliferative (borderline) tumors. Type II tumors include high-grade serous carcinoma, carcinosarcoma, and undifferentiated carcinoma. Type I tumors usually present at an early stage and are low grade except for clear cell, which is considered high grade. Type I proliferative activity is usually low. They are diagnosed early and have a good prognosis. In comparison, Type II tumors are high-grade tumors and almost always of advanced stage. They have high proliferative activity with rapid and aggressive progression and a high degree of chromosomal instability compared to type I with the presence of p53 mutations in most of the cases. [8]

Ovarian serous carcinoma is the most common subtype of ovarian carcinoma. It presents as low-grade (10% of all the serous subtype tumors) or high-grade carcinoma (90% of all the serous subtype tumors). The high-grade subtype (HGSOC) shows significant nuclear atypia and mitosis (>12

per 10 high-power fields) with more copies of molecular abnormalities as seen by cytogenetic analysis. HGSOCs are usually diagnosed at an older age with a 10-year mortality rate of 70%. Further analysis revealed that a high frequency of KRAS and BRAF mutations are found in low-grade serous carcinoma, whereas high-grade serous carcinoma shows a high frequency of p53 and BRCA1 and BRCA2 gene mutations with an absence of KRAS/BRAF mutation. [8]

2.1.4 Disease Diagnosis

There is currently no reliable screening method for ovarian cancer. Most women are diagnosed based on symptoms, with the majority presenting at an advanced stage. [36] Currently, ovarian cancer can be diagnosed through medical history evaluation combined with a gynecological exam, serum Cancer Antigen 125 quantification, imaging tests, magnetic resonance imaging, and/or positron emission tomography. Novel technologies in detecting ovarian cancer are being discovered and tested. One prominent and novel technology, that could help the early detection of Ovarian Cancer is the analysis of cell-free DNA, through Next Generation Sequencing. In the study published by Zhou et. al. [100], it has been developed a cfDNA testing method for the detection of ovarian cancer based on whole-genome sequencing data including nucleosome distribution, terminal signature sequence, DNA fragmentation, and copy number variation. This testing method achieved high sensitivity (94.74%) and high specificity (98%). An FDA-approved test for the diagnosis of Ovarian cancer is the Foundation One Liquid CDx [28], it is a test based on cfDNA that uses targeted high throughput hybridization-based capture technology to detect and report substitutions, insertions, and deletions in 311 genes, rearrangements in four genes, and copy number alterations in three genes.FoundationOne Liquid CDx test is the companion diagnostic for the therapy with RUBRACA (rucaparib) if it detects mutations in BRCA1 and BRCA2. FoundationOne Liquid CDx.

2.1.5 HGSOC Treatment

Treatment of ovarian cancer conventionally includes a combination of chemotherapy and surgery. Neoadjuvant chemotherapy is recommended to reduce the tumor burden in patients deemed poor surgical candidates. Neoadjuvant chemotherapy should be evaluated after a histological diagnosis of invasive ovarian cancer confirmed by biopsy. For ovarian cancers in

advanced disease, complete debulking is often not doable, these patients can be initially treated with neoadjuvant chemotherapy, and if there is a treatment response, an interval debulking resection can be conducted, followed by adjuvant chemotherapy. In advanced Epithelial Ovarian Cancer, a successful surgery, that achieves a macroscopic tumor clearance with no residual visible disease, significantly increases Overall Survival and Progression-Free Survival. Primary cytoreductive surgery is the gold standard, and it is done for patients who can undergo surgery and in which the complete resection seems achievable. Systemic Chemotherapy after the surgery is recommended for all advanced ovarian cancer, and consideration should be given to the inclusion of anti-angiogenic and maintenance therapies. Standard Chemotherapy consists of six cycles of paclitaxel-carboplatin. Bevacizumab is a monoclonal antibody targeting the Vascular Endothelial Growth Factor (VEGF), its addition to paclitaxel-carboplatin in the first-line therapy followed by bevacizumab as maintenance gives a significant increase in Progression Free Survival versus Chemotherapy alone, but without an overall survival benefit. [8] Almost 50% of HGSOCs are HRD-positive, this is a well-established predictive factor of the magnitude of response to PARPis. The incorporation of PARPis as maintenance after first-line chemotherapy gives great benefits in patients with HRD-positive cancers. Up to 70% of patients with stage III-IV high-grade ovarian cancer will relapse within 3 years. Systemic therapy of recurrent disease is based on platinum-containing or non-platinum-containing regimens. There are currently no molecular biomarkers to predict the efficacy of platinum rechallenge.

Maintenance Therapy Maintenance therapy is conceptualized to ensure the effective killing of residual slowly dividing cells by decelerating the cell turnover so that the dormant population of cancer cells does not progress to grow enough to be detected by either elevation of biomarkers or clinical evidence of recurrent disease. Several randomized trials have been done to compare maintenance therapy versus observation.

Olaparib was the first FDA-approved Poly(ADP)-ribose polymerase (PARP) inhibitor indicated to treat advanced BRCA mutated ovarian cancer after platinum-based chemotherapy, based on SOLO-1, phase III randomized double-blind, placebo-controlled trial. It showed a reduction in disease progression or death by 70%. PAOLA-1 trial, a phase III randomized controlled trial of 806 women with stage III-IV high-grade serous or endometrioid ovarian cancer, showed a Progression-Free Survival (PFS) benefit of 4.5 months

in the group that received olaparib and bevacizumab maintenance versus placebo and bevacizumab. This combination of olaparib and bevacizumab achieved FDA approval as a first-line maintenance treatment for these patients with ovarian cancer after initial platinum-based chemotherapy with partial or complete response or tumors associated with homologous recombination deficiency (HRD) defined by the presence of deleterious BRCA mutation. Further noted clinical trials include the VELIA trial and PRIMA trial using Veliparib and Niraparib maintenance therapy, respectively, showing markedly improved PFS compared to the placebo group in patients with newly diagnosed advanced-stage ovarian cancer who initially responded to first-line platinum-based chemotherapy.

Recurrent Ovarian Cancer About 80% of women with advanced-stage ovarian cancer more commonly have tumor progression or recurrence. Platinum- free interval (PFI) is one of the most reliable predictors indicating the response of recurrent ovarian cancer to subsequent chemotherapy. PFI refers to the interval between the completion of the last platinum-based chemotherapy and the occurrence of relapse. However, platinum sensitivity generally refers to an interval of greater than 6 months between the last platinum-based chemotherapy cycle and the commencement of subsequent platinum-based chemotherapy. [8]

Large phase III trials have also resulted in the approval of bevacizumab which was studied in combination with chemotherapy for the treatment of recurrent ovarian cancer as well as for maintenance therapy (GOG 218, or OCEANS and AURELIA trials). The studies have shown an objective improvement of PFS. However, they failed to prove a benefit in overall survival. PARP inhibitors have been under clinical development at various stages and have shown their efficacy in patients with germline BRCA mutations. They were first approved as monotherapy in ovarian cancer patients with deleterious germline or somatic BRCA mutations who have not responded to chemotherapy. An overall survival benefit is yet to be proven, which requires a longer follow-up. SOLO-2 study assessed maintenance monotherapy with olaparib in patients with platinum-sensitive recurrent ovarian cancer and BRCA mutation showing significantly improved PFS for the patients receiving olaparib with no significant detrimental effect on the patient's quality of life. PAOLA-1, a phase III trial, studied olaparib with bevacizumab, an antiangiogenic agent that can be used in conjunction with PARPis, in platinum-sensitive recurrent ovarian cancer showing PFS benefit

in the patients receiving the combination. The results were quite consistent with those observed in the SOLO 1 trial. The safety profile of olaparib was quite consistent in the trials, with a higher incidence of serious adverse events noted in the group receiving a combination of olaparib and bevacizumab than with placebo plus bevacizumab, the most common one being anemia. Many phase III trials have shown PARP inhibitor maintenance therapy in patients with platinum-sensitive recurrent ovarian cancer with clinical benefits. Platinum resistance poses a very poor prognosis, where these patients have a recurrence of the disease within 6 months of completion of cytoreductive surgery and adjuvant chemotherapy, for them additional targets like tumor vasculature, DNA repair, intracellular signaling inhibition, and other molecular targets will provide more avenues to be explored for optimizing the treatment of recurrent ovarian cancer. To conclude, advanced-stage ovarian cancer patients are treated with primary reductive surgery, followed by platinum-based chemotherapy. But poor surgical candidates or patients who might not achieve effective cytoreductive surgery are recommended to undergo neoadjuvant chemotherapy. Optimal cytoreductive surgery is very important to achieve as it is one of the most powerful predictors of survival of these patients. There is a high rate of relapse in patients with advanced stage whose response to subsequent platinum-based chemotherapy depends on various factors. Targeted therapies are the new emerging treatment strategies where bevacizumab and PARP inhibitors have become first-line therapies for maintenance and PARP inhibitors as the first line for recurrent cases. Genetic screening for all newly diagnosed ovarian cancer is recommended. [8]

2.1.6 ESMO recommendations

The European Society for Medical Oncology (ESMO) recommends the following clinical decisions in regard to HRD in metastatic Ovarian Cancer:

- All patients with high-grade ovarian cancer should be tested for BRCA1 and BRCA2 mutation (germline/somatic) at diagnosis.

- Patients with a BRCA mutation and a partial or complete response to front-line platinum-based chemotherapy should receive maintenance treatment with a PARP inhibitor: 2 years for olaparib and 3 years for niraparib. The combination of olaparib and bevacizumab should be used when bevacizumab is added to front-line chemotherapy, though it is not clear that this provides superior results to the use of olaparib alone.

- Testing for genomic instability (HRD) is recommended. It identifies a subgroup of women who are BRCA wild type but derive greater benefit from a PARP inhibitor. Patients with a positive HRD test and a partial or complete response to front-line platinum-based chemotherapy, with or without bevacizumab, should receive maintenance treatment with a PARP inhibitor, either olaparibbevacizumab (if started with ChT) or niraparib monotherapy.

- Patients receiving bevacizumab with front-line chemotherapy and who are HRD negative do not have a PFS benefit from the addition of olaparib to maintenance bevacizumab. This is not a licensed indication and consequently is not recommended.

- Niraparib monotherapy is licensed for all patients with stage III-IV ovarian cancer who have responded to chemotherapy. Long-term outcome data are not available; a decision about using the drug as first-line or at recurrence in the HRD-negative population, or in the absence of knowledge about HRD status, needs to be made on a case-by-case basis. [62]

2.2 Breast Cancer

Breast cancer is currently one of the most prevalently diagnosed cancers and the 5th cause of cancer-related deaths with an estimated number of 2.3 million new cases worldwide according to the GLOBOCAN 2020 data. [52]

2.2.1 Etiology

The number of risk factors of breast cancer is significant and includes both modifiable factors and non-modifiable factors. Breast cancer is 100 times more prevalent in women than men, due to a higher estrogen and progesterone stimulation. In postmenopausal women, the amount of circulating estrogens and androgens is positively correlated with the risk of breast cancer. In men, the increase in estrogen to androgen ratio is positively correlated with the risk of breast cancer. The majority of breast cancers are diagnosed in women older than 50 years, and breast cancer risk increases with advancing age. The increased breast cancer incidence with advancing age is partly due to age-related increases in carcinogenesis and the accumulation of cellular modifications throughout time. Personal history of breast cancer is correlated to an increased risk of developing breast cancer in the opposite breast. A positive familial history of breast cancer constitutes a high risk of developing breast cancer, the risk increases as more closely related

relatives are affected. The increased risk due to a positive familial history is mainly correlated to gene abnormalities. BRCA1 and BRCA2 deleterious mutations are highly correlated to an increased risk of developing breast cancer, for a deleterious mutation in BRCA1 the collective risk is 72%, and for BRCA2 is 69%. Breast cancer is also positively correlated to modifiable factors such as obesity, physical activity and nutrition, alcohol consumption, and smoking. [5, 1]

2.2.2 Epidemiology

Breast cancer is the most frequently diagnosed cancer in women worldwide with 2.26 million new cases in 2020. In the United States, breast cancer alone is expected to account for 29% of all new cancers in women. The 2018 GLOBOCAN data shows that age-standardized incidence rates (ASIR) of breast cancer are strongly and positively associated with the Human Development Index (HDI).

Besides being the most common, breast cancer is also the leading cause of cancer death in women worldwide. Globally, breast cancer was responsible for 684,996 deaths at an age-adjusted rate of 13.6/100,000. Although incidence rates were the highest in developed regions, the countries in Asia and Africa shared 63% of total deaths in 2020. In 2020 breast cancer mortality-to-incidence ratio (MIR) as a representative indicator of 5-year survival rates was 0.30 globally. [52]

2.2.3 Breast Cancer Classification

Invasive breast cancers comprise wide-spectrum tumors that show a variation concerning their clinical presentation, behavior, and morphology. The World Health Organization distinguishes at least 18 different histological breast cancer types. Invasive breast cancer of no special type (NST), formerly known as invasive ductal carcinoma is the most frequent subgroup (4080%). This type is diagnosed by default as a tumor that fails to be classified into one of the histological special types. About 25% of invasive breast cancers present distinctive growth patterns and cytological features, hence, they are recognized as specific subtypes (e.g., invasive lobular carcinoma, tubular, mucinous A, mucinous B, neuroendocrine). Molecular classification is done independently from histological subtypes, invasive breast cancer can be divided into molecular subtypes based on molecular expression levels, in the Cancer Genome Atlas Project (TCGA) over 300 primary tumors were

thoroughly profiled (at DNA, RNA, and protein levels) and combined in biological homogenous groups of tumors. The consensus clustering confirmed the distinction of four main breast cancer intrinsic subtypes based on mRNA gene expression levels only (Luminal A, Luminal B, HER2-enriched, and basal-like). Additionally, the 5th intrinsic subtypeclaudin-low breast cancer was discovered in 2007 in an integrated analysis of human and murine mammary tumors. The cancer type that most commonly is HRD positive is the Triple-Negative Breast Cancer. [52]

Basal-Like/Triple-Negative Breast Cancer Triple-Negative Breast Cancer (TNBC) is a heterogeneous collection of breast cancers characterized as ER-negative, PR-negative, and HER2-negative. They constitute about 20% of all breast cancers. The majority (approximately 80%) of breast cancers arising in BRCA1 germline mutation are TNBC, while 11 - 16% of all TNBC harbor BRCA1 or BRCA2 germline mutations. TNBC tends to be biologically aggressive and is often associated with a worse prognosis. The most common histology seen in TNBC is infiltrating ductal carcinoma, but it may also present as medullary-like cancers with a prominent lymphocytic infiltrate; metaplastic cancers, which may show squamous or spindle cell differentiation; and rare special type cancers like adenoid cystic carcinoma (AdCC). The terms basal-like and TNBC have been used interchangeably; however, not all TNBC are of the basal type. On gene expression profiling, TNBCs can be subdivided into six subtypes: basal-like, mesenchymal, mesenchymal stem-like, immunomodulatory, and luminal androgen receptor, as well as an unspecified group. [52]

2.2.4 Diagnosis of Breast Cancer

An early diagnosis of Breast cancer is essential for the patient's survival. Mammography is an x-ray of the breast that can reveal benign or malignant abnormalities, it's the most cost-effective diagnostic method and it has high specificity and sensitivity. Another method is the Breast MRI, a non-invasive and non-ionizing diagnostic imaging tool that uses low-energy radio waves and magnetic fields to obtain detailed images of the structures within the breasts, it's used to recognize tumors with size less or equal to 2 cm and metastatized tumors. MRI can detect suspected breast malignancies that often are not recognized by mammography and ultrasound detection. Ultrasounds are a supplemental tool to Mammography when it gives inconclusive results, but they fail to detect microcalcifications and may miss some

early signs of cancer. [11]

Cell-free DNA and Circulating tumor cells are being evaluated in studies as diagnostic biomarkers for the detection, staging, response to therapy, and recurrence of Breast cancer. [59] Nowadays, there are commercial tests that use cfDNA for the diagnosis of particular gene mutations in Breast cancer. FoundationOne Liquid CDx [28] is the companion diagnostic for PIQRAY (alpelisb) if specific point mutations are found in PIK3CA.

2.2.5 Treatment Strategies

Chemotherapy Chemotherapy for Breast cancer can be either neoadjuvant or adjuvant. Neoadjuvant chemotherapy is used for locally advanced breast cancer, inflammatory breast cancers, or small tumors with worse prognostic molecular subtypes (HER2 or TNBC). Currently, treatment includes a simultaneous application of drugs like carboplatin. The choice of the proper drug is of major importance since different molecular breast cancer subtypes respond differently to preoperative chemotherapy. Preoperative chemotherapy is comparably effective to postoperative chemotherapy. Even though chemotherapy is considered to be effective, its usage very often leads to several side effects. TNBC does not benefit from endocrine or HER2-targeted drugs, therefore the standard of care for nonsurgical operable TNBCs (the majority of TNBCs) is nonspecific chemotherapy, such as taxane or anthracyclines. However, less than 30% of TNBC patients achieve a complete response. [48] Establishing PD-L1 and germinal BRCA mutational status is fundamental to optimizing management. [32] Patients with BRCA-mutant TNBC show a high overall response rate to cisplatin and carboplatin treatment, compared to docetaxel (taxane). Approximately, 80% of TNBCs have mutations (germline or somatic) in the BRCA1 gene, which is linked to HRD and PARPi sensitivity. Current first-line treatment strategies for germinal BRCA-mutated TNBC and metastatic breast cancer involve using olaparib or talazoparib regardless of HR status [32]. For PD-L1 immune cell positivity atezolimumab plus nab-paclitaxel is recommended in first-line treatment

2.2.6 ESMO diagnostic and therapy recommendations for metastatic Breast Cancer

- At first diagnosis of Metastatic Breast Cancer (mBC), a biopsy should be carried out to confirm histology and re-assess tumor biology.
- Other therapeutically relevant biomarkers to be assessed as part of

routine clinical practice include germline BRCA1/2 mutation status in HER2-negative mBC, PD-L1 status in triple-negative breast cancer, and phosphatidylinositol-4,5-bisphosphate 3-kinase catalytic subunit alpha (PIK3CA) in ER/PgRpositive, HER2-negative mBC.

- Genomic profiling and further diagnostic tests on tumor tissue or circulating tumor DNA (ctDNA) should only be carried out as part of routine clinical practice if the result will change the treatment approach, as guided by the ESCAT scale, or if the patient can access appropriate clinical trials.

- For second-line treatment, PARP inhibitor monotherapy (olaparib or talazoparib) should be considered for patients with germline pathogenic BRCA1/2 mutations and as an option for those with somatic pathogenic or likely pathogenic BRCA1/2 or germline PALB2 mutations.

- Patients with HER2-negative mBC and germline pathogenic or likely pathogenic variants in BRCA1 or BRCA2 should be offered treatment with a PARP inhibitor (olaparib or talazoparib), independent of HR status, as an alternative to chemotherapy.

- Patients who may be considered for treatment with PARP inhibitors should be offered genetic testing for pathogenic variants in BRCA1 and BRCA2 regardless of age, family history, or BC subtype. [32]

2.3 Pancreatic Cancer

Approximately 60,430 new diagnoses of pancreatic cancer were anticipated in the US in 2021. The incidence is rising at a rate of 0.5% to 1.0% per year, and pancreatic cancer is projected to become the second-leading cause of cancer death by 2030 in the US. Pancreatic ductal adenocarcinoma (PDAC) accounts for the majority (90%) of pancreatic neoplasms, and the other subtypes include acinar carcinoma, pancreaticoblastoma, and neuroendocrine tumors. Most patients with pancreatic cancer present with nonspecific symptoms at an advanced stage with disease that is not amenable to curative surgery. No effective screening exists. The 5-year survival rate approached 10% for the first time in 2020, compared with 5.26% in 2000. The survival improvements have been modest and attributed primarily to multiagent cytotoxic therapies. Recently, comprehensive germline and somatic genomic sequencing became the standard of care for small subgroups of patients with targeted treatment opportunities. Olaparib, a poly (adenosine diphosphate[ADP]-ribose) polymerase inhibitor, can prolong cancer control in patients with a BRCA1/2 pathogenic germline variant. [67]

2.3.1 Etiology

Pancreatic cancer is correlated to unmodifiable factors such as age, and genetics, and modifiable factors such as cigarette smoking, alcohol use, chronic pancreatitis, and obesity. About 3.8% to 9.7% of patients with PDAC have pathogenic germline gene variants that increase susceptibility to PDAC. These variants occur mostly in DNA damage repair genes. The most common variants in PDAC include BRCA1, BRCA2, and ATM. In 2019, the National Comprehensive Cancer Network guidelines recommended that all patients newly diagnosed with PDAC undergo germline testing with a gene panel including BRCA1/2, ATM, MLH1, MSH2, MSH6, and PMS2.[16]

Whole-genome structure analysis can provide insight into genomic instability and the relationship with DNA maintenance genes (BRCA1/2 and PALB2) and, specifically, genetic signature 3. The identification of genomic instability can enable platinum-based therapy and poly (ADP-ribose) polymerase inhibitors may be effective for patients with pathogenic variants in BRCA1/2 and PALB2. One prospective trial building on these observations has led to the approval of the targeted agent olaparib in select patients with BRCA1/2 pathogenic germline variants.

2.3.2 Epidemiology

PDAC is the third-leading cause of cancer mortality in the US and the seventh-leading cause worldwide. The median age at diagnosis in the US is 71 years, and PDAC is slightly more common in men than in women (5.5 vs 4.0 per 100,000 individuals). At presentation, 50% of patients have metastatic disease, 10% to 15% have localized disease amenable to surgery, and the remainder (30%35%) have locally advanced mostly unresectable disease due to the extent of tumor-vascular involvement. Pancreatic intraepithelial neoplasms (PanINs) refer to precancerous lesions, of which a small fraction may progress to high-grade dysplasia and PDAC. Low-grade PanINs are common and their potential to transform into a malignancy is unclear. Intraductal papillary mucinous neoplasms are more common precancerous cystic lesions than PanINs and can arise in either the main or branch pancreatic duct. Annual imaging surveillance is recommended; however, there is no consensus as to the optimal surveillance method or frequency of assessment. For asymptomatic average-risk individuals, the US Preventive Services Task Force recommends against routine screening for PDAC. [16][67]

2.3.3 Histopatology of Pancreatic Cancer

Neoplasms of the pancreas comprise a broad spectrum and are generally classified according to their histological differentiation as epithelial or non-epithelial and according to their biological behavior in benign, premalignant, or malignant neoplasms. Epithelial neoplasms can be either exocrine or endocrine, while the group of exocrine neoplasms is further classified as ductal and acinar neoplasms. [38] Pancreatic Ductal Adenocarcinoma affects the exocrine parenchyma and it is the most common type of pancreatic cancer, accounting for about 80% of all pancreas neoplasms, and about 24% to 44% of PDACs are HRD positive. [17] [21]

2.3.4 Diagnosis of Pancreatic Cancer

Pancreas computed tomography (CT) angiography with chest and pelvis CT can be used in the assessment of vascular anatomy and stage of disease and is recommended at diagnosis to also assess the possibility of metastases which happens mostly on the liver, lymph nodes, and lungs. Positron emission tomography/CT is a functional imaging to assess the glucose metabolism of the tumor and to differentiate a benign tumor from a malign tumor. Fine-needle core biopsy of a tumor guided by endoscopic ultrasonography is recommended to obtain a histologic diagnosis. The analysis of cell-free DNA and circulating tumor cells is a new non-invasive technique studied on pancreatic cancer to provide an early diagnosis of pancreatic cancer, stage evaluation, response to therapy, and cancer recurrence. [36] There are still no approved cfDNA and Circulating Tumor Cell liquid biopsy tests for Pancreatic cancer.

2.3.5 Pancreatic Cancer Therapy

Resection of PDAC is one of the first treatments, the resectability of the cancer depends on the degree of tumor contact and invasion. PDAC is relatively resistant to chemotherapy, the recommended adjuvant chemotherapy after resection of PDAC, in most patients, is either modified FOLFIRINOX for individuals with high functional status or gemcitabine and capecitabine or gemcitabine alone for individuals with poorer functional status. Meanwhile, radiotherapy for PDAC is controversial because older studies highlighted no overall survival advantage.

Neoadjuvant therapy can eradicate micro-metastases and increase the

number of patients eligible for systemic therapy. There are genetic alterations in PDAC which are actionable mutations that define the type of neoadjuvant therapy. In PDAC with germline BRCA1, BRCA2 or PALBB2 mutations are highly responsive to cisplatin plus gemcitabine. [85] Based on the result of phase 3 trial POLO, the FDA has approved PARPi maintenance therapy with olaparib for adult patients with BRCA-mutated metastatic pancreatic adenocarcinoma [14].

2.3.6 ESMO Reccomendations

- BRCA testing is recommended to patients with pancreatic cancer
- For first-line treatment, patients with BRCA mutations should receive platinum-chemotherapy.
- Regarding patients with metastatic Pancreatic Cancer, BRCA genetic testing should be executed to determine the eligibility for selection of platinum-based chemotherapy, followed by maintenance with olaparib. [21]

2.4 Prostate Cancer

2.4.1 Introduction

Prostate cancer affects middle-aged men between the ages of 45 and 60 and it's the main cause of cancer-associated deaths in Western countries. Prostate cancer is usually diagnosed through prostate biopsy and analysis, prostate-specific antigen (PSA) testing, and digital rectal examination. The main risks associated with prostate cancer are family history, ethnicity, age, obesity, and other environmental factors. [79]

Genetic mutations in prostate cancer are heterogeneous, and the prostate cancer risk is inheritable. Candidate genes for prostate cancer predisposition are genes involved in the androgen pathway and metabolism of testosterone Prostate cancer can either be classified as androgen-sensitive or androgen insensitive which indicates testosterone stimulation and the possible treatment options. The treatment options depend on the nature of the tumor, PSA level, grade and stage, and possible recurrence. [79]

2.4.2 Etiology

Prostate cancer is multifactorial and its etiology is still not well comprehended. [49] Many risk modifiable and unmodifiable risk factors contribute to its development. Ages is a well-known risk factor, Prostate cancer is rarely present in men of age below 40 years, and the risk increases with age. A positive family history poses a great risk of developing prostate cancer, the risk of developing prostate cancer is highest if a brother is diagnosed, and increases the probability of developing it early. Another associated risk is a positive familial history of breast cancer. Germline DNA sequencing of men with Prostate cancer revealed that 5.5% of the men had germline mutations in DNA repair genes such as ATM, BRCA1, and BRCA2 genes. [79]

Men with a positive familial history of breast cancer and prostate cancer have the highest probability of developing prostate cancer. BRCA gene mutations are linked to an increased risk of developing Prostate cancer. The incidence of prostate cancer is also affected by ethnicity and geographic variations, men of black African descent have the highest incidence. Smoking and alcohol usage are risk factors linked to increased prostate cancer susceptibility, where the magnitude of the risk, severity, and mortality are directly linked with tobacco smoke and alcohol intake. Obesity and increased body mass index are associated with an increased risk of developing prostate cancer. [49]

2.4.3 Epidemiology

Prostate cancer is one of the most common cancers diagnosed in men worldwide. In 2020, it was the third most commonly diagnosed malignancy, 1,400,000 new cases of prostate cancer and 375,00 deaths were reported with an incidence from 6.3 to 83.4 per 100.000 people, it has a higher prevalence in developed countries, like Europe and North America. It has been reported that people of African descent are more prone to develop prostate cancer, whereas people of Asian descent are less prone to develop it.

2.4.4 Histopathology of Prostate Cancer

Prostate cancer involves malignancy primarily of the epithelium and is thus classified as a carcinoma. There are rarer subtypes of prostate cancers such as sarcomas and lymphomas. About 90-95% of prostate cancers are acinar adenocarcinomas that arise from the peripheral prostatic gland. [49]

Approximately, 20% of metastatic prostate cancers harbor mutations in DNA damage and repair genes and BRCA2 is the most commonly altered.

2.4.5 Diagnosis of Prostate Cancer

A higher mortality rate and failure of therapy are linked to a diagnosis in later stages. There is no single specific test for prostate cancer, a digital rectal examination usually diagnoses it, high Prostate-specific antigen levels in blood is a biomarker positively correlated with the presence of prostate tumor because higher levels are also present in benign prostatic hyperplasia. Biopsy analysis is one of the most reliable methods for the diagnosis of prostate cancer. The common genes used as biomarkers for prostate cancer are BRCA genes, HOX genes, ATM gene, RNase L, and ELAC2/HPC2. Biomarkers can be used in diagnostic procedures, staging, and to evaluate the therapeutic process. A novel method for Prostate cancer diagnosis is the analysis of mutations and epigenome in cfDNA. There are commercial tests available to detect Prostate cancer-specific mutations by sequencing the cfDNA with actionable results in case of a positive test, one of these tests is FoundationOne Liquid CDx [28] which is the companion diagnostic for LYNPRARZA (olaparib) if it detects mutations in BRCA1, BRCA2, and ATM, and for RUBRACA (rucaparib) if it detects mutations in BRCA1, and BRCA2.

2.4.6 Prostate cancer therapy

Androgens are essential for normal prostate development and differentiation and are also involved in prostate cancer initiation and progress. Thus, androgen-deprivation therapy, which blocks androgen receptor signaling, is the standard treatment for prostate cancer. This therapy is not curative, because most cancers become insensitive to it, acquiring the castration-resistant phenotype. Primary surgery is a viable treatment for prostate cancer, decreasing the mortality and the likelihood of disease progression and metastasis. Radiation therapy is another therapy widely used, even in combination with androgen-deprivation therapy. [49] Recent studies highlight the benefits of rucaparib and olaparib (two types of PARPis) usage in metastatic castration-resistant prostate cancer harboring mutations in BRCA1 and BRCA2 genes. Prostate cancer with mutations in HRR genes such as ATM, CDK12, CHECK2, CHECK1, PALB2, PP2R2A, and RAD54L responded well to olaparib treatment.

2.4.7 ESMO Recommendations

- Germline testing for BRCA2 and other DDR genes associated with cancer predisposition syndromes is recommended in patients with a family history of cancer and should be considered in all patients with metastatic prostate cancer.
- Olaparib can be considered after new hormonal agents for patients with mCRPC with alteration in BRCA1 or BRCA2.

2.5 Homologous Recombination Repair

2.5.1 Overview of the Double Strand Breaks Repair

The Homologous Recombination Repair (HRR) pathway is usually used when a chromosome suffers a Double Strand Break (DSB). The DNA damage response mechanism coordinates the cellular pathways to allow genomic stability and cell survival, in which are present in the DNA repair pathway of DSBs. The DSBs can be repaired through many pathways, the main pathways are the Non-homologous End Joining (NHEJ), Micro-Homology End Joining (MMEJ), and the Homologous Recombination Repair. [95]

The HRR is an error-free DNA repair pathway, where the DSBs are repaired using the sister chromatid as a template, this allows the maintenance of heterozygosity. For this reason, HRR happens mostly in the phase S/G2 in response to replication stress. The DNA repair pathways such as NHEJ and MMEJ are available throughout the whole cell cycle, they require minimum homology of the DNA strands for the repair (MMEJ) or no homology (NHEJ). Those systems are faster but much more error-prone since deletions, translocations, and inversions usually may happen. [27]

The HRR may happen through different subpathways, but the initial steps are functionally the same and they involve common proteins, The HR starts with an extensive resection of 5′ - 3′ of the broken ends by a nuclease MRN complex (MRE11 - RAD50 - NSB) to form 3′ ssDNA overhangs. The ssDNA gets coated by the Replication Protein A (RPA). The Breast and Ovarian Cancer Susceptibility Protein 2 (BRCA2) loads the recombinase RAD51 on the ssDNA, replacing RPA and forming a nucleo-protein strand to begin the homology search to find homologous sequences. Once the complementary strand has been found, a displacement loop (D-loop) is formed, where a primer-template junction allows DNA repair synthesis to proceed. After

repair synthesis completion, HR can proceed by the displacement of the extended break end from the D-loop and annealing to the complementary sequence at the non-invading end, a subpathway referred to as synthesis-dependent strand annealing (SDSA). An alternative mechanism involves the formation of a joint structure containing a four-way junction between the recombining strands, known as a Holliday junction (HJ). This can occur through the annealing of the non-invading end to the displaced strand of the D-loop in a second-end capture step, or possibly by simultaneous invasion of the two resected ends into the donor and subsequent extension. To allow proper chromosome segregation, the two intertwining strands must be separated, which can occur through two mechanisms with distinct genetic outcomes. Double HJs (dHJs) are prominent HR intermediates and are predominantly processed by helicase- and topoisomerase-dependent dissolution that separates the recombining molecules without genetic exchanges. Alternatively, these joint molecules can be resolved by the structure-selective nucleases to give rise to crossover (CO) or non-CO products at an expected equal frequency. HR can also proceed through a third, non-canonical subpathway termed break-induced replication (BIR), which is characterized by long-range conservative DNA synthesis from the invading DSB end without engagement of the second end and displaying a high propensity to form genomic rearrangements and point mutations.[27]

Non-Homologous End Joining is a fast, always available, and error-prone mechanism for DSB repair. Upon a DSB break the Ku70/80 heterodimer, a ring-shaped molecule, binds the DNA ends. DNA-PKcs, a protein kinase, binds DNA-Ku70/80 and its kinase activity is stimulated which phosphorylates many NHEJ and DNA repair factors. The critical event for DSB repair is the auto-phosphorylation of DNA-PKcs. The ligation process is highly dependent on the proximity of the two ends, to diminish the distance between the two ends, a long-range evolving synaptic complex is formed, which involves a multi-protein complex mainly composed of Ku70/80, DNA-PKcs, XRCC4-LIG4, and XLF which allow the transition to a short-range synaptic complex. The ligase LIG-4 catalyzes the ligation. LIG-4 can tolerate mismatches and damaged bases. DSBs frequently yield damaged DNA ends that are not suitable for immediate ligation by LIG-4. Thus, the NHEJ pathway uses different end-processing enzymes that modify the DNA ends until they are compatible for ligation. The role of the nuclease Artemis is pivotal for DSB repair, but its mode of function in NHEJ, outside of V(D)J recombination, is not yet known. After the nuclease action of Artemis, NHEJ

polymerases pol lambda, pol mu, and terminal deoxynucleotidyl-transferase (TdT) are recruited to the DSBs via an interaction with Ku70/80 and XRCC4-LIG4. [88]

2.5.2 Homologous Recombination Repair Mechanism

The DSBs repair through HRR is a pathway with different branches, the starting steps are the same, but the ending is different. HRR begins with the nucleic degradation of the DSBs ends, also known as DNA end resection. DNA end resection requires the enzymatic activity of the nuclease MRE11 and CtIP. MRE11 creates a complex with RAD50 and NSB to form the MRN complex (MRE11 - RAD50 - NSB). BRCA1 regulates the DNA end resection through its interaction with the MRN complex and CtIP. Then, the end resection is completed by Exo1, DNA2, and BLM helicase, forming a 3' overhanging ssDNA tail.

The ssDNA ends are coated with the protein RPA, making them resistant to further degradation. The RAD51 recombinase displaces RPA, and BRCA2 mediates the displacement. BRCA1 and PALB2 regulate the protein DSS1. BRCA1 stimulates the RAD51-ssDNA nucleoprotein filament to start the homology search and strand invasion on the homologous DNA, forming a displacement loop. [99]

Some pathways result in the formation of Holliday Junctions, a branched DNA structure that contains four double-stranded arms joined, the annealing of the second end is catalyzed by the protein Rad52, which mediates the annealing of the ssDNA bound to RPA to the complementary DNA. The resulting Holliday Junction can be resolved through a non-crossover way using the BLM helicase and the topoisomerase TOPOIIIα, or it can be resolved through the structure-sensible nuclease Resolvase A, giving crossover/ non-crossover products.

In the Synthesis Dependent Strand Annealing (SDSA) pathway, the D-loop gets dissolved after the DNA synthesis and the unbound strand binds the second extremity of the DSB, forming non-crossover products. The re-annealing of the second end of the DSB always involves the RAD52 protein. [47]

Homologous Recombination Repair is active only during the S - G2 phase because it needs the sister chromatid as a homologous template for the DNA repair. It has two main pathways: the synthesis-dependent strand annealing (SDSA) and Double Holliday Junction formation with or without crossover

(Figure.

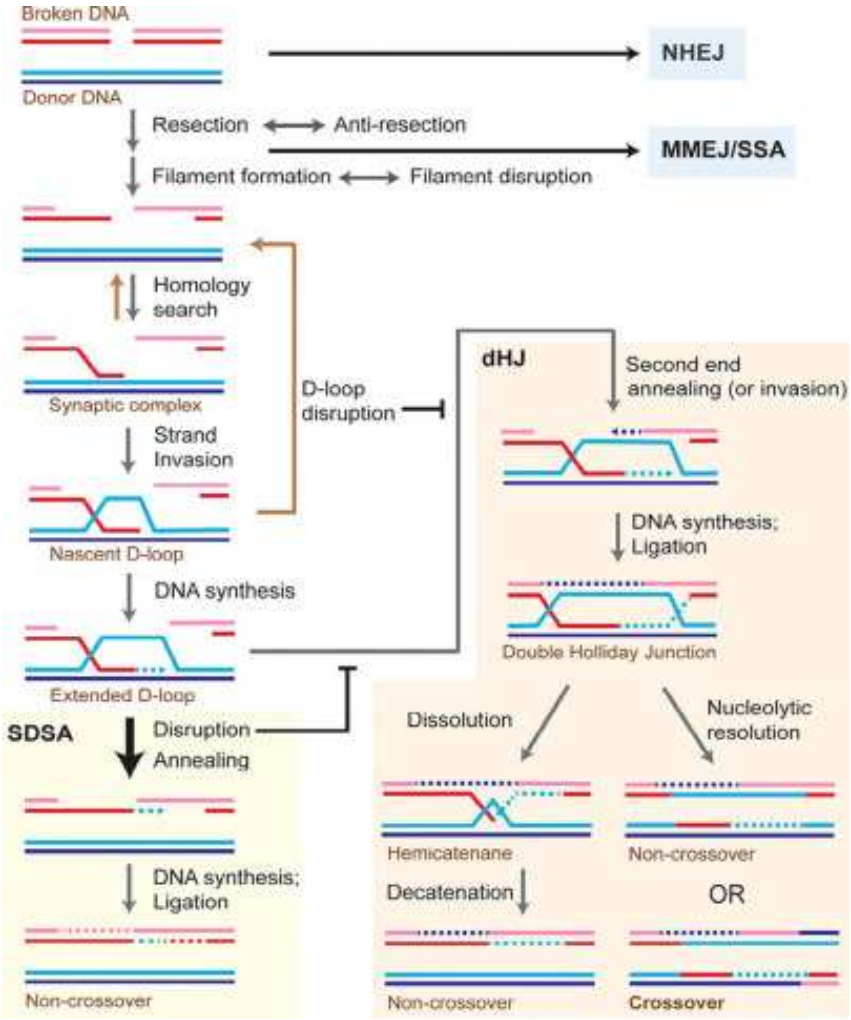

Figure 2.1: Graphical representation of HRR pathways from [95] . After DSB detection the DNA is resected by the MRN complex leaving a 3'OH end, this end gets coated by RAD51 through BRCA2 interaction. RAD51-DNA proceeds with the homology search to find the homologous filament in the sister chromatid. After binding to the homologous filament the DNA synthesis starts to form an extended 3' end. This end can be processed through the Synthesis Dependent Strand Annealing where it binds to its original chromatid to restore the DNA integrity, or it may form a double Holliday Junction through second strand invasion, this may be resolved through a deleterious crossover event or a noncrossover event.

Double Strand Break resection In HRR, the DSB is resected 5' to 3' on one strand of the DSB ends producing terminal 3'-OH single-stranded DNA tails. After DNA resection the DNA must proceed towards HRR instead

of NHEJ. The nuclease MRE11-RAD50-NBS1 (the MRN complex) and its cofactor Sae2 initiate resection with the capability of acting on DSB ends with nonstandard DNA chemistry or covalently attached proteins by delivering an endonucleolytic incision to release terminal 5'-ending oligonucleotide.

The resected DSB ends must find, synapse with, and invade a homologous donor locus to prime repair DNA synthesis. [95]

Assembly of the nucleoprotein filament scaffold on ssDNA RAD51 family proteins form right-handed helical filaments on ssDNA that act as nucleoprotein scaffolds to direct their own activities and the activities of interacting proteins. Nucleation of RAD51 to the filament competes with the ssDNA binding protein RPA. RAD51 to nucleate in the ssDNA filament requires the interaction with mediator proteins to overcome the nucleation-inhibition by RPA, the interaction with the mediators allows the displacement of RPA and the nucleation. In vertebrates, the interaction of the BRCA2-DSS1 complex with Rad51 is critical to the RAD51 filament nucleation. BRCA2 acts in concert with the human RAD51 paralogs. In BRCA2-deficient human cells, RAD52 becomes essential, and it was suggested that RAD52 exterts a mediator function in BRCA2-deficient cells.

In vertebrates, the core HR protein is less autonomous, its ATPase slows, and it has a greater number of interactors. vertebrates have five different RAD51 paralogs, and each one is required for a normal RAD51 foci formation. RAD51 paralogs function in the integration of RAD51 to the filament, and their interaction with RAD51 filaments mediates a change of Rad51 conformation. In vertebrates, the SWI3-MEI5 heterodimer is pivotal for mitotic and meiotic recombination. It enhances the RAD51 ATPase function promoting the ADP-ATP exchange. Eukaryotic cells have evolved the Rad54 protein, a tightly coupled dsDNA-dependent motor activity complementing the RAD51 filament. Rad54 requires its ATPase activity but it associates with Rad51-ssDNA filaments and stabilizes them, independent of its ATPase activity. Rad51 regulation by the nucleotide-binding/hydrolysis cycle, associated proteins, and other potential cofactors are critical in its assembly and function. Once the nucleoprotein scaffold is assembled, other Rad51 filament-interacting proteins enhance the homology search and DNA strand invasion activities. [95]

The homology search The DSB end, now resected to ssDNA and assembled with the RAD51 filament and cofactors must find a homology donor

from which to initiate DNA synthesis. The ssDNA filament must interact with the genomic dsDNA as it scans for sequence complementarity. One strand of dsDNA is destabilized to open the helix and to allow bases to be sampled for complementarity via base flipping to those within the ssDNA filament. RAD51 requires additional proteins in this step, the bridging of RAD51 filaments to dsDNA has been proposed for the proteins RAD51Ap1, PALB2, and HOP2-MND1. Extrinsic factors can enhance dsDNA probing by RAD51. For efficient homology search, dsDNA must be transiently bound and turned over rapidly when the sequence is incorrect. Microhomologies of as few as eight nucleotides promote extended lifetimes of RAD51-ssDNA-dsDNA complexes. It's not clear whether RAD51 ATPase activity plays a role in dsDNA release during homology search or whether additional protein cofactors are required. The synaptic complex, also known as a paranemic joint, forms upon identification of homology in a donor dsDNA. All three strands pass into the filament along the paired region until they exit again. The arrangement of base pairing in these three-stranded intermediates is poorly understood, but there is no net intertwining of the invading strand with its complement in the donor, such that the removal of proteins results in total disruption of the structure. However, synaptic complexes are more stable than filament interactions observed with nonhomologous dsDNA. The structure, size, and lifetimes of synaptic complexes in vivo are not known; however, it was recently proposed that they exist for an extended time before being triggered to proceed to form the D-loop. When three or more nucleotides are consecutively base-paired, the dsDNA untwists in the same pattern of triplet stacked bases intervened by unstacked and stretched intertriplet gaps. This arrangement may facilitate the homology search by preventing cooperative base stacking interactions in the absence of homology, to favor stabilization through Watson-Crick interactions. This also explains why negatively supercoiled DNA donors are highly favored for the formation of metastable synaptic complexes. As the dsDNA is stretched the negative supercoils are relaxed to provide energy to drive the expansion of the paired region. [95]

Formation of heteroduplex DNA in the D-loop and the ATP-dependent role of Rad54 After the formation of the synaptic complex, the 3′ end of the invading strand must form a primer-template junction with the homologous DNA to begin the DNA synthesis. This intermediate is known as the Displacement loop (D-loop), where the invading strand forms a heteroduplex

(hDNA) with the homologous DNA. Human RAD54 activity is tightly coupled to the activity of RAD51 and it highly stimulates the calcium-supported RAD51 reaction. RAD51 stimulates RAD54 ATPase activity which induces RAD51 dissociation The regulation via RAD54 and other protein factors allows a greater function and versatility it can operate in almost any kind of coiled DNA. Also, the different cofactors allow a greater regulation. [95]

DNA topology and structure regulation in HRR The extension of the hDNA creates a supercoiling opposing the further expansion of the hDNA, negatively supercoiled filaments favor the initial synaptic complex formation and subsequent invasion. In vivo, the supercoiling status is dynamic and highly regulated, by motor proteins and topoisomerases to facilitate strand invasion, DNA synthesis, and hDNA disruption. The Sgs1-Top3-Rmi1 complex is composed of a 3'-5' helicase, a type 1A topoisomerase, and its cofactor, Top3-Rmi1 specifically are important in dissociation of the D-loop. Other type I and II topoisomerases are involved in HR outcomes, even indirectly. The 3' end of the invading strand is required to be in hDNA to form a primer-template junction for DNA synthesis, but the hDNA region can be hundreds of base pairs long. Longer hDNA can favor double Holliday Junction formation thereby promoting crossovers, with the correlated risk of loss of heterozygosity in critical genes, thus the favored pathway usually involves the SDSA pathway to avoid the loss of heterozygosity. [95]

D-loop reversal activities ensure high-fidelity DSB repair and CO avoidance In SDSA, the disruption of the extended D-loop is required for chromosome resolution, for the rejection of the formation of hDNA with homologous donor DNA, to lower the probability of a double invasion of the donor DNA, and to prevent the multi-invasion (one ssDNA end invading two donors) which can lead to translocations of the two donors and a plethora of rearrangements. In vertebrates, the enzymes/complexes involved in D-loop disruption are: Sgs1-Top3-Rmi1, the 3'-5' helicases, Srs2 and Mph1, and, five helicases of the RecQ family. Often these factors have roles in support of DNA replication in addition to DSB repair. D-loop disruption activities maintain a dynamic balance with hDNA formation and extension, enhancing overall HR fidelity and promoting cross-over avoidance. [95]

DNA synthesis at the D-loop Once the 3' end has been incorporated into hDNA in the D-loop or a 3' end has been generated by cleavage, the

DNA synthesis can start. DNA synthesis mediated by Polymerase δ and other cofactors (like PCNA) creates a positive supercoil that opposes further DNA synthesis. To overcome this block, invading DNA is peeled off from the 5′ side to create a migrating bubble to prevent topological stalling. In Drosophila, the BLM helicase is required for long SDSA events, its function is to carry out the bubble migration. Alternatively, topoisomerases can relax the donor DNA ahead of the extending D-loop, as they normally do in DNA synthesis. However, these topoisomerases cannot resolve roadblocks in the DNA template, such as RNA-DNA loops, transcription machinery, and bound proteins. [95]

Extended D-loop disruption, second-end annealing, and crossover avoidance Polymerase δ DNA synthesis must elongate the invading strand to an extent where when the D-loop is disrupted the invading strand can anneal with the other broken end of the DSB. A popular theory suggests that the synthesis of the invading strand is achieved through cycles of invasion, short DNA synthesis, and D-loop disruption. Srs2 and Mph1 have a role in disrupting the extended D-loops, they are 3′-5′ ssDNA translocases concerning the DNA strand the motors translocate on. To disrupt the hDNA, they must first load onto a strand in the D-loop substrate, then Srs2, for example, can interact with the modified PCNA and 3′ proximal hDNA and translocate on the invading strand starting at the 3′ end to disrupt hDNA. Another possible mode of action proposed is the loading of a helicase at the 5′ hDNA branch point on the donor template strand and translocating toward the 3′ side of the hDNA tract. The unwound ssDNA will then be bound by RPA. Cell signaling can promote D-loop disruption through Srs2 interaction with protein complexes like PCNA-SUMO. The two DSB ends can now anneal in the region of homology created by the DNA synthesis, in human the annealing of the ssDNA RPA-coated strands is carried on by, at least, the RAD52 protein, but in the presence of RAD52 lof the phenotype is subtle and mild. BRCA2 in vertebrates is not involved in this step. Another model called the modified SDSA model, replaces a second-end annealing step with a second-end DNA strand invasion step, removing the need for an annealing protein. Regardless of the model, another unidentified DNA polymerase is involved in the second-end DNA synthesis. The ligation of the nicks restores the integrity of the chromosomes and avoids any crossover. [95]

Double Holliday junction processing and the possibility of a crossover A fraction of DSB repair through HRR proceeds through the formation of a double Holliday junction (dHJ). To form a dHJ, two events may happen: the second resected DSB end anneals to the displaced strand of the D-loop, or both DSB ends simultaneously invade the donor and extend through DNA synthesis. Ligation of the resultant nicked duplexes then creates a dHJ, where each HJ is a four-way branched DNA joint molecule. These dHJs are processed by either dissolution, giving strictly noncrossover, or endonucleolytic resolution that generates crossover or noncrossover products. Human resolvases MUS81-EME1 have been proposed to cooperate with another pair of resolvases: SLX1-SLX4, where SLX1-SLX4 introduces the initial cut to form nicked HJ, which is further processed by MUS81-EME1 which prefers nicked dsDNA molecules. SLX-MUS complex often cleaves asymmetrically, leaving products with gaps and protruding ends that require further processing. As a last measure of crossover avoidance, the cell can dissolute dHJ through the Sgs1-Top3-Rmi1 complex leading to a noncrossover outcome. The Sgs1 helicase promotes branch migration of the two HJs toward each other to converge into a hemicatenane. Top3 is required to resolve topological constraints during branch migration and to dissolve the topological connection by passing the two DNA strands of the hemicatenane to result in noncrossover products. Whether migration of HJs is random or directed is unknown. Dissolution is important to avoid excessive inter-sister crossovers and to prevent loss of heterozygosity in somatic cells. This is exemplified in Blooms syndrome, in which the human Sgs1 homologBLMis mutated, resulting in excessive sister chromatid exchanges and genome instability. [95]

2.6 Biological Functions of Important Proteins in HRD

2.6.1 BRCA1 and BRCA2 functions

BRCA1 and BRCA2 are two main genes in HRR, their loss of function is usually associated with the HRD phenotype and genotype.

BRCA1 and BRCA2 proteins have a crucial role in DSB repair through the regulation of the repair through homologous recombination.

BRCA1

BRCA1 is a tumor suppressor gene mainly involved in DNA damage repair, cell cycle regulation, maintenance of genome stability, etcetera. BRCA1 is located in 17q21, it has an N-terminal RING domain with E3 ligase activity, with it can interact with its partner protein, the BRCA1-associated RING domain protein 1 (BARD1). BRCA1 C-terminal domain (BRCT domain) is associated with different phosphorylated interacting proteins. Upstream of the BRCT domain, there is a coiled-coil domain that binds to the N-terminal coiled-coil domain of PALB2, PALB2 also binds BRCA2, and their interaction forms the BRCA1-PALB2-BRCA2 complex, which stimulates RAD51-mediated localization and repair at DNA breaks. The majority of lof mutations registered in BRCA1 are located in the BRCT domain and N-terminal RING domain. [30] BRCA1 can form four different complexes in cells, through the association of different adaptor proteins with the BRCT domain, such as BRCA1/ RAP80/ Abraxas complex, BRCA1/ BACH1 (BRCA1 associated C-terminal helicase) complex, BRCA1/ PALB2 (partner and localizer of BRCA2 / BRCA2 complex), and BRCA1/CtIP complex- BRCA1/RAP80- / Abraxas complex is recruited to DNA DSBs through RAP80, a ubiquitin-binding protein. RAP80 could target this complex to MDC1-rH2AX-dependent K6 and K63-linked ubiquitin polymers at DSBs. BRCA1 /RAP80/ Abraxas complex prevents excessive end resection and potentially deleterious homology-directed DSB repair mechanisms. The helicase catalytic function of BRCA1/BACH1 is not only important for BRCA1-mediated DDR but also necessarily required to maintain DNA damage-induced G2/M checkpoint. BRCA1 is also involved in the repair and restart of stalled and damaged DNA replication forks and in the protection from nucleolytic attack and degradation. BRCA1-mediated fork protection functions independently from its role in the HR-mediated repair of DNA DSBs. Upon replication fork stress, BRCA1 protects nascent DNA strands from degradation by stabilizing RAD51 nucleofilaments that affect the exonuclease activity of MRE11. RAD51 is also required for fork restart once halted forks are repaired in response to short replication blocks. BRCA1 is a component of the SWI/SNF chromatin remodeling complex and controls the transcription through the modulation of chromatin structure. [30] In addition to its role in HR-dependent DNA repair, BRCA1 also regulates the non-homologous end-joining (NHEJ) repair pathway. BRCA1 is involved in both, classical-NHEJ and alternative-NHEJ pathways. BRCA1 interaction with the C-NHEJ factor Ku80 stabilizes the Ku heterodimer at DSB sites that is re-

quired for precise end-joining repair. Evidence suggests that BRCA1 blocks A-NHEJ through phosphorylation of BRCA1 at S988 by checkpoint kinase 2 (Chk2), but the exact mechanism of this regulation is unknown.[37] BRCA1 promotes HR-dependent DNA repair by dephosphorylation of 53BP1 (p53-binding protein 1) that consequently results in the repair pathway switch from NHEJ to HR. Interaction between BRCA1, CtIP, and MRN complex is important for activation of HR by the mechanisms involving CDK (cyclin-dependent kinase)-mediated phosphorylation of CtIP at Ser327. BRCA1 is important for BRCA2 recruitment to the sites of DNA DSBs during HR, and the association between these two proteins is mediated through interaction with PALB2/FANCN (Fanconi anemia, complementation group N) protein. [37]

BRCA2

BRCA2 is located in 13q12.3, it seems to have no enzymatic activity, and it exists predominantly as a homodimer. BRCA2 presents several key domains: the BRC repeats, the DNA-binding domain (DBD), and the C-terminal TR2 domain. BRCA2 acts as a hub and recruits several regulatory proteins including RAD51, PALB2, FANCN, and FANCD2. [29] BRCA2 binds RAD51 via its BRC repeats to promote RPA displacement from ssDNA and RAD51 nucleation to the ssDNA filament. BRCA2 then can interact again with RAD51-ssDNA through its C-terminal TR2 domain to stabilize RAD51 nucleofilaments. CDK phosphorylation of the TR2 domain reduces BRCA2-RAD51 binding and it promotes the disassembly of RAD51 complexes at the beginning of mitosis, to, in a way, turn off HR-mediated DSB repair in mitosis, to maintain genomic stability by avoiding the disruption of chromosome segregation. BRCA2 may also function as a complex with RAD51 paralogs such as XRCC2 and XRCC3 to facilitate an assembly of RAD51 with ssDNA. [37]Phosphorylation of BRCA2 C-terminus by the checkpoint kinases CHK1/CHK2 can be also important for BRCA2 functions in HRR. BRCA2 can bind the ssDNA through the DBD and through the DNA binding it promotes RAD51 loading. The DBD can also interact with deleted in split hand/split foot 1 (DSS1) protein, this interaction is critical for DSB repair and for the BRCA2 ability to limit R-loops (RNA-DNA hybrids). DSS1 is involved in masking a Nuclear Export Signal in BRCA2 and thus controlling both BRCA2 and RAD51 nuclear localization. DSS1 also physically interacts with RPA to promote its unloading and its replacement by RAD51 on ssDNA. BRCA2's BDB binds to poly(ADP-ribose) (PAR). PARylation of BRCA2

mediates a quicker recruitment of BRCA2 to DNA lesions. Besides BRCA2 interactions with RAD51, which involves a big portion of the BRCA2 structure, BRCA2 is involved in additional protein interactions. The N-terminal domain can interact with PALB2/FANCN, which links BRCA1 and BRCA2 in a cell cycle-dependent manner. This interaction is critical for the recruitment of BRCA2 to DSBs and for its role in HRR. BRCA2 can also interact with EMSY protein which is involved in chromatin remodeling in DSBs. BRCA2 interacts also with PDS5B/APRIN through its BRC repeat in a cell cycle-dependent manner, the loss of this interaction is responsible for a significant reduction in HR. BRCA2 seems to play an important role in stalled replication forks processing, where BRCA2 protects the nascent DNA strand from degradation of MRE11 through RAD51 nucleofilament stabilization. [29] BRCA2 is also recruited by 3'-repair exonuclease 2 (TREX-2) complexes for processing of R-loops, the structures formed during transcription and composed of a DNA-RNA hybrid and associated ssDNA. BRCA2 can protect telomere integrity via loading of RAD51 on telomeres during S/G2 phase which is evidenced by the accumulation of telomere dysfunction-induced foci and telomere shortening in Brca2- but not Brca1-deficient mice. [37]

Poly (ADP-Ribose) polymerase

Poly (ADP-ribose) polymerases are a family of proteins that catalyze the transfer of ADP-ribose to target proteins. PARPs play an important role in various cellular processes, including chromatin structure modulation, transcription, replication, recombination, and DNA repair.

The accumulation of DNA lesions significantly increases PARP levels in cells. PARP is involved in base excision repair (BER) in response to ssDNA breaks and is a component of the BER complex, composed of DNA ligase 3, DNA polymerase beta, and the XRCC1 protein (a scaffolding protein for other DNA repair enzymes). PARP-1 senses SSB through its DNA-binding domain and undergoes poly ADP PARylation, activating PARP-1, which binds to XRCC1, which in turn binds DNA ligase-3, DNA polymerase beta, and bifunctional polynucleotide kinase 30 phosphatase (PNKP) to form the SSB repair complex, which ultimately repairs the damaged DNA. [97]

The PARP enzyme tightly binds ssDNA strand breaks, and following auto-poly ADP-ribosylation, it is released, allowing the repair enzyme to access the damaged DNA. Both PARP1 and PARP2 interact with common partners in SSB repair and BER pathways, but PARP2 also has unique partners such as the telomeric protein TRF-2. PARP1 plays a role in nucleotide

excision repair (NER), as NER processes are reduced following PARP1 inhibition. Both BER and NER are major pathways that allow for the repair of DNA damage that can be caused by certain alkylating agents and chemotherapeutic drugs. [64]

2.6.2 PARP Inhibition in Chemotherapy and PARPis

PARP inhibition PARP inhibition results in genomic instability and accumulation of damaged cells with an arrested cell cycle. This demonstrates that ADP ribosylation is necessary for cells to progress through the G2-M phases of the cell cycle following DNA damage. Inhibition of PARP activity results in increased apoptosis partially due to reduced DNA repair capacity. It has been suggested that PARP is a fundamental component of the G2 cell cycle checkpoint, preventing entry into cell division with DNA strand breaks. Expression of a dominant negative for PARP's DNA binding domain sensitizes cells to SSBs caused by alkylating agents and resulting DNA damage leads to rapid apoptosis, underscoring the importance of PARP in post-DNA-damage repair. PARP -/- is not embryonically lethal but is essential for survival in the face of DNA damage.

There is evidence of upregulation of PARP activity in some cancers; for example, high expression of PARP1, but not PARP2, is observed in some triple-negative breast cancer (TNBC) tumors.

Deficiencies in the homologous recombination system due to the loss of function of genes such as BRCA1, BRCA2, RAD51, DSS1, RPA1, and CHK1 make cells highly dependent on PARP activity and therefore sensitive to its inhibition. Cells deficient in BRCA1 or BRCA2 are respectively 57 times and 133 times more sensitive to PARP inhibitors than normal cells.

Loss of 53BP1, a DNA damage response factor, in BRCA1 -/- tumors alleviates their recombination defect and reverses their hypersensitivity to DNA damage. Further loss of 53BP1 appears to be common in both TNBC and tumors with BRCA1/2 mutations, this could be an important biomarker for determining sensitivity to PARPi and/or DNA damaging agents. [41]

PARPis PARP inhibitors are mainly composed of NAD+ analogs that compete with NAD+ to bind the active site of PARP, causing inhibition of PARP activity, which in turn affects the formation of PARP1-ADP ribose branched chains and prevents them from recruiting DNA damage-associated repair proteins, ultimately resulting in failure of DNA damage repair. [97] PARPis have a different degree of trapping (talazoparib > niraparib >= olaparib =

rucaparib> veliparib) with consequently proportional cellular cytotoxicity. Three types of PARPis exist based on their allosteric impact on the PARP-1-DNA complex: type I, allosteric proretention on DNA, which induces Helical subdomain conformational changes that reinforce contacts with DNA break resulting in a slow release. Type II has mild o no allosteric effects. Type III results in allosteric prorelease from DNA, which induce helical subdomain conformational changes opposite to type I inhibitors. [18] The killing mechanism induced by PARPis in HRD/BRCA mutated cells is called synthetic lethality, where the mutation in HRR genes, which gives the HRD phenotype, and the inhibition of PARP leads to cell death. In HRD cells, ssDNA breaks are repaired through PARP activity, its inhibition leads to an accumulation of stalled PARPs in ssDNA breaks, these unrepaired ssDNA breaks can encounter replication forks and tend to collapse them, turning ssDNA breaks into DSBs. [48] The collapse of replication forks and the formation of many DSBs has a catastrophic effect on the cell leading it to apoptosis. [23] PARPis are approved in ovarian cancer for the treatment of recurrent disease and for maintenance if the cancer is responsive to platin agents. [68] In the randomized, placebo-controlled, double-blind phase III SOLO2 trial, patients with relapsed epithelial ovarian, fallopian tube, or primary peritoneal cancer carrying a BRCA1/2 mutation demonstrated a significantly longer median progression-free survival (PFS) under olaparib maintenance treatment than those receiving placebo. The antitumor activity of olaparib was highlighted in phase III SOLO3 (NCT02282020) and OlympiAD trials, in germline BRCA-mutated ovarian cancer and HER breast cancer, respectively. Similarly, the ABRAZO study, and the latest EMBRACA trial, where patients underwent talazoparib monotherapy, showed a significant PFS advantage and higher objective response rate over standard chemotherapy with greater HRQoL in favor of talazoparib. Several trials including POLO and PROfound also demonstrated the benefits of PARPi (olaparib or rucaparib) over placebo or androgen receptor-directed therapy, respectively, in patients with metastatic pancreatic ductal adenocarcinoma harboring germline BRCA mutation and in patients with castration-resistant prostate cancer with confirmed HRD phenotype. [18]

2.7 Homologous Recombination Deficiency

2.7.1 Overview of Homologous Recombination Deficiency

Homologous Recombination Deficiency is a cellular condition caused by the loss of function of one or more genes belonging to the Homologous Recombination Repair pathway, in particular: BRCA1, BRCA2, ATR, ATM, BARD1, BRIP1, H2AX, MRE11, PALB2, RAD51, RAD51C/D, RPA e Fanconi Anemia Complementation Group genes. [58]

Inactivating mutations on BRCA1 are located on genomic regions corresponding to the BRCT and RING domains together with exons 11-13 encoding for the Nuclear Localization Signal essential for BRCA1 functions and binding sites for various interacting proteins with BRCA1 such as c-MYC, RAD50, PRB, RAD51, BRCA2, and PALB2. Most mutations in BRCA1 are frameshift insertions/deletions, nonsynonymous truncations, and splice site disruptions leading to missense mutations or expression of non-functional proteins. Another common mechanism found in cancers for inactivating BRCA1 functionality is through complete promoter methylation, inducing epigenetic silencing of BRCA1 expression; the promoter methylation level correlates with the amount of BRCA1 mRNA expression, and a partial suppression allowing residual expression is attributed to a non-response to cisplatin. [15]

Mutations in BRCA2 in cancers are usually insertions/deletions resulting in frameshifts, missense, and nonsense mutations, with exon 11 being the most common mutation site, which is where the BRC domain is located, thus hindering the interaction with RAD51. BRCA2 mutations predispose to ovarian, prostate, breast, and other types of cancer. 70-80% of observed mutations in BRCA2 result in a dysfunctional protein or absence of protein product.[45]

Mutations in other HRR genes are partly correlated with the HRD phenotype, and the single gene contribution to the phenotype is not yet fully understood; somatic mutations in non-BRCA HRR genes have been shown to offer a Progression-free survival (PFS) and survival advantage similar to BRCA mutations in patients undergoing platinum treatment.[58] The mutational status of the HRR genes is the cause of the appearance of the HRD phenotype and can manifest as genomic scars (the consequences) due to repair events of DSBs in the genome with error-prone repair systems (NHEJ, MMEJ) leading to insertions, deletions, inversions, and translocations of

genomic sections. Testing for the consequences of a dysfunctional HRR pathway is performed by probing the genome to detect genomic abnormalities. Several studies on ovarian and breast cancer have identified genomic patterns or signatures of genetic instability associated with the HRD phenotype. These instability signatures may include genomic patterns of loss of heterozygosity (LOH), which are intermediate-sized regions (>15Mbp and < the entire chromosome), the number of telomeric allelic imbalances (TAI), which are the number of regions with allelic imbalances extending to the subtelomere but not crossing the centrosome, and large-scale transitions (LST), which are chromosome breaks (translocations, inversions, or deletions). These approaches assess the presence of genomic signatures correlated with HRD (called scars), thought to be the consequence of error-prone DNA repair systems (such as Non-Homologous End Joining, NHEJ) [87]. Definitions:

- Loss of Heterozygosity (LOH): It's the loss of one of the two alleles of a gene. Loss of the second allele can lead to tumor progression.
- Telomeric Allelic Imbalance (TAI): The proportion of alleles at the end of the chromosome (in the telomeres) in a pair of chromosomes does not match, indicating that one of the chromosomes has lost alleles and therefore one chromosome has more alleles than the other.
- Large-Scale Transitions (LST): Chromosome breaks generating fragments of sizes equal to or greater than 10 Mbp causing discrepancies in the pair of chromosomes, resulting from translocations, deletions, and inversions. [58]

Genomic instability in HRD tumors causes a range of genetic abnormalities of various sizes that are detectable through sequencing and single nucleotide polymorphism analysis. Large structural variations of 0.1 - 10 Mbp in size and interchromosomal rearrangements occur at the chromosomal scale. At the gene scale, deletions and tandem duplications of less than 100 kbp with flanking microhomologies are identifiable. Events at both scales contribute to a high rate of somatic copy number alterations (SCNAs) in HRD tumors. At the nucleotide scale, single-base substitutions and indels contribute to mutational signature characteristics. [25] Somatic Copy Number Alterations (SCNA) have been targeted for genomic scar assays, and measurement has often been done by quantifying loss of heterozygosity (LOH) on high-density SNP arrays or by analyzing a large panel of genes to calculate the %LOH. LOH, TAI, and LST can be combined or used individually to provide a measurement of genomic instability reflecting the extent of HRD in tumors. Various endogenous and exogenous processes damage

and repair the cell genome during its existence. Some of these processes can result in characteristic patterns of alterations, which can be classified according to the combination and frequency of recurring nucleotide triplets identified within the tumor genome. As of now, there are 49 observed mutational signatures in cancers, many of which have been attributed to specific mutational processes. For HRD, signature 3 is associated with the loss of BRCA1 or BRCA2. Mutational signatures are usually measured using Whole Genome Sequencing (WGS) or Whole Exome Sequencing (WES) [25]. Mutational signatures are physiological imprints of DNA damage and the repair process that occurred during tumorigenesis. The BRCA1 or BRCA2-null phenotype leads to the formation of 6 genomic signatures that include two single-base substitutions (SBS3 and SBS8), 630 indels (ID6, a microhomology-mediated deletion), and two rearrangement signatures (RS3 duplications and RS3 tandem duplications). These multiple signatures are a direct consequence of HRD, and when combined, they provide excellent sensitivity and specificity in a composite assay [44]. Copy Number Variations (CNVs or CNA) are one of the major forms of genetic alterations in cancer. They can influence gene expression levels through dosage effects. Since CNVs are much more stable than gene expression, they can be a more robust and stable biomarker compared to gene expression signatures, which can be easily altered. Several studies have shown that CNVs can be a good biomarker for cancer diagnosis and subtyping [40]. Copy Number Variation is a generic term used to describe a molecular phenomenon in which genome sequences are repeated and the number of repetitions varies among individuals of the same species. CNVs can substantially contribute to both rare and common genetic disorders. CNVs are a subtype of structural genomic variants and range in size from 50bp to several Mb.

Cancer sensitivity to cisplatin salts and PARPi can be correlated with both the causes of HRD (the non-functionality of HRR genes) and the consequences (the presence of genomic scars). Instances where cancer is resistant to PARPi despite demonstrating the causes and/or consequences essentially derive from three causes:

- Selective pressure leading to reversion of inactivating mutations of HRR genes and/or demethylation of the BRCA1 promoter [25]
- Gene mutations may involve genes not directly related to HRR but that can provide drug resistance, such as increased drug efflux [34].
- The presence of consequences but not causes: genomic scars can be events that occurred during cancer progression due to genetic insta-

bility; subsequently, cancer lost genetic instability but maintained the genomic scars, the effects of such instability.

2.7.2 PARP inhibitor resistance

DSBs are repaired through the unstable NHEJ repair pathway, especially when HRR repair is defective, and the two repair pathways counteract each other. Therefore, any factor that promotes the restoration of HRR repair function or inhibits the NHEJ repair pathway can cause resistance to PARP inhibitors. Additionally, the number and functional site of PARP inhibitors also influences drug action sensitivity to some extent. [96]

The HR function recovery Deletion of the methylation of the BRCA1 gene promoter is sufficient to restore HRR and cause resistance to PARPis. The transcription factor FOXM1 can cause overexpression of genes associated with the HRR repair pathway in tumor cells, related to resistance to olaparib. When patients take olaparib, the FOXM1 pathway can be activated thus leading to the expression of BRCA1 and RAD51, acquiring partial resistance. Thiobacillomycin can reduce the expression of FOXM1 and increase the expression of some apoptosis-related genes. It also helps PARP inhibitors trap PARP1. USP15 promotes the maintenance of BARD1/BRCA1, which prevents terminal damage from resection. USP15 overexpression causes resistance to PARP inhibitors. The molecular chaperone protein HSP90 functions to resist misfolding of proteins due to BRCA mutations. So, it forms unstable structures and causes protein degradation. HSP90 stabilizes the mBRCA protein and helps load RAD51 onto replication forks to promote DNA damage repair. [96]

Inhibition of NHEJ pathway The NHEJ repair pathway is more unstable and sometimes produces more errors in repair, whereas the HR repair pathway is more reliable. NHEJ leads to the accumulation of damaged DNA and ultimately causes apoptosis. The functions of the NHEJ repair pathway and the HR pathway are in competition. Therefore, when the NHEJ repair function is inhibited, through 53BP1 deletion for example [53], some DNA damage may only pass through HR repair, which also leads to resistance to PARP inhibitors. [96]

CCNE1 copy number increase Cyclin E1 (CCNE1) is a gene correlated with the Homologous Recombination Proficiency (HRP) phenotype in tumors and insensitivity to treatment with platinum salts and PARPi if this gene is present in the genome in multiple copies or with an upregulated expression. The amplification/upregulation of CCNE1 is associated with the activation of HR DNA damage repair proteins and DNA damage checkpoint proteins such as Rad51, RAD51C, RAD54L, BRCA1, and BRCA2, ATR signaling, and cell cycle checkpoint pathways. Cells with amplified CCNE1 demonstrate consistently high expression of RAD51, ATR, CHK2, and the activated forms of ATR (pATR) and CHK2 (pCHK2).

It was observed that CCNE1 expression correlated with PI3K/AKT, DNA damage proteins, and checkpoint pathways, and mTOR signaling was significantly co-expressed with CCNE1 in ovarian cancer samples. The mTOR pathway regulates protein synthesis and is therefore a candidate for regulating the upregulated expression of checkpoint and HR proteins.

The hyperactivation of HR could be the mechanism for resistance to PARPi-based chemotherapy in tumors with amplified CCNE1 and HRP tumors. Studies have suggested that mTOR could be a therapeutic target to overcome primary resistance and potentially increase the response to PARPi. The expression of the mTOR pathway correlates with the expression of CCNE1 and is critical for the expression of RAD51, ATR, and CHK2. As expected, mTOR inhibitors (mTORi) downregulate these proteins in HRP/PARPi-resistant tumors and provide an increased in vivo response to PARPi. Inhibitors such as mTORi and ATR inhibitors can significantly impact the growth of tumors with amplified CCNE1 and synergize with PARPi. [9]

Changes in the mode of drug action

Change of actional target PARP1 is an important member of the PARP family and is involved in repairing DNA damage sites. After PARylation of the PAR chain, PARP1 can recruit some DNA damage repair factors to help realize its function. PARylation of PARG counters and prevents HR from occurring. PARP family members primarily work by binding to PARP1. Therefore, any factor that affects PARP1 function will result in the failure or resistance of PARP inhibitors. [96]

PARP1 decreases Reducing the number of PARP leads to a lack of PARP inhibitor targets, leading to resistance. Recent studies have observed primary

resistance to PARP inhibitors in cells with low PARP1 expression. Gogola et al. observed resistance to PARP inhibitors in tumor cells through the introduction of two shRNA-mediated losses of PARG, which is more common in tumors with BRCA2 mutations. Therefore, the endogenous activity of poly(ADP-ribose) glycohydrolase (PARG) influences the action of PARP inhibitors. [35] When PARPi does not completely block PARP accumulation, loss of PARG activity causes downstream PARP1 proteins to continue to perform DNA damage repair functions, a possible cause of resistance.

PARP1 domain mutation In addition to changes in the number of PARPs, any factor that affects the ability of PARP inhibitors to bind to PARP may be related to resistance. Mutations in the zinc finger (ZnF) DNA-binding domain of PARP1 lead to abnormal trapping of PARP inhibitors, affecting its function and leading to drug resistance. [96]

2.7.3 How to Identify HRD

Current clinical methods for detecting HRD are limited to assessing genomic disruptions within tumors due to mutations in the HRR pathway or detecting genomic scars that reflect genomic instability. However, there are HRR proficient/HRD negative and BRCA1/2 wild-type patients who respond to PARPi.

HRD causes

BRCA1/2 mutations: BRCA1 and BRCA2 mutations lead to homologous recombination deficiency (HRD) by disrupting key HR DNA repair pathway processes. These mutations prevent the proper repair of DNA double-strand breaks through HRR, resulting in increased genomic instability caused by NHEJ repair and the cancer sensibility to PARPis. BRCA1 and BRCA2 can be mutated in the germinal line or just in the somatic cells of the cancer. PARPis are recommended by all medical guidelines after a positive analysis of deleterious mutations of BRCA1 and BRCA2. [92].

Non-BRCA HR pathway mutations: In addition to BRCA1/2, germline or somatic homozygous mutations in genes encoding proteins involved in the HRR pathway such as RAD51B/C/D, BRIP1, PALB2, NBN, ATM, CHK1, CDK12, and Fanconi Anemia genes, and others, are thought to confer HRD or a "BRCAness" phenotype given their cooperative role in HRR. Up to 30%

of ovarian cancers have mutations in the HRR pathway. Preclinical data have suggested that deficiency of RAD51C/D and mutations in genes such as ATM and CHK1/2 may confer synthetic lethality when treated with DNA repair-targeting drugs. The presence of mutations in ATM, ATR, FANCA, FANCD2, FANCM, or PALB2 was not associated with high LOH scores or platinum sensitivity. Only homozygous deletions in CHK1 and PTEN led to high LOH scores associated with HRD. Study19 and ARIEL2 trials have described that mutations or methylation of RAD51C were associated with long-term response to PARPi therapy. Similar findings were reported by Study19 where patients with mutations in HRR-related genes such as CDK12, RAD51B, and BRIP1 had benefits similar to those with mutations in BRCA1/2. It appears that individual mutations in HRR genes have distinct platinum and PARPi therapy sensitivities, but further confirmatory data is needed. [92].

Epigenetic modifications: Epigenetic silencing of BRCA1 and other HRR genes like RAD51C are part of an additional 11-15% of HRD-positive HGSOC. Gene silencing occurs through aberrant methylation of cytosine in CpG regions at promoter regions and leads to reduced gene expression. Confirmatory studies using immunohistochemistry validated that epigenetic silencing of BRCA1 led to a lack of BRCA1 protein expression. Both BRCA1-methylated HSOC and RAD51-methylated HGSOC have high HRD scores. Epigenetic modifications to BRCA1 have also been associated with BRCA-deficient genomic signatures and have been observed to have similar effects on HRR as BRCA1/2 mutations. Such epigenetic modifications are not analyzed by current NGS sequencing methods. Additionally, the clinical implications of such epigenetic modifications in HRR-related genes appear to be variable. Studies are presenting inconclusive data regarding the predictive power of HRR gene methylation. Some studies have drawn attention to the zygosity of BRCA1 promoter methylation, which is a critical factor in determining its relationship with PARPi response. In HGSOC patient-derived xenograft models, it was noted that demethylation of a single BRCA1 allele was capable of restoring HRR proficiency and reducing PARPi sensitivity. Exposure to chemotherapy has also been shown to drive demethylation of methylated BRCA1 copies, which can occur more readily than reversion mutations in non-functional BRCA1/2. [92]

2.7.4 Identifying HRD Genotype

The HRD phenotype causes a pattern of mutations, deletions, and insertions (mutational signatures), as well as Copy Number Variations (CNVs) and structural rearrangements (genomic scars). The most significant genomic alterations are called genomic scars and currently form the basis of clinical assays for HRD identification, which can only be performed on tumor tissue. These genomic scars include Loss of Heterozygosity (LOH), Telomeric Allelic Imbalance (TAI), and Large Scale Transitions (LST). [94] Genomic alterations associated with HRD must be distinguished from other genomic alterations found in cancer genomes. Therefore, the measurement of these three markers in the context of HRD tumors has been defined using Single Nucleotide Polymorphism arrays in respective cohorts. It has been demonstrated that the number of subchromosomal segments with LOH greater than 15 Mb but smaller than an entire chromosome is associated with the functional inactivation of BRCA1, BRCA2, or RAD51C. Telomeric allelic imbalances extend from the breakpoint to the subtelomeric region of a chromosome without including the centromere. High levels of these aberrations have been detected in tumors with a deficiency in BRCA1 and BRCA2 and in tumors sensitive to platinum-based chemotherapy. LOH, TAI, and LST are independently associated with HRD, but the combination of all three scores allows for robust prediction. A composite HRD score has been developed in three clinical cohorts of TNBC using the unweighted sum of the three individual scores. Furthermore, a threshold for HRD positivity has been selected based on the probability of a positive response to platinum-based chemotherapy. Commercially available tests often combine the mutational status of BRCA with a composite HRD score or just the evaluation of LOH. Therefore, to detect HRD, an estimate given by the HRD score can be used. Although alterations in genes involved in HR are assessed by standard mutation methods or expression analysis, the HRD score can be computed by combining measurements of large genomic defects including LOH, TAI, and LST. To detect individual or concurrent DNA repair defects, a wide range of technologies are currently available.[94]

Single Nucleotide Polymorphism (SNP) Arrays SNP arrays are one of the primary assays capable of measuring chromosomal abnormalities, such as CNVs and genomic scars (LOH, TAI, and LST). The major drawback is the lack of reliable determination of the mutational status of BRCA1 and BRCA2. Chromosomal microarray analysis includes an SNP-based microarray where

probes for SNPs are immobilized on a special matrix which is then followed by hybridization. Differences in fluorescence signal can be read by an array reader. These genome-wide polymorphism assays allow for the simultaneous analysis of up to 850,000 SNPs. Two commonly used SNP assays include OncoScan Dx (Affymetrix) and Infinium CytoSNP-850k BeadChip (Illumina) which can be applied to determine LOH, LST, and TAI after bioinformatic analysis using respectively 80 ng or 250 ng of FFPE DNA.[94]

Whole Genome Sequencing A comprehensive testing of HRD including both detection of HRR gene alterations and an HRD score can be conducted using parallel sequencing tools. An option that has already shown a good correlation between SNP array-based scores and parallel sequencing-based scores is unbiased whole genome sequencing using from 100 ng to 500 ng of tumor and normal DNA. WGS facilitates the detection of somatic mutations, rearrangements, and CNVs. Apart from identifying pathogenic alterations of BRCA1 and BRCA2, this testing approach allows for the detection of LOH, TAI, and LST. In combination with a suitable bioinformatics approach based on evaluation algorithms, such as HRDetect and scarHRD, scores including all three parameters can be estimated. With the Classifier of Homologous Recombination Deficiency (CHORD) algorithm, at least the LOH status can be determined for potential HRD detection. Although parallel sequencing is a commonly used tool in routine diagnostics, WGS analysis used in this way is cost-effective when using sequencing platforms such as Illumina HiSeq or NovaSeq. Since the number of laboratories with such expensive equipment is limited, a low-cost alternative uses low-coverage WGS. This low-pass/shallow WGS is defined by reducing the read depth in the range of 0.1X-3X, allowing for lower sequencing capacity. Using the shallowHRD algorithm, LOH, TAI, and LST can still be detected even though reliable detection of BRCA1/2 mutations at a low coverage level is no longer possible. Despite downsampling, there is a good correlation between HRD scores from SNP arrays, WGS, and sWGS. [94]

Targeted Panel Sequencing Most of the HRR genes are integrated into a comprehensive sequencing panel and targeted sequencing panels range from 13 to 500 genes. To detect large deletions and insertions in exons and intronic boundaries, technologies based on hybrid capture-based parallel sequencing are preferably used over those based on amplicons for mutation detection. Illumina's TruSight Tumor 170 or TrueSight Oncology 500,

as well as various Oncomine panels from Thermo Fisher Scientific, provide the opportunity to use extensive panels on HRR genes based on different technologies among laboratories, facilitating rapid integration into the laboratory. In case an in-house pipeline is not available, all mentioned panels also offer a bioinformatics solution on their website. Comprehensive cancer panels are not common as there are reimbursement difficulties in various nations for genetic analysis without diagnostic markers; some manufacturers also offer only BRCA1 and BRCA2 mutation analysis or in combination with LOH status and/or combined HRD score.[94]

2.7.5 Functional HRD Assays

Functional Analysis of RAD51 Foci To directly determine HRR ability, functional assays have been developed that, although not in clinical use, allow estimation of nuclear RAD51 quantity. RAD51 is a DNA recombinase involved in the invasion of the template filament. However, the RAD51 assay has several limitations:

- Requires immunofluorescence.
- Is labor-intensive: requires quantification of RAD51 foci in 40 cells by a pathologist.
- Defects in downstream pathways to RAD51 are not detected.
- Radiation is used to induce DNA damage and obtain the RAD51 signal for the assay.

These limitations make this assay impractical in the clinical setting. However, refinement of the assay using FFPE samples has been achieved, making it a useful tool in laboratories for a future functional homologous recombination capacity assay, with a simpler workflow and 90% sensitivity in BRCA-deficient tumors [25]. Recently, it has been shown that analysis of basal levels of RAD51 foci is possible in clinical samples and appears to correlate highly with the response to PARPi [87].

Platinum Sensitivity Status Platinum salt sensitivity has been shown to be a surrogate marker of HR proficiency and a predictive marker for PARPi response. Platinum sensitivity status was found to be a superior biomarker for predicting the benefits of PARPi in the NOVA, ARIEL, and Study19 trials compared to myChoice CDx or %LOH. [92]

DNA Fiber Assay DNA Fiber Assay evaluates the dynamics of the replication forks by incorporating DNA labeled with two thymidine analogs, iododeoxyuridine, and chlorodeoxyuriridine, which can be visualized by an immunofluorescence-based approach. The degradation of the stalled forks, caused by BRCA1/2 or RAD51 lof mutations, leads to the shortening of the thymidine-labeled tract. While DNA fiber assay can predict PARPi sensitivity, it is better suited to detect platinum sensitivity. [19]

2.7.6 Somatic and Germline Testing

A portion of patients with germline BRCA1/2 mutations may have a negative BRCA1/2 status in the tumor, and therefore, exclusively performing BRCA1/2 testing in the tumor could exclude patients who could benefit from preventive maintenance treatment with PARPi. Ideally, patients should be tested for BRCA1/2 mutations and HRD testing in the tumor, as well as germline BRCA testing. From a therapeutic standpoint, if only one test could be performed, tumor BRCA/HRD testing would be the most practical to identify the greatest number of patients for PARPi treatment. Germline testing has significant implications for family members who could benefit from BRCA1/2 testing, prophylactic interventions, and advanced cancer screening. Early knowledge of BRCA1/2 mutations and HRD status is crucial for selecting an appropriate management plan for patients with advanced ovarian cancer. [92].

2.7.7 HRD score calculation methods

HRD can be identified through the detection of mutations that induce a loss of function in genes involved in HRR, particularly in BRCA1 and BRCA2. To do this, it is necessary to perform a targeted panel sequencing of the genes involved and analyze the variants using information on the pathogenicity of the variant under examination. Genome status can be analyzed to observe the HRD genotype through various techniques: whole genome sequencing (WGS), whole exome sequencing (WES), sequencing or an array of a panel of Single Nucleotide Polymorphisms (SNPs), sequencing of a gene panel to derive %LOH, and Shallow Whole Genome Sequencing (sWGS). All these techniques calculate an HRD score (also called Genome Instability Score (GIS)) or a %Loss of Heterozygosity associated with the degree of observed genomic alterations. At a certain HRD score/%LOH threshold, obtained through statistics of the determined data, the HRD and HRP phenotypes are

assigned. [92]

The methods developed for HRD detection can be mainly classified into four approaches. [50] The most popular approach is based on an HRD index related to genomic instability, which includes LOH, TAI, and LST. To calculate these HRD indexes, accurate quantification of the allelic frequencies of high-frequency SNP sites is necessary, and usually, such assays are based on probe hybridization to capture tens of thousands of SNPs across the human genome, which is experimentally complicated and commercially expensive. The second approach is based on the mutational signatures characteristic of HRD. Methods like signature3 and sigMA use this approach, which can accurately identify HRD patients. However, such analysis requires a wide range of somatic mutations, whole exome sequencing, or a large sequencing panel on hundreds of genes related to tumors with high sequencing depth and thus shares the same problem as the first approach. The third approach aggregates different signatures associated with HRD to predict HRD status. For example, HRDetect uses a combination of the HRD index, the proportion of deletions with microhomology, rearrangement signatures RS5 and RS3, and substitution signatures 3 and 8. CHORD uses a combination of single-base substitutions, structural duplications, and deletions of flanking microhomologies. Since these methods require multidimensional genomic information, only high-depth WGS is suitable but expensive. [92]

The fourth approach calculates the HRD score based on CNVs, of the computational algorithms that calculate an HRD score, shallowHRD is the first computational algorithm based on genome-wide CNVs. It brings several advantages over previous methods. First, genome-wide CNV is estimated with a resolution in millions of bases, so it is possible to use low-pass WGS (also known a shallow WGS, sWGS) input, where the sequencing and library preparation costs are moderate, while WGS operation is simpler than probe-based methods. In some situations, tumor resection is not possible, especially in severely ill patients who are potentially receiving PARPi treatment. Unlike existing methods, sWGS requires only a small amount of input DNA, so shallowHRD is suitable for patients with samples from core-needle biopsy or even circulating tumor cells can be used. shallowHRD also incorporates Large Genomic Alterations, defined as intra-chromosome arm CNA breaks to its HRD score equation, as well as CCNE1 amplification. [26]

An advantage of CNV-based methods is the robustness of CNV calling. Unlike other methods based on germline variants, the CNV pattern may not be influenced by population characteristics or mutational patterns of

different tumor types, making shallowHRD suitable for a pan-cancer test. It should be noted that the shallowHRD pipeline was developed for sWGS, but it can also be applied to data generated from WES, genome-wide SNP-panel sequencing, or SNP array. Therefore, this method can be integrated into other existing HRD detection methods and improve their performance.

2.7.8 Shallow Whole Genome Sequencing

Shallow Whole Genome Sequencing (sWGS) is a whole-genome sequencing technique that uses a coverage range of 0.3x-1x. It can be used to determine the genomic HRD status by detecting LOH, TAI, and LST and calculating a genomic instability score with appropriate bioinformatics tools. sWGS was compared against Myriad's myChoice HRD for the prediction of HRD in Triple Negative Breast Cancer. [15] It was observed that My-Choice-like HRD scores (CGH scores) were highly correlated with shallow HRD scores ($r = 0.93$, $p < 0.0001$, Pearson correlation analysis) with 95% concordance in HRD prediction. In the set of 44 Patient-Derived Xenografts, the sensitivity and specificity in predicting cisplatin response were similar (76% and 61% for MyChoice-like-HRD and 81% and 65% for ShallowHRD).

The strong correlation, high concordance in HRD prediction, and similar predictive performance between shallowHRD in sWGS and Myriad MyChoice GIS score calculation suggest that the two methods are fundamentally measuring similar aspects of genomic instability and HRD, despite differences in methodology and sequencing depth.

2.8 FDA and EMA-approved HRD companion diagnostic tests

HRD tests offer interesting economic prospects, for this reason, pharmaceutical companies specialized in the diagnostic sector such as Myriad, Foundation Medicine, and AB ANALITICA have invested in developing a CE-IVD certified HRD kit. Myriad participated in three phase III studies on Ovarian Cancer: PAOLA, PRIMA, VELIA, NOVA, SOLO1, and SOLO2. [74] [36] [63] The successful completion of these studies allowed the FDA-approval and CE-IVD certification in 2020 and it's recommended by ASCO and NCCN guidelines for HGSOC patients of MyChoice CDx. MyChoice CDx [65] is the companion diagnostic for olaparib, in case of deleterious or suspected deleterious BRCA1 and BRCA2 mutations and/or a positive

Genomic Instability Score (GIS). MyChoice test analyzes DNA from Ovarian Cancer tissue in FFPE form through NGS and SNP arrays. BRCA1 and BRCA2 are sequenced at high depth and their sequence is analyzed through a knowledgebase of known BRCA1 and BRCA2 mutations. The SNP array uses 27.000 Single Nucleotide Polymorphisms in the whole genome to asses the LOH, TAI, and LST status of the cancer tissue, which are used to calculate the GIS, patients above a threshold are considered HRD positive. In 2022, Myriad released MyChoice CDx Plus, an upgraded version of MyChoice CDx, it has been approved by the FDA and the CE, and it analyze through NGS the mutational status of HRR-related genes in addition to BRCA1 and BRCA2, such as ATM, BARD1, BRIP1, CDK12, CHEK1, FANCL, PALB2, PPP2R2A, RAD51B, RAD51C, RAD51D, AND RAD54L. FoundationOne CDx [61] test for HRD detection and BRCA1 and BRCA2 status has been validated in phase III trials ATHENA-MONO and, ARIEL3. This test is FDA-approved and CE-IVD certified, it's the companion diagnostic for olaparib for BRCA1 and BRCA2 alterations. Also, rucaparib is recommended for ovarian cancers bearing tumor BRCA 1 and BRCA2 positive mutational status and/or a high Loss of Heterozygosity. This test analyzes 324 clinically relevant genes (BRCA1 and BRCA2 included) through NGS, and from their sequencing results, an informatic pipeline computes the %LOH, if it's above a pre-determined threshold the ovarian cancer is considered HRD positive. Besides BRCA1, BRCA2, and HRD status this test also determines TMB and MSI and it's the companion diagnostic for many other cancer-related drugs based on molecular biomarkers. MyChoice and FoundationOne CDx are tests executed only at Myriad or Foundation Medicine labs respectively, the clinicians must deliver the FFPE tumor tissue to their laboratories where it will be analyzed. AmoyDx HRD Focus is a CE-IVD-certified diagnostic kit for HRD that doesn't require sending the FFPE tumor tissue to the central laboratory because the kit includes everything necessary for HRD assessment. The kit targets BRCA1 and BRCA2 whole coding regions and intron/exon boundaries, and about 24.000 genome-wide SNPs to calculate the Genomic Scar Score. AmoyDx HRD Focus Panel CE-IVD certification has been conceded through comparative studies against the already certified CE-IVD test Myriad MyChoice, AmoyDx showed high positive concordance with MyChoice (87.8%) and 100% negative concordance. [31] [7]

2.9 Cell Free-DNA

2.9.1 Overview of Cell Free-DNA

The cell-free DNA (cfDNA) is released by cells into the circulatory system. cfDNA can be found in plasma and various bodily fluids [98]. The majority of cfDNA in plasma derives from the hematopoietic system of healthy individuals. Under certain physiological and pathological conditions such as pregnancy, organ transplants, and cancer, affected/correlated tissues may release additional DNA into the circulation. Therefore, detecting cfDNA in peripheral blood could identify abnormalities non-invasively. In recent years, several technologies have been developed to analyze cfDNA with various applications, such as cancer monitoring.

The analysis of cfDNA offers several advantages in the diagnosis and management of cancer. cfDNA can provide a comprehensive picture of the tumor's genomic landscape, allowing for the detection of various genetic alterations that drive cancer development and progression. This includes point mutations, insertions, deletions, copy number variations, and chromosomal rearrangements. The identification of these genetic alterations is essential for selecting appropriate targeted therapies. [75]

Moreover, cfDNA analysis can offer insights into tumor heterogeneity, which refers to the presence of different genetic subpopulations within a single tumor. Tumor heterogeneity analysis is fundamental in cancer treatment, as different subpopulations may respond differently to therapy and contribute to treatment resistance. By analyzing cfDNA from different tumor sites or at different time points during the course of the disease, it's possible to monitor changes in tumor heterogeneity and adapt treatment strategies accordingly. [75]

In addition to providing diagnostic information, cfDNA analysis can also be used for monitoring treatment response and detecting minimal residual disease. Changes in the abundance or composition of cfDNA during or after treatment can indicate whether the therapy is effective or if residual tumor cells are present. This real-time monitoring enables clinicians to make timely adjustments to treatment plans, potentially improving patient outcomes. [13]

Furthermore, cfDNA analysis can guide the selection of targeted therapies based on the presence of specific genetic alterations in the tumor. [28] PARP inhibitors, for example, have shown efficacy in treating ovarian

tumors with homologous recombination deficiency (HRD), a genomic instability phenotype characterized by defects in DNA repair pathways. By identifying HRD status through cfDNA analysis, patients who are likely to benefit from PARPi therapy can be identified, sparing others from unnecessary treatment and potential side effects.

Overall, sequencing and analyzing cfDNA offer a non-invasive and comprehensive approach to cancer diagnosis, prognosis, and treatment selection. As technology advances and our understanding of cancer biology improves, cfDNA analysis is likely to play an increasingly important role in personalized cancer care, facilitating more precise and effective treatments for the individual characteristics of each patient's tumor.

Typically, cfDNA appears as double-stranded fragments of approximately 150-200 base pairs in length, corresponding to the nucleosome's unit size, or multiples of the nucleosome unit size (up to 500 - 700bp).[54] Circulating tumor DNA (ctDNA), the fraction of DNA released by tumor cells into the circulation, tends to be shorter by about 20 bases. ctDNA has a half-life ranging from 2.5 to 16 hours.

According to quantitative studies, it has been found that the concentration of cfDNA in healthy subjects ranges from 0 to 100 ng/ml of blood with an average of 30 ng/ml, while the concentration of cfDNA in cancer patients varies from 0 to 1,000 ng/ml, with an average of 180 ng/ml. The size and stage of tumors are reported to be correlated with the level of ctDNA in the blood. There are, on average, 100 to 1,000 copies of ctDNA per 5 ml of blood in patients with stage IV or advanced tumors, and only 10 copies of ctDNA in those with early-stage tumors. [98]

Patients with cancer usually have high levels of cfDNA in their serum and plasma as a result of the necrosis and apoptosis of cancer cells, as these cells divide more rapidly than normal cells and release cfDNA in higher proportions. In recent years, both cfDNA and ctDNA have attracted a lot of attention as new blood biomarkers because the quantification and kinetic analysis of cfDNA and the molecular profiling of ctDNA have suggested their predictive and prognostic value. [98] Several liquid biopsy tests, designed for the identification of specific cancer mutations, have been recommended as companion diagnostic tests (CDx) by the European Medicines Agency (EMA) and the United States Food and Drug Administration (FDA) to guide therapeutic decision-making. These tests include the cobas EGFR mutation test for non-small cell lung cancer or BRAC Analysis CDx for breast and ovarian cancer. Epi proColon R, based on the analysis of the methylation

status of the SEPT9 gene, is the first and only FDA-approved blood-based test for detecting colorectal cancer.

2.9.2 cfDNA and FFPE DNA similarities

cfDNA and FFPE-derived DNA share challenges related to sample quality, quantity, and degradation. Preanalytical factors such as such as sample collection, processing, and storage can affect the integrity and yield of extracted cfDNA. Similarly, DNA extracted from FFPE samples may suffer from degradation and cross-linking caused by formalin fixation and paraffin embedding, leading to fragmented DNA molecules and reduced sequencing quality. Also, in both types of analysis, tumoral DNA is a part of the overall DNA in analysis, in fact, ctDNA is mixed with non-ctDNA to constitute cfDNA, while in FFPE tumoral slices, there can be a variable concentration of tumor DNA content mixed with non-tumoral DNA. [42] [89]

2.9.3 Detection of HRD through cfDNA analysis

The detection of HRD through plasma's cfDNA analysis is still in its early stages of development, in date 07/05/2023 searching in PubMed the keywords "HRD" and "Liquid Biopsy" resulted in only 8 scientific papers, whereas, using as keywords "HRD" and "cell-free DNA" returned 4 scientific papers. Nonetheless, the analysis of cfDNA to detect HRD poses as the future of HRD analysis, and in general in cancer diagnosis, because mainly of the non-invasive nature, and the possibility to follow the mutational landscape of the cancer during the therapy. In one of these studies, the researchers developed a probabilistic genomic model to predict HRD status based on the cfDNA DNA analysis of breast cancer patients analyzed through GuardantINFINITY, DNA was sequenced through WGS and they used epigenetic data to better train the model. The model was validated on an independent cohort of breast cancer samples and gave: an AUC of 0.7, 95% LoD of 28%.[10] In another notable study, cfDNA from ovarian cancer ascites was analyzed with targeted NGS including NGS and SNParray for somatic CNA to calculate the genomic instability score. On 20 high-grade ovarian cancer analyzed, GIS analysis was feasible on 17 patients, and 11 had a high GIS, indicating a suspected HRD status. The results of this study were not validated through a standard-of-care genomic instability test. [43]

2.9.4 Challenges in cfDNA extraction and library preparation

cfDNA and ctDNA have a low concentration in plasma, even in patients with late-stage cancer, and the tumor fraction and sensitivity can be heavily altered by genomic DNA contaminations from immune cell-DNA died through necrosis. Given these difficulties, DNA extraction results vary much between different operators and DNA extraction kits. To reduce the technical differences, it is essential to use the same DNA extraction kit, and DNA library preparation kit, and also automation should be considered. [46] To avoid genomic DNA contamination correct blood storage tubes must be used, and blood should be processed to extract plasma as soon as possible. In the cfDNA extraction process, some cfDNA extraction protocols have a size-selection step in which genomic DNA is removed. The cfDNA extraction kits usually involve one of three types of technologies: [72] [70] [55]

- cfDNA extraction with magnetic beads
- cfDNA extraction with silica membranes using a centrifuge
- cfDNA extraction with silica membranes using a vacuum pump

Of these technologies, only the cfDNA extraction through magnetic beads is easily automated by the majority of DNA extraction machines. Vacuum-based technologies tend to be automatable only by the machines sold by the proprietors of the cfDNA extraction kit [73]. Finally, centrifugation-based technologies require expensive machines that not all genetic laboratories may possess. cfDNA library creation kits use particular technologies to allow a high-performance DNA library creation, even with low-quality DNA such as cfDNA. To create cfDNA libraries the cfDNA quantity must be around 5 to 50 ng of cfDNA, which in most cases is not achievable unless large quantities of plasma are used, cfDNA commercial analysis services usually require 10 to 20 mL of plasma to deliver accurate results. [91][28][20] A problem that arises from high volumes of plasma is the high elution volume of purified cfDNA plasma, which may further complicate the following library, elution volume needs to be low to have cfDNA at high concentration.

2.9.5 Cell-free DNA extraction technologies

Commercial kits for cfDNA purification can be used manually and/or with automatic robots. The automation of DNA extraction is essential to

reduce the variations introduced by different operators with different skill levels. Commercial cfDNA extraction kits use mainly three technologies: [72] [70] [55]

- cfDNA extraction with magnetic beads
- cfDNA extraction with silica membranes using a centrifuge
- cfDNA extraction with silica membranes using a vacuum pump

Silica membranes allow the purification of cfDNA from plasma through cfDNA affinity with the silica membrane, where different solutions are used to elute different components that may bind the silica membrane with lower affinity. The force that pushes the solution through the silica membrane can be of two types: through an air-pressure difference (vacuum), or through centrifugation. Vacuum-based technologies are usually automated by specific automatic robots sold by the kit owners [73], meanwhile, centrifugation-based technologies are hardly automatable by automatic robots.[70] [72] [55] Magnetic beads technology uses beads of different materials (usually silica) with a magnetic core, the outer part is functionalized with molecules that have a high affinity for DNA. These kits are automatable with most commercially available automatic extraction robots.

2.9.6 ctDNA analysis

ctDNA is a sub-set of cfDNA and thus is at a lower concentration compared to cfDNA, its concentration in plasma is directly correlated to cancer stage, cancer dimensions, and cancer location, for example, cancers affecting the central nervous system have a low concentration in plasma but a higher concentration in cerebrospinal fluid. Given its low concentration, the methods to identify specific cancer mutations must have a high specificity and sensitivity at low Variant/Mutant Allele Fractions (VAF or MAF)[83, 86, 12].

Low plex approaches to ctDNA analysis Low plex approaches encompass all approaches that target a low number of specific mutations in ctDNA that are informative on cancer presence, molecular biology, and recurrence. Low plex approaches are quantitative real-time PCR (qPCR) and digital droplet PCR (ddPCR)[83, 86, 12]. Low plex approaches mainly test the presence of one or few specific mutations and are mainly used to test if any actionable mutations for a specific cancer are present, thus allowing a binary decision of treating or not treating the patient with a specific therapy. Thus, they

are not suitable for genome analysis for conditions like HRD, also, ddPCR instruments are expensive and not as common as DNA sequencers [83, 86, 12].

NGS methods for cfDNA analysis NGS offers multiplexing capabilities magnitudes higher than low plex approaches, thus is more suited to encapsulate cancer mutational landscape. NGS analysis of cfDNA can be separated into two branches targeted NGS methods and untargeted NGS methods.

Targeted NGS methods Targeted NGS methods cover regions, whole genes, or multiple whole genes. It's suitable for genes without hotspot mutations. Target enrichment in library construction can be achieved by direct amplification (amplicon or multiplex PCR) or hybridization capture of the DNA regions of interest.

Target enrichment through multiplex PCR allows the amplification of multiple genes or loci through PCR primers. Adaptors and indexes are commonly added subsequently through PCR or ligation. Amplification allows a greater enrichment of targeted loci through PCR and it's capable of reaching higher on-target rates than hybrid capture in small NGS panels (< 10 kb) but lower for greater panels (> 100kb).

Target enrichment through hybrid capture uses RNA custom probes for targeted regions. cfDNA, in a common hybrid capture workflow, is initially repaired at the ends to form a blunt dsDNA with protruding 3' poly-A tails. The adaptors are then ligated at both ends of the duplex, and the indexes are added subsequently through PCR using primers against universal sequences in the adaptors. The tagged-cfDNA is separated through hybridization probes ligated to magnetic beads, which ligate to the complementary probes, therefore enriching the remaining cfDNA with the loci of interest. Hybridization capture is preferred for larger panels (>100kb) Both methods have four limitations:

1. PCR amplification and NGS read errors (around 0.1 to 1.5%) resulting in false positive variant calls.

2. Imperfect representation of original cfDNA molecules in the NGS library, leading to false negative variant calls; and sequencing non-uniformity, which either reduces sensitivity to mutations or significantly increases costs.

3. Errors in PCR amplification and NGS reads can cause NGS reads to contain variant sequences even when the sample is completely wild-type.

4. Some panels can be cancer-specific or patient-specific and thus they require prior knowledge of the disease or tumor type.

One of the major recent technological advances is the use of molecular barcodes, which are random sequences introduced before any amplification step. They allow the counting of original DNA molecules instead of PCR duplicates, thereby enabling digital sequencing and resulting in unbiased and accurate mutation profiles with increased sensitivity[83, 86, 12].

Untargeted NGS methods Whole Genome Sequencing (WGS) and Whole Exome Sequencing (WES) are less sensitive than targeted approaches. The sensitivity of these approaches is around 5-10% VAF compared to 0.1% of some targeted sequencing approaches. The higher VAF needed hinders the detection of rare events, especially in situations of early detection or minimal residual disease. WGS and WES are more expensive than targeted sequencing and require high throughput sequencing equipment and highly specialized personnel to interpret the data. However, these approaches may be necessary for the discovery of new alterations in the context of initial profiling at diagnosis, to provide information for the use of more sensitive targeted techniques during disease monitoring. Even if they are not suitable for detecting subclonal events, they may be useful, considering intratumoral heterogeneity, to highlight new drug targets or to track drug resistance clones. WES is a good compromise for the exploration of unknown mutations at a reasonable cost. It can be expanded to promoters and untranslated regions to better identify driver and passenger mutations as well as actionable mutations. Low coverage and sensitivity, compared to targeted NGS technologies do not allow for the detection of rare variants but WES of cfDNA is suitable for mutational analysis of patients with advanced tumors and increased ctDNA fractions (>5% VAF). Beyond SNV detection, WES of cfDNA also allowed analysis of mutational signatures, copy number variations, fusion genes, rearrangements, predicted neoantigens, and tumor mutational burden. WGS technologies are more suitable for detecting ctDNA by identifying structural and non-coding variations such as genome-wide copy number aberrations, methylation profiles, and fragmentation patterns. sWGS allows analysis at a lower price and in less time, sWGS does not detect SNV but can detect CNVs in cfDNA at a depth of 0.1x, with a specificity > 80% when the ctDNA fraction is $\geq$ 10 %[83, 86, 12].

2.9.7 Unique Molecular Identifiers

Mutation-specific VAF in cfDNA can be between 0.01% to 10%, based on cancer progression, location, tumor heterogeneity, and volume. ctDNA may have low VAF because the tumor is in an initial stage or there are subclonal mutations. Subclonal mutations are especially important for therapy selection since rare subclones may carry a mutation that give resistance to the therapy. In a clinical context, it's vital to reach a limit of detection of VAF at about 0.01% or lower. The Unique Molecular Identifiers (UMI) allow to overcome PCR and NGS errors, they allow to detect and quantify mutations with VAF $\leq 0.1\%$. A UMI is a unique sequence associated with a single DNA molecule of the initial cfDNA (1 DNA molecule = 1 UMI). Reads with altered sequences within the same UMI are easily recognized as PCR or sequencing errors. Instead, true mutations will include different UMIs with the same mutation. The bioinformatic interpretation of NGS data with UMIs begins by clustering various NGS reads into 'UMI families' at a DNA locus with an identical UMI sequence. Subsequently, a 'vote' is taken for each UMI family, with the dominant or majority sequence identified as the true sequence of the original DNA molecule. By using UMIs, many PCR and NGS errors can be corrected, and the detection limit of mutation VAFs can be brought below the PCR and NGS error rates. UMIs can be applied in both ligation-based capture and hybrid capture, as well as in multiplex PCR protocols (although it is more challenging for the latter when the number of amplicons is high). Since UMIs can effectively work to correct PCR and NGS errors only when the UMI family sizes are sufficiently large to allow for a majority vote, UMIs increase the required sequencing depth and cost by at least a factor of 5. Additionally, unlike standard NGS, the input cfDNA quantity must be carefully controlled when using UMIs. The bioinformatic interpretation of UMIs is also partly complicated because the UMI sequences themselves might have PCR or NGS errors, which are difficult to distinguish from sequences with small UMI family sizes due to poor PCR amplification efficiency. The typical bioinformatic workflow disregards all sequence information from UMI families with fewer than 5 or 3 reads, effectively mitigating detection and quantification errors due to UMI errors, but it also discards information from a large number of original cfDNA molecules, effectively reducing the conversion yield. An average UMI family size of 12 would therefore result in an effective conversion yield reduction of approximately 30%. Using smaller UMI family sizes would significantly increase the number of original

molecules whose contribution is discarded. [86][83]

2.10 DECIDER Project

AB ANALITICA is participating in the DECIDER project, the goals of this project are to gain an understanding of the mechanism causing chemoresistance in HGSOC patients, deliver tools that enable cost-efficient personalized treatment options for HGSOC patients, and commercialize predictive kits and software for treatment response prediction and finding the right therapeutic regimen to the right patient. The University of Helsinki and the University of Turku are responsible for providing patient data, such as omics data, patient response to PARPis and platinum, and patient HRD score (calculated through Myriad MyChoice) and for clinical samples of Ovarian cancer. The clinical data will be used to develop and test our bioinformatic pipeline for HRD score calculation, while the clinical samples will be used to develop a DNA extraction protocol, and library creation and to further verify our pipeline. [24]

2.11 ONCOFLUID

ONCOFLUID is a project funded by the region Veneto for the development of high-sensitivity NGS technologies for the analysis of ctDNA, to diagnose and characterize a neoplasia with a blood withdrawal. This project aims to the development of a diagnosis kit for the early detection of hepatocarcinoma with performances and reproducibility adequate to the CE-IVD marking. AB ANALITICA, GENARTIS, and Blockchain Solutions are companies participating in this project. In this project participate also public research organs: IRCSS IOV UOSD Oncologia di base sperimentale e traslazionale, UNIPD Dipartimento di Scienze Chirurgiche Oncologiche e Gastroenterologiche, UNIVE Dipartimento di Scienze molecolari e nanosistemi, and FIF Fondazione Italiana Fegato. [66]

3

Development of a diagnostic HRD prediction kit

3.1 Introduction

To be able to request ovarian cancer tissue from hospitals it is required a developed DNA analysis pipeline tested on relevant clinical data. We are still developing the pipeline for HRD prediction based on DNA sequencing data, and we have yet to receive DNA sequencing data from our partners at the University of Helsinki and the University of Turku.

3.2 Bioinformatic Pipeline

We intend to initially use the SeqOne HRD pipeline [80] to test it against clinical data with known HRD status, calculated with the FDA-approved test Myriad MyChoice previously used by the University of Helsinki to determine the HRD status. SeqOne HRD [80] is a proprietary HRD computation algorithm of SeqOne and it's bought as a license, we initially identified this bioinformatic program for HRD prediction since it's already been validated in phase III PAOLA-1 clinical trial, as well as its DNA extraction methods and library creation. Also, we intend to test and then use open-source HRD score-calculating algorithms, such as shallowHRD, that use shallow Whole Genome Sequencing Data to calculate an HRD score.

3.2.1 SeqOne

The core DNA analyzing program that will calculate the HRD score is SeqOne HRD testing. This program is the propriety of SeqOne, a company specialized in DNA analysis, this kit is CE-IVD marked and it has been tested on 364 ovarian cancers coming from PAOLA-1 clinical trial, and it has been tested against Myriad MyChoice results.

The HRD score is calculated using sequencing data obtained in two ways: from sWGS sequencing at a minimum depth of 0.3x and from high-depth (35x) sequencing of the BRCA1 and BRCA2 genes.

From sWGS genome sequencing, two genomic instability features are captured: large genomic alterations (LGA) and loss of parental copy (a type of loss of heterozygosity). LGA is defined as the number of copy number breakpoints in the genome. A breakpoint is considered a variation in chromosome copy number between two genomic segments of minimum size 10 Mb and maximum 3 Mb apart. Loss of Parental Copy is defined as the number of long haploid segments at least 10 Mb in length.

SeqOne also includes the Copy number variation of the CCNE1 gene, whose amplification is computed using sWGS, where the increase in CNV copies is correlated with HRD and poor responses to PARPi.

From high-depth sequencing of BRCA1/2, the program queries the variant knowledgebase to see if they are associated with a mutation that confers sensitivity to PARPi. The pathogenicity of the variants is determined using SeqOneRank+, which is a proprietary machine-learning implementation of the ACMG guideline.

SeqOne's HRD calculation program is a logistic regression model supervised by a reference HRD score. The training dataset was collected in two different centers and consisted of 170 ovarian cancer patients. All samples were prepared using Agilents SureSelect XT-HS1 and XT-HS2 reagents and sequenced on Illuminas NextSeq or NovaSeq platforms.

SeqOne validated its HRD score using a retrospective analysis of 364 ovarian cancer patients from the PAOLA-1 phase 3 clinical trial. SeqOne HRD+ and Myriad Mychoice patients had the same survival benefit from bevacizumab + olaparib compared to bevacizumab alone. In addition, SeqOne HRD testing had a smaller rate of inconclusive results compared to Myriad MyChoice.

SeqOne HRD is already validated for the Agilent XT-HS1 and XT-HS2 extraction kits, Agilent Magnis and Agilent Bravo NGS library preparation

kits, Illumina NextSeq and Illumina NovaSeq sequencers, and the Agilent Great gene panel or other BRCA1/2 panels. SeqOne recommends a depth of 1x for sWGS, a depth of at least 35x for the BRCA1 and BRCA2 panel, and a tumor content of at least 20%. The surface area of tumor content should be above 10mm^2, and the proportion of properly mapped reads should be above 50%.

The calculation of HRD status can be calculated with two different approaches based on turnaround time and economic constraints. The parallel testing approach is time-efficient but more expensive, as sWGS and BRCA1 and BRCA2 sequencing are performed together (on the same flow cell). The sequential testing first performs BRCA1 and BRCA2 sequencing, and if they are wild type, sWGS is performed. This method is more economical but has a longer turnaround time compared to the parallel approach if BRCA1 and BRCA2 are wild type.

SeqOne HRD generates a report based on sequencing data, declaring the HRD score calculated based on the different weights of the analyzed variables.

3.2.2 ShallowHRD

ShallowHRD is a software for HRD testing based on the number of large-scale genomic alterations (LGA) obtained from sWGS. sWGS can robustly detect copy number alterations (CNAs), even in FFPE samples and low-cost liquid biopsies. The concept of LGA follows single nucleotide polymorphism array approaches, exploiting an increased number of large-scale intra-chromosomal CNAs characteristic of HRD.

This algorithm was developed on data from in-house sWGS and down-sampled WGS of normal samples derived from The Cancer Genome Atlas (TCGA) to create an sWGS methodology similar to Large-scale state transitions (LST) in SNP arrays. LGA inferred from sWGS corresponded well to LSTs with identical HRD calls from 8 primary tumors (76-97% match in segments $\geq$ 10Mb). sWGS coverage > 0.3X provided adequate quality, even for FFPE. Validation using down-sampled WGS showed that LGA was consistent with SNP-arrays LST with increased discrepancy in medium-quality samples, and HRD diagnosis was discordant in three cases and borderline in four cases. CCNE1 amplification was found in 4 non-HRD cases, consistent with the previous observation of nearly mutual exclusivity with HRD. Thus, sWGS LGAs are suitable for replacing SNP-array, LSTs, which are clinically

validated methods for HRD detection. Tumor content for sWGS is limited to a minimum of 30% as estimated from TCGA and in silico dilution series. Fifteen and 20 LGAs represent soft and stringent cutoffs with sensitivity of 87.5% and (1.25% (16 HRD cases) and specificity of 90.5% and 95.2% (63 non-HRD cases), respectively, which is comparable with other approaches. ShallowHRD thus implements a fast and direct assessment of tumor HRD in breast cancer, ovarian cancer, and other types of cancer (pancreas and prostate), yielding results similar to approved approaches.

ShallowHRD pipeline has been also validated on simulated data and on real clinical data generated from breast cancer patients and its performance was systematically evaluated on data with different sequencing depths, tumor purities, and DNA input amounts. [50]The results demonstrated that the ShallowHRD pipeline is an accurate and robust method for HRD detection. The methods developed for HRD detection can be mainly classified into three approaches. The most popular approach is based on an HRD-related index of genomic instability that includes LOH, TAI, and LST.

ShallowHRD is the first method that is based on genome-wide CNV. It brings several advantages over previous methods. First, genome-wide CNV is estimated with a resolution in millions of bases, and therefore low-pass WGS input can be used, where the sequencing and library preparation costs are moderate, while WGS operation is simpler compared to probe-based methods. In some situations, tumor resection is not possible, especially in patients in severe conditions who are potentially receiving treatment with PARPi. Unlike existing methods, sWGS requires only a small amount of DNA input, making shallowHRD suitable for patients with samples from core-needle biopsy or even circulating tumor cells can be used. Another advantage of CNV-based methods is the robustness of CNV calling. Unlike other methods based on germline variants, the CNV pattern may not be influenced by population characteristics or mutational patterns of different tumor types, making shallowHRD suitable for pan-cancer testing. The shallowHRD pipeline was developed for sWGS but can also be applied to data generated from WES, genome-wide SNP-panel sequencing, or SNP arrays. This method can be integrated into other existing HRD detection methods and improve their performance. ShallowHRD can be applied to different CNV calling software, in the study they used HMMcopy, a CNV calling algorithm based on a hidden Markov mode, instead of Control-FREEC. Where Control-FREEC requires an estimate of tumor purity and an estimate of ploidy to determine the exact copy number. However, the low sequencing

depth limits the accuracy of the estimate, and the exact copy number is not necessary for shallowHRD. Using simulated sWGS data from 80 patients, the results from using HMMcopy and Control-FREEC were compared and it has been observed that the modified pipeline achieved slightly better performance and could give reliable results with a tumor purity of at least 20%. However, shallowHRD cannot calculate tumor purity using the sequencing data itself, and thus it must be assessed by the pathologist. [50]

3.3 Design of the sequencing panel

While we have yet to try a sequencing panel on ovarian cancer FFPE DNA, we have already decided on the genomic regions that will be sequenced. Our kit will sequence BRCA1, and BRCA2, and perform an sWGS. We have decided to target only BRCA1 and BRCA2 instead of adding other HRR genes (such as PALB2, RAD51, Fanconi Anemia Genes, etc.) because HRR gene mutations, besides BRCA1 and BRCA2, are weakly correlated to the HRD phenotype, and they are responsible for those cases where the HRD phenotype is present but BRCA1 and BRCA2 are still functional. [71] [82] [76] The cases where BRCA1 and BRCA2 are wild-types and the HRD score calculated through sWGS is positive may be caused by two causes:

1. The HRR is non-functional thus the genomic scars are present
2. The HRR is functional and the genomic scars are present because the genomic instability of the tumor caused by HRD was a cancer hallmark that has been lost during tumor generations.

Given these two causes, adding additional HRR genes to the gene panel will inform how the HRD is caused and allow us to rule out those cancers that have an HRD genotype but are not sensible to PARPis. Additional analysis of HRR genes, besides being potentially inconclusive due to Variants of Uncertain Significance (VUS), loss of function (lof) in genes that affect HRR genes function, or epigenetic modifications not detected by our panel, would lead to a substantial increase in the costs of library creation and especially sequencing, as it would significantly increase the number of base pairs to sequence at high depth for a slight improvement in the identification of false positives. Moreover, the use of PARPis in cancers with loss of function mutations in one or more HRR genes, other than BRCA1 and BRCA2, is not yet recommended by ESMO. Thus, given the increase in costs, the redundancy of information provided by extended panels, and the lack of official recommendations based on mutated HRR genes, besides BRCA1 and BRCA2, we

decided that sWGS and BRCA1 and BRCA2 sequencing will prove enough to determine which patients will receive the most beneficial outcomes from PARPi treatment.

4

Development of an HRD diagnostic kit based on cfDNA

4.1 Introduction

The development of a diagnostic HRD detection kit based on FFPE ovarian cancer tissue is still in the early stagesmeanwhile, AB ANALITICA S.r.l. is participating in another funded project called ONCOFLUID, this funded project aims to develop a diagnostic kit for the diagnosis of Hepatocarcinoma and its characterization based on cell-free DNA from plasma. I aided in this project regarding the cell-free DNA extraction methods and library creation methods in perspective for the subsequent development of an HRD diagnostic kit based on cell-free DNA.

4.2 Blood collection tubes, plasma separation, and conservation

To determine which blood collection tubes were the most adequate, we conducted an extensive research based on scientific papers ([33], [54], [60], [84]), internal tests, and expert opinions. According to the data from this research, we have derived the following conclusions about these blood collection tubes:

- Tubes with heparin: tubes with heparin are not suited for molecular biology, gDNA contamination is present immediately after blood collection caused by immediate lysis of the white cells. Also, heparin inhibits DNA polymerases.

- Tubes with EDTA: Tubes with EDTA are cheap and commonly used for blood collection. They can prevent gDNA contamination only if the sample is processed within 4 hours at room temperature or within 24 hours at 4°C.
- Tubes with cell stabilizers: all investigated tubes had analogous performances regarding sample stabilization within 72 hours from blood collection. Also, from the gathered data, these tubes seem suitable for cfDNA analysis even a week after blood collection.
  - PAXgene Blood ccfDNA tubes (Qiagen) and Cell-Free DNA Collection tubes (Roche) have a reduced initial white cell stabilization, increasing the amount of gDNA in plasma
  - Cell-Free DNA BCT tubes (Streck) are correlated to a reduction of the concentration of methylated DNA and they are not suited for cfRNA retrieval

Professor Stefano Indraccolo recommended the collection of blood with Streck tubes, as they noticed little to no gDNA contamination. Despite the long stabilization time of Streck tubes, the experts and scientific articles recommend immediate plasma separation through centrifugation. A separation within 48 hours from blood collection has a lower probability of gDNA contamination and gives a greater yield of plasma, about 8 - 10 mL of plasma for 20 mL of whole blood. Whole blood should never be frozen as the freezing process destroys the majority of red blood cells and white blood cells, making it impossible to separate plasma from blood and it heavily contaminates the sample with gDNA.

Freezing whole blood before plasma extraction should be avoided, especially in the context of cell-free DNA (cfDNA) analysis, to prevent contamination with genomic DNA. The process of freezing and thawing can lead to the lysis of erythrocytes and nucleated cells, releasing genomic DNA into the plasma and compromising the purity of cfDNA samples. The enzymatic degradation of released genomic DNA fragments during the freezing and thawing process can generate short DNA fragments, which may interfere with cfDNA size selection and library preparation steps. This can result in misinterpretation of ctDNA relative quantity and thus underestimating the Variant Allele Frequency and Tumor Fraction. Plasma must be separated from whole blood through centrifugation, one of the methods which have given the best results is double centrifugation, the first centrifugation must be at 800-1200g at 4°C for 10 minutes and then the second one must be at 16000g at 4°C for 10 minutes. The first centrifugation is at low speed to concentrate cells on the bottom of the tube, the second one is at high speed to eliminate cell debris and organelles. This process increases cfDNA purity,

yield, and medium homogeneity. Plasma can be stored for up to 9 months after freezing at -20°C or -80°C for cfDNA quantifications or to determine the degree of cfDNA fragmentation. To avoid cfDNA further fragmentation it's recommended not to subject the plasma to more than 3 cycles of freezing and thawing as it increases fragmentation phenomena. [60]

4.3 cfDNA extraction methods

We evaluated various scientific articles that tested commercial cfDNA extraction kits, both automated and manual, and compared their extraction efficiency. We also conducted a commercial research to evaluate the kit costs and the company's reliability. Based on the results from these researches, we compiled a list of commercial cfDNA extraction kits from plasma and contacted the companies to obtain a trial kit. In these researches, we did not consider the technology used by the extraction kit, as we decided to consider non-automatable kits if their extraction efficiency was significantly superior to automatable kits.

1. **Ease of Automation**: Automation is the best method to reduce technical errors and interpersonal variability among technicians, and it also reduces the manual time dedicated to laboratory activities. By ease of automation, we mean a kit that can be automated by many automatic DNA extraction robots. Kits like CNA (%) and Promega RSC LV ccfDNA, for example, are automatable but only with the proprietary machines of the companies that supply the kit, which might not be widespread in most laboratories.

2. **Cost per Reaction of the Kit**: Reducing the cost of testing for HRD and Hepatocarcinoma is fundamental to allow the majority of the population to access essential diagnostic services like HRD and would facilitate the approval and reimbursement process by the National Health System.

3. **The Time Required and the Number of Steps for cfDNA Extraction from Plasma**: The kits we analyzed can be operated both manually and automatically, except for RSC. A long required time and a high number of steps increase the probability of errors that could result in an incorrect diagnosis with potentially mild or fatal effects, such as the non-administration of PARPi to a PARPi-responsive patient.

We decided to use 3 mL of plasma as the standard plasma volume. This decision was made to harmonize two opposing aspects:

- The first is the need for high volumes of plasma to obtain high quantities of cfDNA for optimal library creation and identification of tumor variants.

- The second is to minimize the volume of blood drawn from the patient to reduce the stress caused by high-volume blood draws.

However, some kits analyzed did not allow operation with 3 mL volumes, so we used the indicated volumes closest to 3 mL. The plasma samples we analyzed came from the Italian Liver Foundation ONLUS in Trieste and were provided by Dr. Devis Pascut. The plasma samples received came from healthy patients and patients with liver cirrhosis, a condition associated with a higher quantity of cfDNA and a greater propensity for developing liver cancer. [6] The plasma extraction protocol used by the Fondazione Italiana Fegato is as follows:

> *Plasma samples were obtained from 18 mL of whole blood collected in 3 EDTA-containing sterilized tubes (DB Vacutainer). Samples were mixed by gently inverting the tubes for 10 times and centrifuged at 3500g for 10 minutes within 2 hours from collection. The supernatant was carefully collected, without disturbing the buffy coat, and transferred into a 15 mL tube. Plasma was mixed by inverting the tube 5 times, aliquoted, and frozen at -80 °C for long-term storage.*

The plasma from patients with the same health status (healthy or cirrhotic) was mixed together and divided into 7 mL aliquots. The mixing was done to reduce interpersonal differences between donors that can alter cfDNA concentration. The division into 7 mL aliquots was done to avoid numerous freeze-thaw cycles of the plasma samples and to have a sufficient volume to perform one technical replicate of the analyzed analysis kit. In all the kits we analyzed, we centrifuged the plasma at 2000g following thawing. This additional centrifugation is recommended to increase cfDNA extraction efficiency from several articles [84], to remove any pellets that may form, and it is also a phenomenon we observed internally, where initial centrifugation improved efficiency.

To analytically compare the extraction efficiency of the different kits with plasma types from healthy patients or patients with liver cirrhosis, we decided to use the Promega Maxwell RSC LV ccfDNA [70] extraction kit as the comparison standard, as it was the only kit available to us that we could easily automate since we had the Maxwell machine in Istituto di Ricerca Pediatrica Città della Speranza. Thus we assumed that the only difference in samples processed with Maxwell RSC LV ccfDNA from patients with hepatic cirrhosis and from healthy patients was the higher concentration of cfDNA in samples from patients with hepatic cirrhosis. We then used

the concentration obtained with the Maxwell to normalize the cfDNA concentration between the kits tested with plasma from healthy patients and cirrhotic patients. The equation we used for the comparison was: the average of cirrhotic samples extracted with Promega using the quantity "DNA extracted per mL of plasma" over the average of healthy samples extracted with Promega using the quantity "DNA extracted per mL of plasma". This ratio gave the quantity called Promega's ratio.

To compare DNA extraction efficiency between kits that use purify from different volumes of plasma, have a different elution volume, and different patient statuses, we used the adjusted concentration, the adjusted concentration has been calculated using the following steps:

1. The kit DNA concentration (ng/μL) was multiplied by the elution volume (μL) to obtain the DNA quantity (ng) extracted
2. The DNA quantity extracted was divided by the plasma volume used (mL) to obtain the DNA quantity extracted per mL of plasma (ng/mL)
3. The DNA quantity extracted per mL of plasma from healthy patients was multiplied by Promega's ratio to obtain a normalized concentration of DNA per mL of plasma, called "Adjusted concentration".

The resulting adjusted concentration is an intensive value that has been used to compare the cfDNA extraction efficiency of the extraction kits analyzed.

4.4 cfDNA quantification

cfDNA quantification may prove challenging due to the different types of DNA (cfDNA and gDNA) present in plasma and the possible RNA carriers used in the extraction, both may alter the cfDNA quantification. After extensive literature research, we concluded that the best-suited DNA quantification methods for cfDNA are the following:

ThermoFisher Scientific Qubit 3 (usually referred to as Qubit) Qubit allows easy and fast comparison of performance between different DNA extraction kits, but it is somehow imprecise due to how it quantifies the DNA: DNA is quantified using a fluorescent dsDNA intercalant which binds to the DNA and emits lightwaves when exposed to light with a determined frequency. Due to its non-specific nature, it quantifies cfDNA and genomic DNA, as long as it is dsDNA, also, it may also partially quantify the carrier RNA used to facilitate the cfDNA extraction from plasma. Thus, this method

does not allow to differentiate between gDNA and cfDNA nor it cannot acknowledge gDNA contamination when it is below or slightly above the normal cfDNA concentration, and carrier RNA makes the concentration analysis unreliable. However, it is a quick and fast method to quantify the DNA. [54] [69] [46] [55]

Agilent Tapestation 4150 (usually referred to as TapeStation) TapeStation is one of the best methods to quantify DNA, due to the nature of how it is analyzed: the quantification mechanism is capillary electrophoresis followed by the fluorescence detection of a fluorescent dye that binds to the dsDNA. This method is really well-suited to quantify DNA and analyze its size distribution, but it suffers from gDNA quantification if gDNA gets degraded to the cfDNA length range. [54] [69] [46] cfDNA concentration is detected through the cfDNA TapeScreen chip, as Agilent recommended. The range of base pairs was chosen according to the guidelines provided by Agilent documentation ([4] [3]. Therefore, the region from 50 to 700 bp was identified as the region where cfDNA is present, while regions larger than 700 bp are considered High Molecular Weight DNA for the samples analyzed with the cfDNA chip. We used cfDNA tapescreen chips that expired in November 2023, we deemed them still usable. The cfDNA peaks of the samples analyzed with the D1000 HS TapeScreen chip were integrated in the cfDNA that ranges from 50 to 700 bp. However, Agilent does not recommend the D1000 HS TapeScreen chip for cfDNA analysis. These chips were used only for comparison purposes and to identify potential differences between the two chips.

5

Testing of commercial cfDNA extraction kits

5.1 QIAGEN: QIAamp Circulating Nucleic Acid Kit

5.1.1 Description of the kit

QIAamp Circulating Nucleic Acid Kit (CNA) [72] is a RUO kit that uses a silica membrane and vacuum to purify cfDNA from plasma, the kit can only be automated by the automatic extractor QIAcube Connect. [73] The protocol is characterized by the addition of carrier RNA to increase yield. The carrier RNA was added to the samples at a final concentration of 0.2 $\mu g/\mu L$, with a volume of 11.3 μL added to each sample. This protocol requires a vacuum device and a vacuum pressure of 800-900 mbar. We extracted cfDNA from 3 mL of plasma and the final elution volume was 45 μL.

5.1.2 Limitations

This kit had a limitation regarding vacuum pressure control: the aspiration step using an unregulated vacuum collector resulted in a faster-than-expected solution passage, indicating a lack of pressure control. This could potentially lead to suboptimal extraction efficiency, sample loss, or a lower cfDNA purity.

5.1.3 Results

Plasma from Healthy Patients Fragment distribution via TapeStation was performed with both D1000 HS TapeScreen, which is not specifically designed for cfDNA but has an adequate DNA size range, and the dedicated cfDNA TapeScreen kit, designed specifically for cfDNA size distribution analysis.

Qubit Analysis From Qubit Analysis, the following concentrations and adjusted concentrations were obtained:

- Sample 1 concentration measured with Qubit: 0.552 ng/μL.
- Sample 2 concentration measured with Qubit: 0.448 ng/μL.
- Sample 1 adjusted concentration measured with Qubit: 20.45 ng/mL.
- Sample 2 adjusted concentration measured with Qubit: 16.60 ng/mL.

TapeStation Analysis

D1000 HS TapeScreen From the analysis with D1000 HS TapeScreen we obtained the following concentrations and we calculated the following cfDNA quantity per mL of plasma:

- Sample 1 concentration measured with TapeStation (range: $\sim$ 50 -700 bp): 0.209 ng/μL.
- Sample 2 concentration measured with TapeStation (range: $\sim$ 50 -700 bp): 0.252 ng/μL.
- Sample 1 concentration per mL of plasma measured with TapeStation (range: $\sim$ 50 -700 bp): 3.135 ng/mL.
- Sample 2 concentration per mL of plasma measured with TapeStation (range: $\sim$ 50 -700 bp): 3.78 ng/mL.

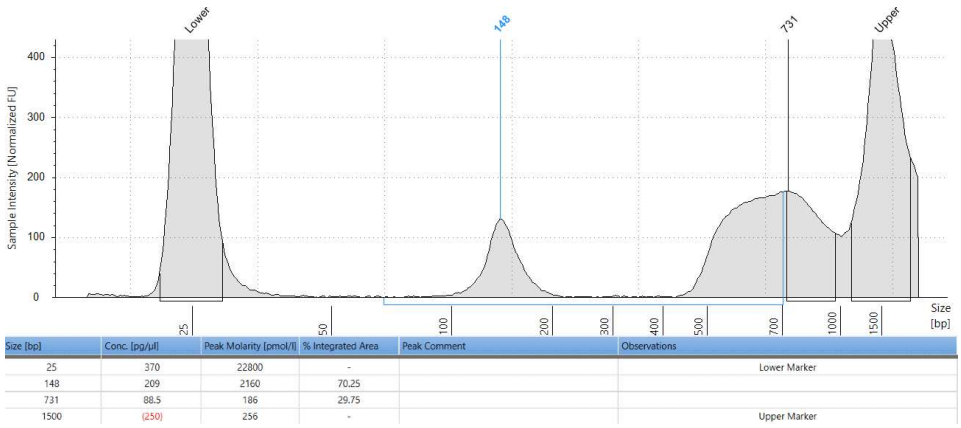

Size [bp]	Conc. [pg/µl]	Peak Molarity [pmol/l]	% Integrated Area	Peak Comment	Observations
25	370	22800	-		Lower Marker
148	209	2160	70.25		
731	88.5	186	29.75		
1500	(250)	256	-		Upper Marker

Figure 5.1: Qiagen sample 1 analyzed with D1000 HS Tapescreen

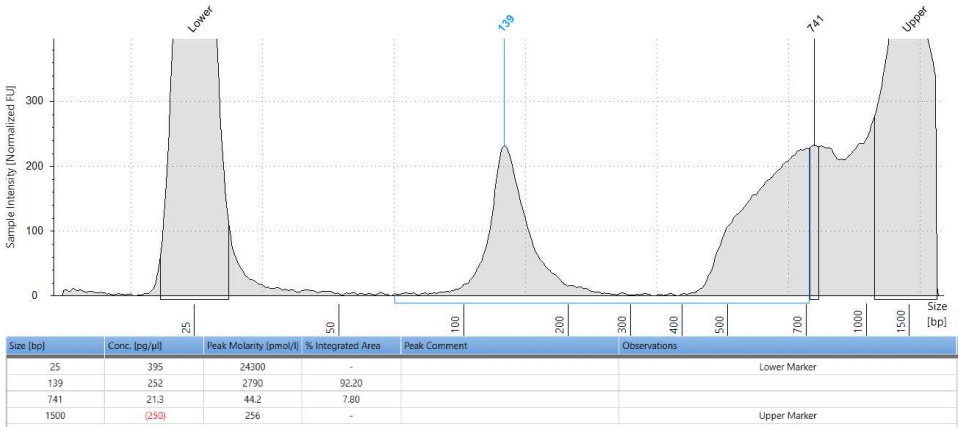

Size [bp]	Conc. [pg/µl]	Peak Molarity [pmol/l]	% Integrated Area	Peak Comment	Observations
25	395	24300	-		Lower Marker
139	252	2790	92.20		
741	21.3	44.2	7.80		
1500	(250)	256	-		Upper Marker

Figure 5.2: Qiagen sample 2 analyzed with D1000 HS TapeScreen

cfDNA TapeScreen From the analysis with cfDNA TapeScreen we obtained the following concentrations and we calculated the following adjusted concentration:

- Sample 1 concentration measured with TapeStation (range: 50 -700 bp): 0.219 ng/μL.
- Sample 2 concentration measured with TapeStation (range: 50 -700 bp): 0.249 ng/μL.
- Sample 1 adjusted concentration measured with TapeStation (range: 50 -700 bp): 8.84 ng/mL.
- Sample 2 adjusted concentration measured with TapeStation (range: 50 -700 bp): 10.04 ng/mL.

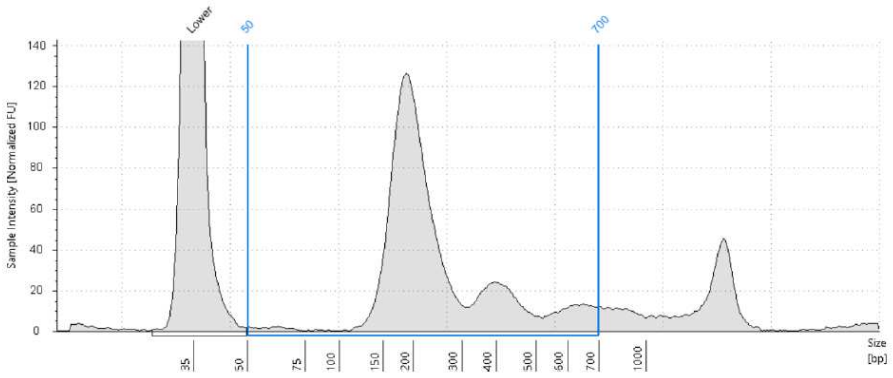

Sample Table

Well	%cfDNA	Conc. [pg/µl]	Sample Description	Alert	Observations
C1	78	281	q1	⚠	Caution! Expired ScreenTape device

Region Table

From [bp]	To [bp]	Average Size [bp]	Conc. [pg/µl]	Region Molarity [pmol/l]	% of Total	Region Comment	Color
50	700	264	219	1570	77.80	%cfDNA	

Figure 5.3: Qiagen sample 1 analyzed with cfDNA TapeScreen

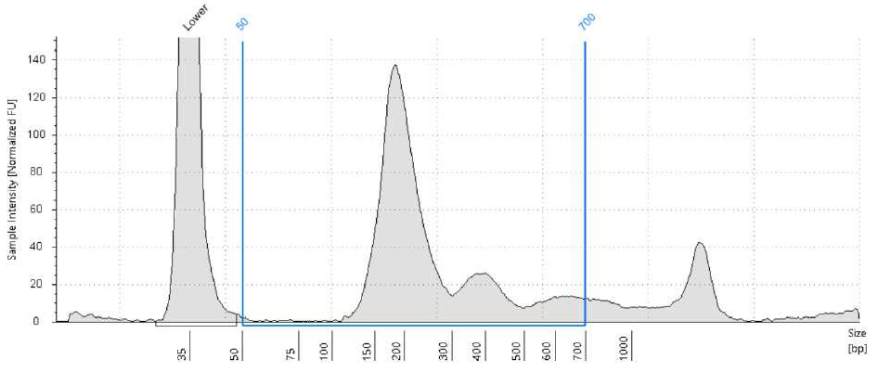

Sample Table

Well	%cfDNA	Conc. [pg/µl]	Sample Description	Alert	Observations
B1	78	319	q2	⚠	Caution! Expired ScreenTape device

Region Table

From [bp]	To [bp]	Average Size [bp]	Conc. [pg/µl]	Region Molarity [pmol/l]	% of Total	Region Comment	Color
50	700	262	249	1790	78.16	%cfDNA	

Figure 5.4: Qiagen sample 2 analyzed with cfDNA TapeScreen

5.1.4 Discussion of Results

In the TapeStation results using D1000 HS TapeScreen, a high molecular weight peak reflecting genomic DNA (gDNA) contamination is observed; however, this peak disappears when using the cfDNA TapeScreen. We believe this is because low molecular weight DNA migrates more easily than high molecular weight DNA, due to both the smaller gel pore sizes

and the use of different buffers. Despite the differences between the two TapeScreens, a well-defined peak around 200 base pairs, corresponding to the cfDNA in the extraction eluate, is observable in both cases.

5.2 Promega: Maxwell RSC ccfDNA LV Plasma Kit

5.2.1 Description of the kit

Maxwell RSC ccfDNA LV Plasma Kit (Promega) [70] is a RUO kit that uses magnetic beads to separate DNA that can purify cfDNA from 2 - 8 mL of plasma. This protocol is only usable with the Maxwell RSC instrument. We extracted cfDNA from 3 mL of plasma and we used 60 μL of the elution buffer for NGS instead of the default, as our future applications will be for NGS. The kit was tested under two conditions: with plasma from healthy patients and with plasma from patients with hepatic cirrhosis, using the same protocol in both conditions. This kit was chosen as the reference standard for comparing samples from healthy and cirrhotic patients, due to its ease of use and reproducibility with the automated machine.

5.2.2 Results

Plasma from Healthy Patients Fragment distribution via TapeStation was performed with both D1000 HS TapeScreen, which is not specifically designed for cfDNA but has an adequate DNA size range, and the dedicated cfDNA TapeScreen kit, designed specifically for cfDNA size distribution analysis.

Qubit Analysis From Qubit Analysis, the following concentrations and adjusted concentrations were obtained:

- Sample 1 concentration measured with Qubit: 0.226 ng/μL.
- Sample 2 concentration 2 measured with Qubit: 0.212 ng/μL.
- Sample 1 adjusted concentration measured with Qubit: 11.17 ng/mL.
- Sample 2 adjusted concentration measured with Qubit: 10.47 ng/mL.

Tapestation Analysis

D1000 HS TapeScreen From the analysis with D1000 HS TapeScreen we obtained the following concentrations and we calculated the following cfDNA quantity per mL of plasma:

- Sample 1 concentration measured with TapeStation (range: ~ 50 -700 bp): 0.299 ng/μL.
- Sample 2 concentration measured with TapeStation (range: ~ 50 -700 bp): 0.237 ng/μL.
- Sample 1 concentration per mL of plasma measured with TapeStation (range: ~ 50 -700 bp): 5.98 ng/mL.
- Sample 2 concentration per mL of plasma measured with TapeStation (range: ~ 50 -700 bp): 4.74 ng/mL.

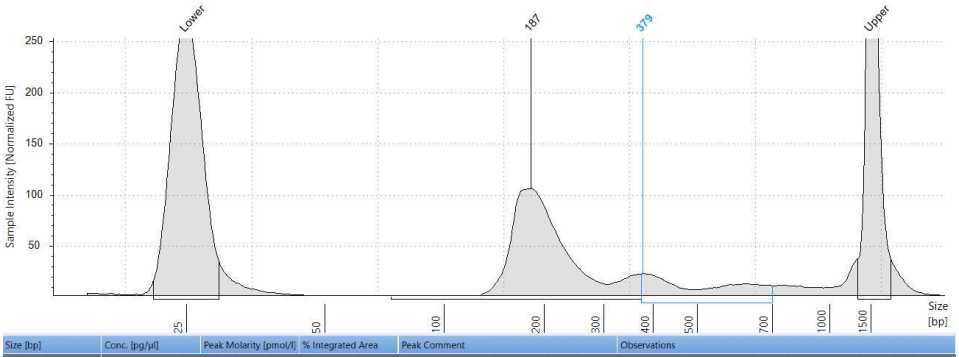

Size [bp]	Conc. [pg/µl]	Peak Molarity [pmol/l]	% Integrated Area	Peak Comment	Observations
25	355	21900	-		Lower Marker
187	242	1990	80.92		
379	57.0	232	19.08		
1500	(250)	256	-		Upper Marker

Figure 5.5: Promega sample 1 analyzed with D1000 HS TapeScreen

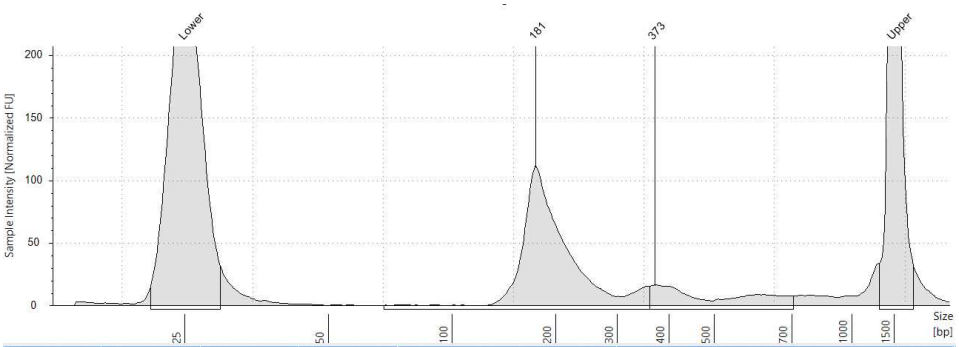

Size [bp]	Conc. [pg/µl]	Peak Molarity [pmol/l]	% Integrated Area	Peak Comment	Observations
25	371	22900	-		Lower Marker
181	193	1640	81.28		
373	44.4	183	18.72		
1500	(250)	256	-		Upper Marker

Figure 5.6: Promega sample 2 analyzed with D1000 HS TapeScreen

cfDNA TapeScreen From the analysis with cfDNA TapeScreen we obtained the following concentrations and we calculated the following adjusted concentrations:

- Sample 1 concentration measured with TapeStation (range: 50 -700 bp): 0.266 ng/μL.

- Sample 2 concentration measured with TapeStation (range: 50 -700 bp): 0.257 ng/μL.

- Sample 1 adjusted concentration measured with TapeStation (range: 50 -700 bp): 14.31 ng/mL.

- Sample 2 adjusted concentration measured with TapeStation (range: 50 -700 bp): 13.83 ng/mL.

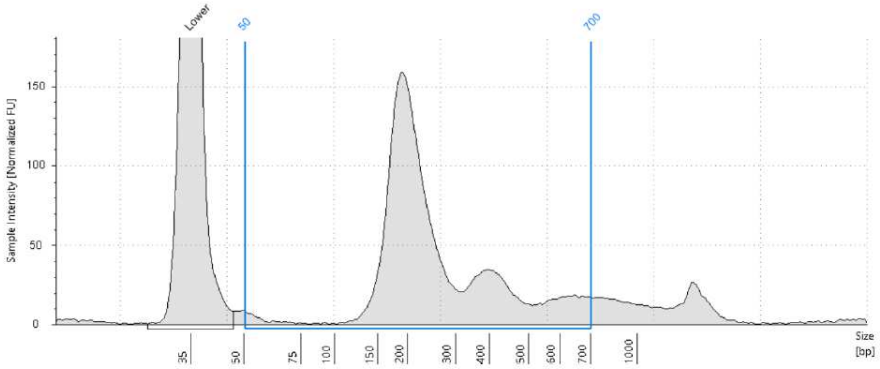

Sample Table

Well	%cfDNA	Conc. [pg/µl]	Sample Description	Alert	Observations
D1	82	323	p1	⚠	Caution! Expired ScreenTape device

Region Table

From [bp]	To [bp]	Average Size [bp]	Conc. [pg/µl]	Region Molarity [pmol/l]	% of Total	Region Comment	Color
50	700	275	266	1860	82.30	%cfDNA	

Figure 5.7: Promega healthy sample 1 analyzed with cfDNA TapeScreen

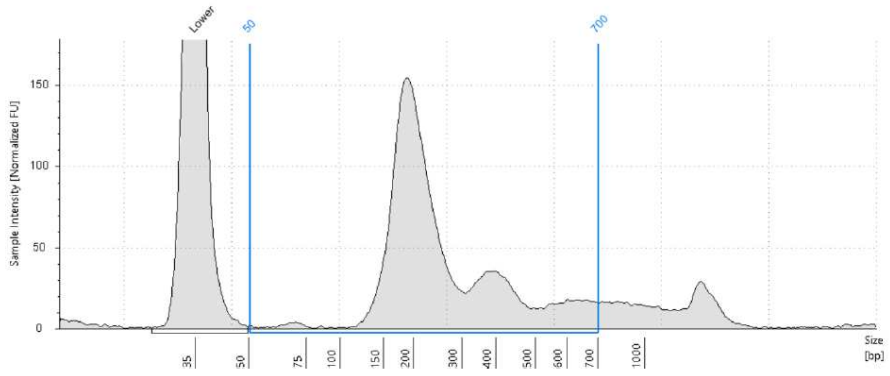

Sample Table

Well	%cfDNA	Conc. [pg/µl]	Sample Description	Alert	Observations
E1	82	312	p2	⚠	Caution! Expired ScreenTape device

Region Table

From [bp]	To [bp]	Average Size [bp]	Conc. [pg/µl]	Region Molarity [pmol/l]	% of Total	Region Comment	Color
50	700	274	257	1790	82.45	%cfDNA	

Figure 5.8: Promega healthy sample 2 analyzed with cfDNA TapeScreen

Plasma from Patients with Hepatic Cirrhosis

Qubit Analysis From Qubit Analysis, the following concentrations and adjusted concentrations were obtained:

- Sample 1 concentration measured with Qubit: 0.546 ng/μL.
- Sample 2 concentration 2 measured with Qubit: 0.536 ng/μL.
- Sample 1 adjusted concentration measured with Qubit: 10.92 ng/mL.
- Sample 2 adjusted concentration measured with Qubit: 10.82 ng/mL.

Tapestation Analysis cfDNA TapeScreen was used to determine cfDNA concentration and size distribution. The following concentrations and adjusted concentrations were obtained:

- Sample 1 concentration measured with TapeStation (range: 50 -700 bp): 0.71 ng/μL.
- Sample 2 concentration measured with TapeStation (range: 50 -700 bp): 0.697 ng/μL.
- Sample 1 concentration measured with TapeStation (range: 50 -700 bp): 14.2 ng/mL.
- Sample 2 concentration measured with TapeStation (range: 50 -700 bp): 13.94 ng/mL.

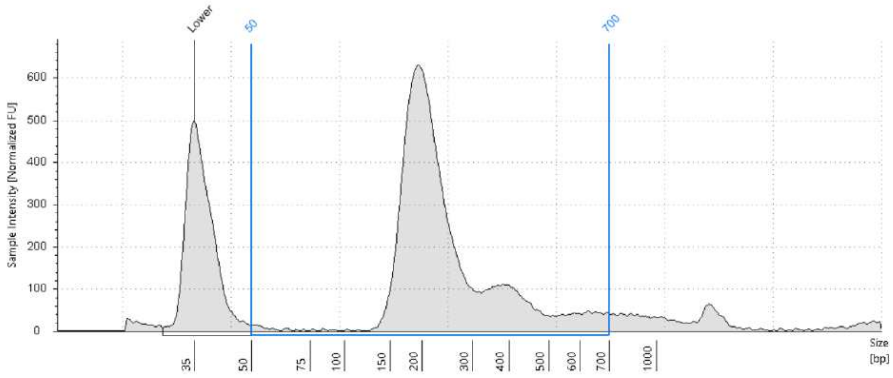

Sample Table

Well	%cfDNA	Conc. [pg/µl]	Sample Description	Alert	Observations
B1	89	797	Promega 1	⚠	Caution! Expired ScreenTape device

Region Table

From [bp]	To [bp]	Average Size [bp]	Conc. [pg/µl]	Region Molarity [pmol/l]	% of Total	Region Comment	Color
50	700	260	710	5000	89.05	%cfDNA	

Figure 5.9: Promega cirrhotic sample 1 analyzed with cfDNA TapeScreen

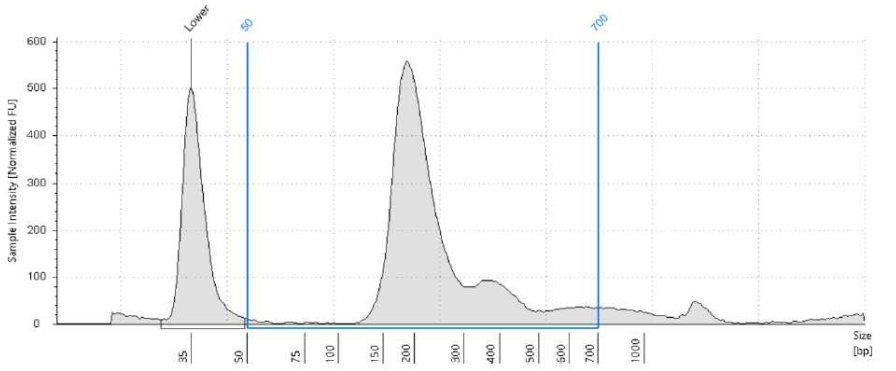

Sample Table

Well	%cfDNA	Conc. [pg/µl]	Sample Description	Alert	Observations
C1	89	782	Promega 2	⚠	Caution! Expired ScreenTape device

Region Table

From [bp]	To [bp]	Average Size [bp]	Conc. [pg/µl]	Region Molarity [pmol/l]	% of Total	Region Comment	Color
50	700	253	697	5010	89.13	%cfDNA	

Figure 5.10: Promega cirrhotic sample 2 analyzed with cfDNA TapeScreen

5.2.3 Discussion of Results

As indicated with the CNA kit, the electropherograms with D1000 HS TapeScreen show a high molecular weight peak, whereas with cfDNA TapeScreen, the peak disappears due to the higher selectivity for small DNA fragments like cfDNA. In all electropherograms shown above, a sharp peak around 200 bp, corresponding to the extracted cfDNA, is noticeable.

5.3 Magen: HiPure Circulating DNA Kit (Spin Protocol)

5.3.1 Description of the kit

The Magen HiPure Circulating DNA Kit (Magen Spin) [55] is a RUO kit that uses a silica membrane and centrifugation to purify cfDNA, the kit requires the addition of 1 μg of carrier RNA, this kit cannot be easily automated. The kit can purify cfDNA from 1 to 5 mL of plasma. It was tested on samples of plasma from healthy and cirrhotic patients. We extracted cfDNA from 3 mL of plasma and the final elution volume was 40 μL.

5.3.2 Limitations:

During cfDNA extraction from healthy patients, issues with centrifugation arose as the centrifuge rotor did not allow the speeds reported in the protocol. Plasma from patients with hepatic cirrhosis was processed according to protocol instructions.

5.3.3 Results

Plasma from Healthy Patients

Qubit Analysis From Qubit analysis, the following concentrations and adjusted concentrations were obtained:

- Sample 1 concentration measured with Qubit: 1.03 ng/μL.
- Sample 2 concentration measured with Qubit: 0.908 ng/μL.
- Sample 1 adjusted concentration measured with Qubit: 33.92 ng/mL.
- Sample 2 adjusted concentration measured with Qubit: 29.91 ng/mL.

Tapestation Analysis cfDNA TapeScreen was used to determine cfDNA concentration and size distribution. The following concentrations and adjusted concentrations were obtained:

- Sample 1 concentration measured with TapeStation (range: 50 -700 bp): 0.363 ng/μL.

- Sample 2 concentration measured with TapeStation (range: 50 -700 bp): 0.262 ng/μL.
- Sample 1 concentration measured with TapeStation (range: 50 -700 bp): 13.02 ng/mL.
- Sample 2 concentration measured with TapeStation (range: 50 -700 bp): 9.39 ng/mL.

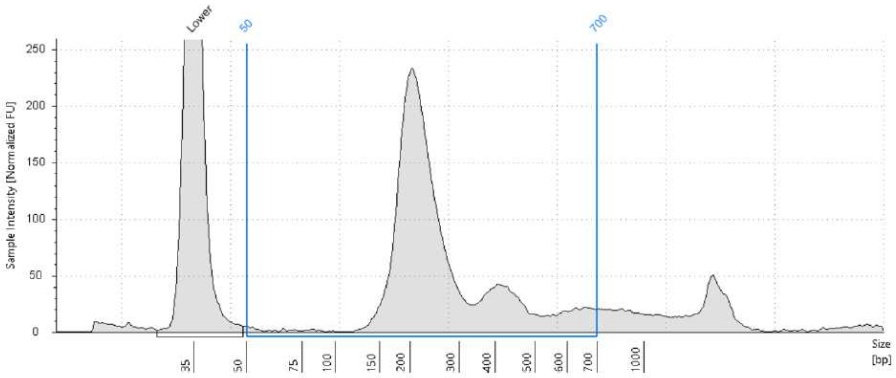

Sample Table

Well	%cfDNA	Conc. [pg/µl]	Sample Description	Alert	Observations
F1	80	452	Spin Magen 1	⚠	Caution! Expired ScreenTape device

Region Table

From [bp]	To [bp]	Average Size [bp]	Conc. [pg/µl]	Region Molarity [pmol/l]	% of Total	Region Comment	Color
50	700	277	363	2410	80.29	%cfDNA	

Figure 5.11: Magen Spin healthy sample 1 analyzed with cfDNA TapeScreen

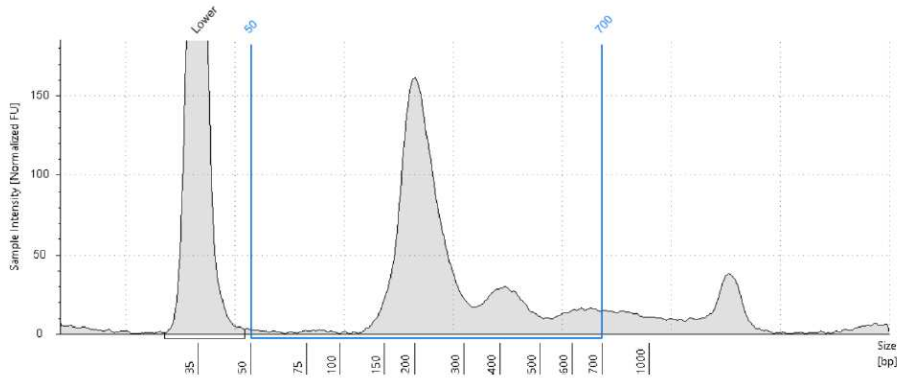

Sample Table

Well	%cfDNA	Conc. [pg/µl]	Sample Description	Alert	Observations
G1	79	329	Spin Magen 2	⚠	Caution! Expired ScreenTape device

Region Table

From [bp]	To [bp]	Average Size [bp]	Conc. [pg/µl]	Region Molarity [pmol/l]	% of Total	Region Comment	Color
50	700	274	262	1770	79.46	%cfDNA	

Figure 5.12: Magen Spin healthy sample 2 analyzed with cfDNA TapeScreen

Plasma from Patients with Hepatic Cirrhosis

Qubit Analysis From Qubit analysis, the following concentrations and adjusted concentrations were obtained:

- Sample 1 concentration measured with Qubit: 0.966 ng/μL.
- Sample 2 concentration measured with Qubit: 0.916 ng/μL.
- Sample 1 adjusted concentration measured with Qubit: 12.88 ng/mL.
- Sample 2 adjusted concentration measured with Qubit: 12.21 ng/mL.

Tapestation Analysis cfDNA TapeScreen was used to determine cfDNA concentration and size distribution. The following concentrations and adjusted concentrations were obtained:

- Sample 1 concentration measured with TapeStation (range: 50 -700 bp): 1.02 ng/μL.
- Sample 2 concentration measured with TapeStation (range: 50 -700 bp): 1.00 ng/μL.
- Sample 1 adjusted concentration measured with TapeStation (range: 50 -700 bp): 13.60 ng/mL.
- Sample 2 adjusted concentration measured with TapeStation (range: 50 -700 bp): 13.33 ng/mL.

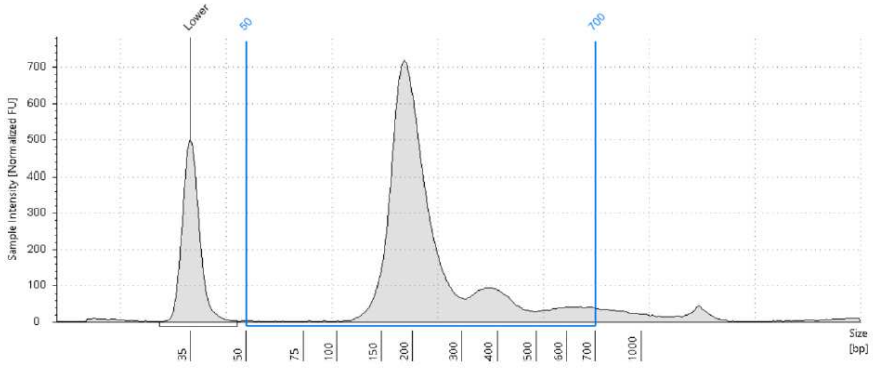

Sample Table

Well	%cfDNA	Conc. [pg/µl]	Sample Description	Alert	Observations
D1	92	1110	Spin 1	⚠	Caution! Expired ScreenTape device

Region Table

From [bp]	To [bp]	Average Size [bp]	Conc. [pg/µl]	Region Molarity [pmol/l]	% of Total	Region Comment	Color
50	700	247	1020	7390	91.78	%cfDNA	

Figure 5.13: Magen Spin cirrhotic sample 1 analyzed with cfDNA TapeScreen

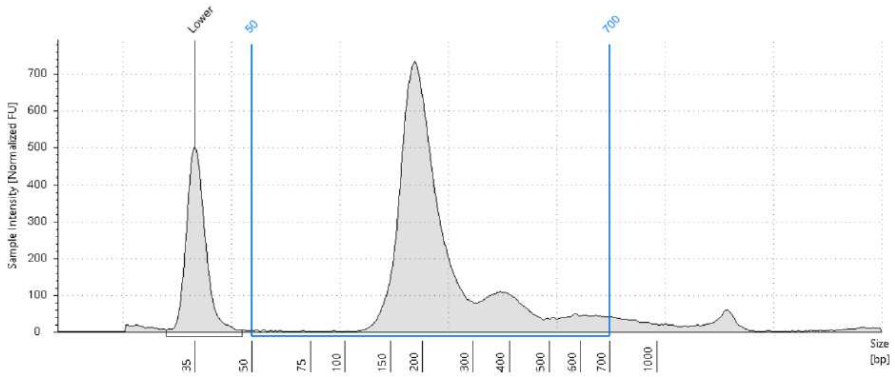

Sample Table

Well	%cfDNA	Conc. [pg/µl]	Sample Description	Alert	Observations
E1	91	1110	Spin 2	⚠	Caution! Expired ScreenTape device

Region Table

From [bp]	To [bp]	Average Size [bp]	Conc. [pg/µl]	Region Molarity [pmol/l]	% of Total	Region Comment	Color
50	700	252	1000	7180	90.81	%cfDNA	

Figure 5.14: Magen Spin cirrhotic sample 2 analyzed with cfDNA TapeScreen

5.3.4 Discussion of Results

Resolutions to the issues were implemented in the extractions with cirrhotic plasma, resulting in similar concentrations between samples from healthy and cirrhotic patients. The difference becomes evident when observing TapeStation results: in cirrhotic plasma samples, a defined peak around 200 bp is observed, decreasing for larger fragments. In healthy patients, the distribution decreases less, likely due to fragmented genomic DNA contamination, resulting in a similar concentration. The generally high values in Qubit analysis may also be explained by the presence of carrier RNA, which alters cfDNA quantification using both Qubit as reported in their protocol.

5.4 Magen: MagPure Circulating DNA Maxi Kit

5.4.1 Description of the kit

MagPure Circulating DNA Maxi Kit (Magen Maxi) [56] uses magnetic beads technology to separate cfDNA from plasma, it can purify cfDNA from 1 to 6 mL of plasma, and it can be automated. The Magen Maxi was tested on plasma samples from healthy and cirrhotic patients. Reagents were prepared following the protocol instructions, and to avoid interference in DNA quantification due to carrier RNA presence, it was not used since

its addition is optional. For healthy samples, due to the lack of a magnetic grid for 15 mL tubes, the sample was centrifuged at 2000g for 5 minutes to precipitate beads and facilitate adhesion to the magnetic separator for 2 ml tubes. For cirrhotic plasma, a magnetic separator for 15 mL tubes was available. We purified cfDNA from 3 mL of plasma, the elution volume was 70 μL.

5.4.2 Limitations

Problems with the magnetic separator in healthy samples: the lack of a magnetic separator for 15 mL tubes required an alternative centrifugation step, potentially causing interruptions and inefficiencies. Additionally, using a 2 ml magnetic separator could negatively impact the bead adhesion efficiency. It was not possible to analyze the second sample with Tapestation as it didn't detect any marker and it gave a highly fragmented spectrum.

5.4.3 Results

Plasma from Healthy Patients

Qubit Analysis From Qubit analysis, the following concentrations and adjusted concentrations were obtained:

- Sample 1 concentration measured with Qubit: 0.242 ng/μL.
- Sample 2 concentration measured with Qubit: 0.252 ng/μL.
- Sample 1 adjusted concentration measured with Qubit: 15.94 ng/mL.
- Sample 2 adjusted concentration measured with Qubit: 16.60 ng/mL.

Tapestation Analysis cfDNA TapeScreen was used to determine cfDNA concentration and size distribution. The following concentration and adjusted concentration were obtained:

- Sample concentration measured with TapeStation (range: 50 -700 bp): 0.151 ng/μL.
- Sample adjusted concentration measured with TapeStation (range: 50 -700 bp): 10.83 ng/mL.

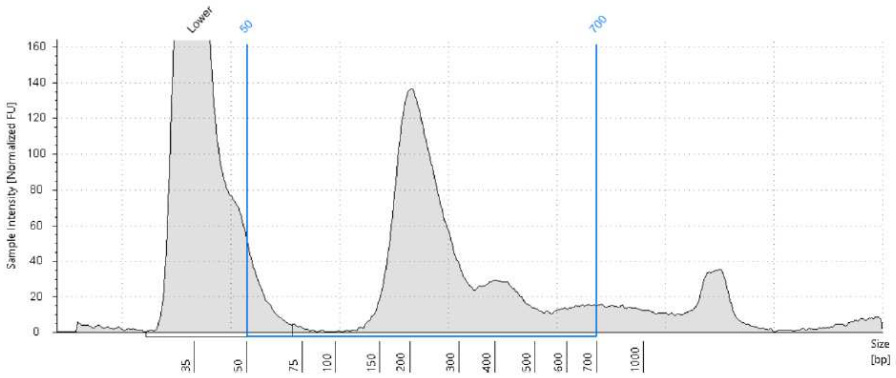

Sample Table

Well	%cfDNA	Conc. [pg/µl]	Sample Description	Alert	Observations
D1	78	194	MagPure Maxi 1	⚠	Caution! Expired ScreenTape device

Region Table

From [bp]	To [bp]	Average Size [bp]	Conc. [pg/µl]	Region Molarity [pmol/l]	% of Total	Region Comment	Color
50	700	282	151	1370	77.76	%cfDNA	

Figure 5.15: Magen Maxi healthy sample analyzed with cfDNA TapeScreen

Plasma from Patients with Hepatic Cirrhosis

Qubit Analysis From Qubit analysis, the following concentrations and adjusted concentrations were obtained:

- Sample 1 concentration measured with Qubit: 0.448 ng/μL.
- Sample 2 concentration measured with Qubit: 0.304 ng/μL.
- Sample 1 adjusted concentration measured with Qubit: 10.45 ng/mL.
- Sample 2 adjusted concentration measured with Qubit: 7.09 ng/mL.

Tapestation Analysis cfDNA TapeScreen was used to determine cfDNA concentration and size distribution. The following concentrations and adjusted concentrations were obtained:

- Sample 1 concentration measured with TapeStation (range: 50 -700 bp): 0.582 ng/μL.
- Sample 2 concentration measured with TapeStation (range: 50 -700 bp): 0.451 ng/μL.
- Sample 1 adjusted concentration measured with TapeStation (range: 50 -700 bp): 13.58 ng/mL.
- Sample 2 adjusted concentration measured with TapeStation (range: 50 -700 bp): 10.52 ng/mL.

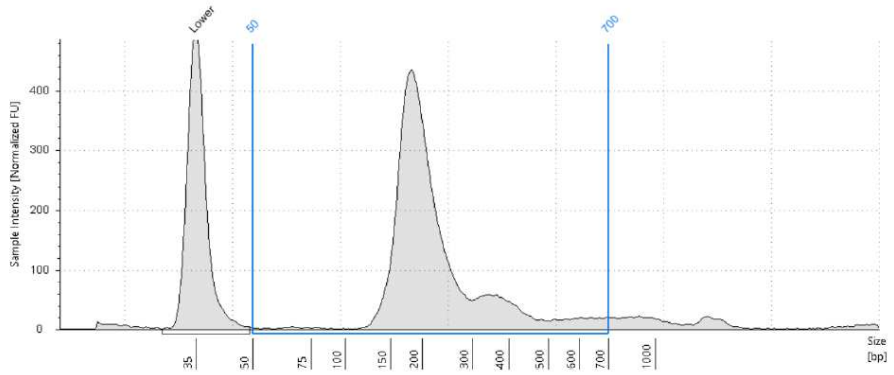

Sample Table

Well	%cfDNA	Conc. [pg/µl]	Sample Description	Alert	Observations
H1	91	637	Maxi 1	⚠	Caution! Expired ScreenTape device

Region Table

From [bp]	To [bp]	Average Size [bp]	Conc. [pg/µl]	Region Molarity [pmol/l]	% of Total	Region Comment	Color
50	700	237	582	4400	91.42	%cfDNA	

Figure 5.16: Magen Maxi cirrhotic sample 1 analyzed with cfDNA TapeScreen

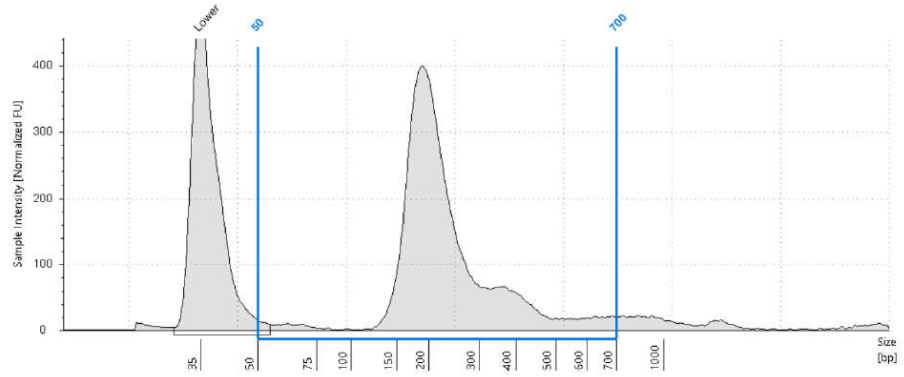

Sample Table

Well	%cfDNA	Conc. [pg/µl]	Sample Description	Alert	Observations
A2	92	489	Maxi 2	⚠	Caution! Expired ScreenTape device

Region Table

From [bp]	To [bp]	Average Size [bp]	Conc. [pg/µl]	Region Molarity [pmol/l]	% of Total	Region Comment	Color
50	700	246	451	3390	92.19	%cfDNA	

Figure 5.17: Magen Maxi cirrhotic sample 2 analyzed with cfDNA TapeScreen

Discussion of Results The difference between improperly processed healthy samples with an additional centrifugation step and cirrhotic samples processed exactly according to the protocol is significant. Cirrhotic patients show higher DNA purity around 200 bp, while healthy samples show greater

contamination with higher molecular weight DNA. The second distribution in healthy samples does not present sufficient low-size DNA concentration for detection by TapeStation, likely due to DNA dissociation from magnetic beads into the supernatant during extraction, resulting in DNA loss.

5.5 MAGEN: MAGPURE CIRCULATING DNA RICH MAXI KIT

5.5.1 DESCRIPTION OF THE KIT

MagPure Circulating DNA Rich Maxi Kit (Rich Maxi) [57] is a RUO kit that uses magnetic beads to purify cfDNA from 5 mL of plasma, it cannot be easily automated since it has centrifugation steps during its extraction protocol. The kit was tested on plasma samples from both healthy patients and patients with hepatic cirrhosis. The final elution volume was 100 μL.

5.5.2 LIMITATIONS

No limitations were encountered during the execution of the protocol.

5.5.3 RESULTS

Plasma from Healthy Patients

Qubit Analysis From Qubit analysis, the following concentrations and adjusted concentrations were obtained:

- Sample 1 concentration measured with Qubit: 0.298 ng/μL.
- Sample 2 concentration measured with Qubit: 0.290 ng/μL.
- Sample 1 adjusted concentration measured with Qubit: 14.72 ng/mL.
- Sample 2 adjusted concentration measured with Qubit: 14.32 ng/mL.

Tapestation Analysis cfDNA TapeScreen was used to determine cfDNA concentration and size distribution. The following concentrations and adjusted concentrations were obtained:

- Sample 1 concentration measured with TapeStation (range: 50 -700 bp): 0.143 ng/μL.

- Sample 2 concentration measured with TapeStation (range: 50 -700 bp): 0.153 ng/μL.
- Sample 1 adjusted concentration measured with TapeStation (range: 50 -700 bp): 7.69 ng/mL.
- Sample 2 adjusted concentration measured with TapeStation (range: 50 -700 bp): 8.23 ng/mL.

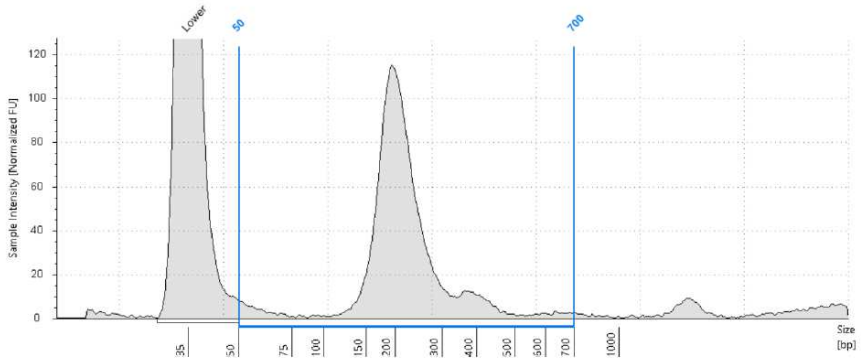

Sample Table

Well	%cfDNA	Conc. [pg/µl]	Sample Description	Alert	Observations
B1	89	160	MagPure Rich Maxi 1	⚠	Caution! Expired ScreenTape device

Region Table

From [bp]	To [bp]	Average Size [bp]	Conc. [pg/µl]	Region Molarity [pmol/l]	% of Total	Region Comment	Color
50	700	226	143	1160	89.47	%cfDNA	

Figure 5.18: Magen Rich Maxi healthy sample 1 analyzed with cfDNA TapeScreen

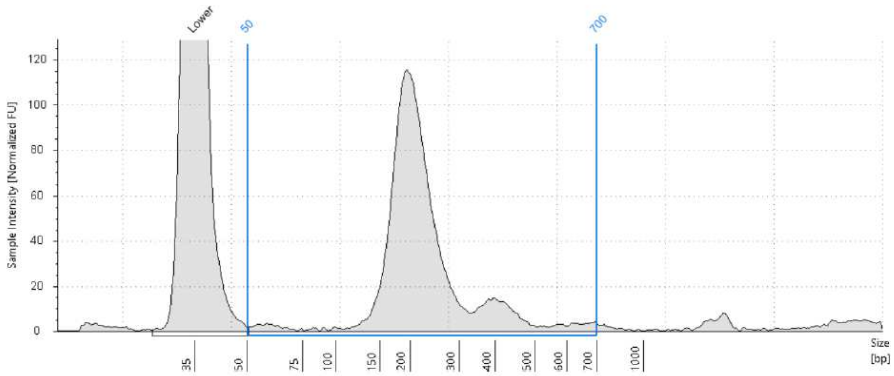

Sample Table

Well	%cfDNA	Conc. [pg/µl]	Sample Description	Alert	Observations
C1	92	167	MagPure Rich Maxi 2	⚠	Caution! Expired ScreenTape device

Region Table

From [bp]	To [bp]	Average Size [bp]	Conc. [pg/µl]	Region Molarity [pmol/l]	% of Total	Region Comment	Color
50	700	235	153	1180	91.82	%cfDNA	

Figure 5.19: Magen Rich Maxi healthy sample 2 analyzed with cfDNA TapeScreen

Plasma from Patients with Hepatic Cirrhosis

Qubit Analysis From Qubit analysis, the following concentrations, and adjusted concentrations were obtained:

- Sample 1 concentration measured with Qubit: 0.356 ng/μL.
- Sample 2 concentration measured with Qubit: 0.63 ng/μL.
- Sample 1 adjusted concentration measured with Qubit: 7.12 ng/mL.
- Sample 2 adjusted concentration measured with Qubit: 12.6 ng/mL.

Tapestation Analysis cfDNA TapeScreen was used to determine cfDNA concentration and size distribution. The following concentrations and adjusted concentrations were obtained:

- Sample 1 concentration measured with TapeStation (range: 50 -700 bp): 0.883 ng/μL.
- Sample 2 concentration measured with TapeStation (range: 50 -700 bp): 0.729 ng/μL.
- Sample 1 adjusted concentration measured with TapeStation (range: 50 -700 bp): 17.66 ng/mL.
- Sample 2 adjusted concentration measured with TapeStation (range: 50 -700 bp): 14.58 ng/mL.

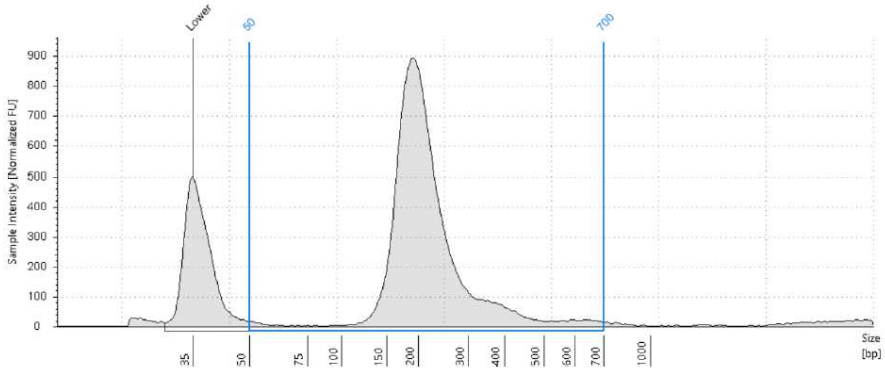

Sample Table

Well	%cfDNA	Conc. [pg/µl]	Sample Description	Alert	Observations
F1	96	918	Rich Maxi 1	⚠	Caution! Expired ScreenTape device

Region Table

From [bp]	To [bp]	Average Size [bp]	Conc. [pg/µl]	Region Molarity [pmol/l]	% of Total	Region Comment	Color
50	700	227	883	6730	96.25	%cfDNA	

Figure 5.20: Magen Rich Maxi cirrhotic sample 1 analyzed with cfDNA TapeScreen

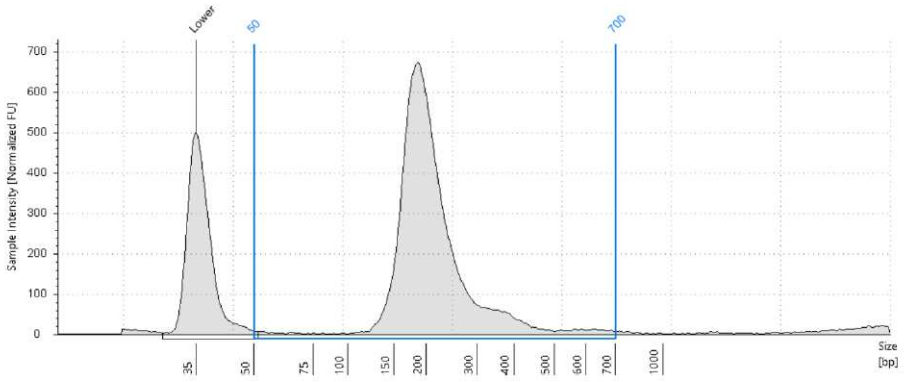

Sample Table

Well	%cfDNA	Conc. [pg/µl]	Sample Description	Alert	Observations
G1	96	760	Rich Maxi 2 (material loss)	⚠	Caution! Expired ScreenTape device

Region Table

From [bp]	To [bp]	Average Size [bp]	Conc. [pg/µl]	Region Molarity [pmol/l]	% of Total	Region Comment	Color
50	700	220	729	5670	95.85	%cfDNA	

Figure 5.21: Magen Rich Maxi cirrhotic sample 2 analyzed with cfDNA TapeScreen

Discussion of Results This kit produces good results with cirrhotic plasma, but it is difficult to observe similar results with healthy samples due to excessive background noise in TapeStation results. The overall lower average cfDNA concentrations in samples from healthy patients likely reflect the differences in cfDNA concentration in cirrhotic samples. Lower purity of extracted cfDNA in cirrhotic samples and poorer cfDNA yields in healthy samples may be attributed to protein or lipid contamination not efficiently removed during extraction. The low concentration observed in sample 1 of cirrhotic patients' plasma may be attributed to an error during Qubit analysis and sample preparation or to a high abundance of ssDNA.

5.6 Beckman Coulter: Apostle MiniMax High Efficiency Isolation Kit

5.6.1 Description of the kit

Apostle MiniMax High Efficiency Isolation Kit(Apostle) [22] is a RUO kit that uses magnetic beads to separate cfDNA from 1, 2, and 4 mL of plasma and it can be automated. We tested it on 3 mL of plasma from patients with hepatic cirrhosis, but it gave no results, we hypothesized that the kit was not suited for the extraction of 3 mL, because in its protocol there were no

specific volumes of reagents indicated for 3 mL, but there was for 1, 2, 4 mL which volumes and concentrations increased linearly. We then tested the kit on 2 mL of plasma from patients with hepatic cirrhosis. The final elution volume was 40 μL.

5.6.2 Limitations

Besides the failure to extract cfDNA from 3 mL of plasma, no limitations were encountered during the execution of the protocol.

5.6.3 Results

Plasma from Patients with Hepatic Cirrhosis

Qubit Analysis From Qubit analysis, the following concentration and adjusted concentration were obtained:

- Sample concentration measured with Qubit: 0.256 ng/μL.
- Sample adjusted concentration measured with Qubit: 5.12 ng/mL.

Tapestation Analysis cfDNA TapeScreen was used to determine cfDNA concentration and size distribution. The following concentration and adjusted concentration were obtained:

- Sample concentration measured with TapeStation (range: 50 -700 bp): 0.247 ng/μL.
- Sample adjusted concentration measured with TapeStation (range: 50 -700 bp): 4.94 ng/mL.

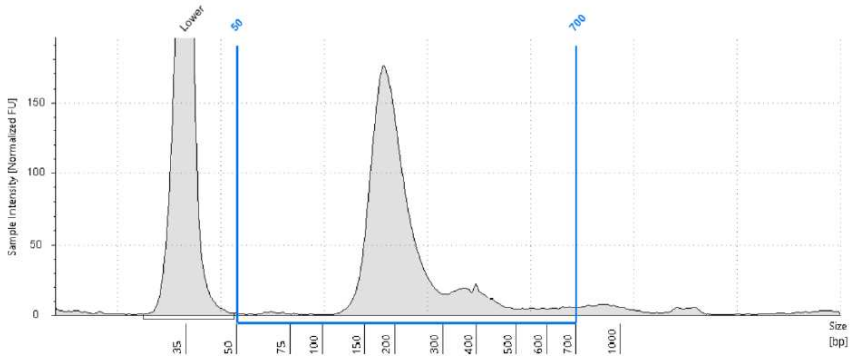

Sample Table

Well	%cfDNA	Conc. [pg/µl]	Sample Description	Alert	Observations
B1	93	265	apostle 11-03-2024 CIR	⚠	Caution! Expired ScreenTape device

Region Table

From [bp]	To [bp]	Average Size [bp]	Conc. [pg/µl]	Region Molarity [pmol/l]	%of Total	Region Comment	Color
50	700	227	247	1930	93.46	%cfDNA	

Figure 5.22: Apostle cirrhotic sample analyzed with cfDNA TapeScreen

Discussion of Results As seen in Figure 5.22, Apostle extracted specifically cfDNA as no DNA with a length higher than 700 bp is present. While there aren't any size selection steps, the protocol has many elution passages that may increase cfDNA selection over gDNA, these steps may also be responsible for the low DNA quantity per mL of plasma observed.

5.7 Vazyme: VAHTS Serum/Plasma Circulating DNA Kit

5.7.1 Discussion of the protocol

VAHTS Serum/Plasma Circulating DNA Kit (Vazyme) [93] is a RUO kit that uses magnetic beads to separate cfDNA from 200 μL to 2 mL of plasma. This kit can be used with automated nucleic acid extraction instruments. We decided to extract 2 mL of plasma from patients with hepatic cirrhosis because it's closer to 3 mL. The final elution volume was 100μL.

5.7.2 Limitations

No limitations were found in the protocol and during cfDNA extraction

5.7.3 Results

Plasma from Patients with Hepatic Cirrhosis

Qubit Analysis From Qubit analysis, the following concentrations and adjusted concentrations were obtained:

- Sample 1 concentration measured with Qubit: 0.336 ng/μL.
- Sample 2 concentration measured with Qubit: 0.422 ng/μL.
- Sample 1 adjusted concentration measured with Qubit: 16.8 ng/mL.
- Sample 2 adjusted concentration measured with Qubit: 21.1 ng/mL.

Tapestation Analysis cfDNA TapeScreen was used to determine cfDNA concentration and size distribution. The following concentrations and adjusted concentrations were obtained:

- Sample 1 concentration measured with TapeStation (range: 50 -700 bp): 0.286 ng/μL.
- Sample 2 concentration measured with TapeStation (range: 50 -700 bp): 0.279 ng/μL.
- Sample 1 adjusted concentration measured with TapeStation (range: 50 -700 bp): 14.3 ng/mL.
- Sample 2 adjusted concentration measured with TapeStation (range: 50 -700 bp): 13.95 ng/mL.

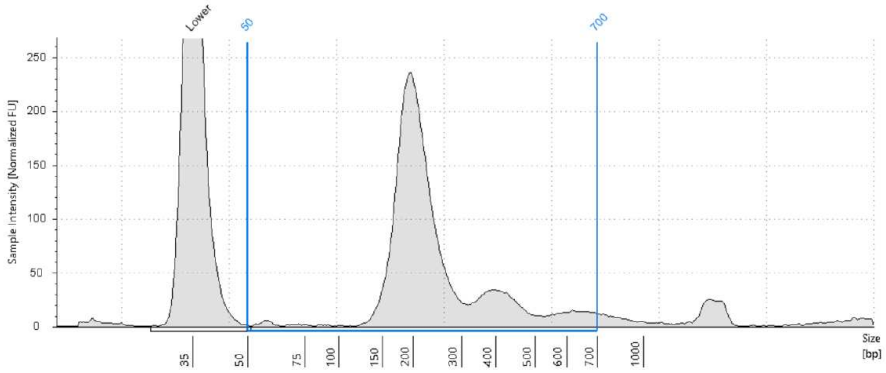

Sample Table

Well	%cfDNA	Conc. [pg/µl]	Sample Description	Alert	Observations
D1	89	320	Vazhyme 1	⚠	Caution! Expired ScreenTape device

Region Table

From [bp]	To [bp]	Average Size [bp]	Conc. [pg/µl]	Region Molarity [pmol/l]	% of Total	Region Comment	Color
50	700	256	286	2060	89.30	%cfDNA	

Figure 5.23: Vazyme cirrhotic sample 1 analyzed with cfDNA TapeScreen

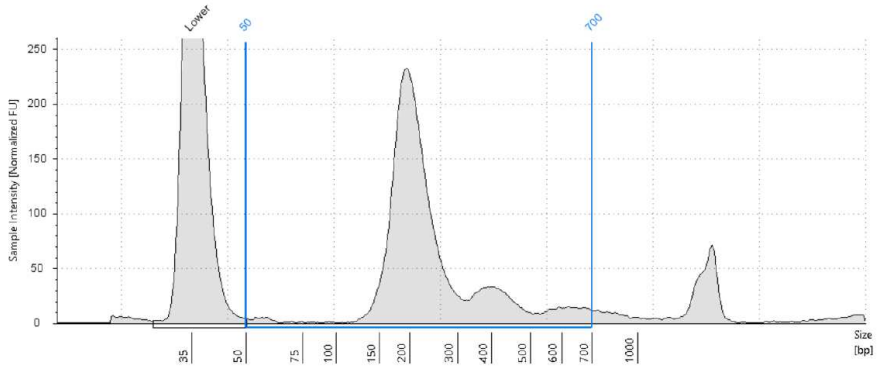

Sample Table

Well	%cfDNA	Conc. [pg/µl]	Sample Description	Alert	Observations
E1	84	333	Vazhyme 2	⚠	Caution! Expired ScreenTape device

Region Table

From [bp]	To [bp]	Average Size [bp]	Conc. [pg/µl]	Region Molarity [pmol/l]	% of Total	Region Comment	Color
50	700	255	279	2020	83.67	%cfDNA	

Figure 5.24: Vazyme cirrhotic sample 2 analyzed with cfDNA TapeScreen

5.7.4 Discussion of the results

This kit yielded really good results, the kit is easy to use and it takes about 1.30-2 hours of time to extract DNA. The kit performed better than we expected from the bibliography research, where it was shown on par with CNA for cfDNA extraction efficiency. [51]

5.8 Thermo Fisher Scientific: MagMAX Cell-Free DNA (cfDNA) Isolation Kit

5.8.1 Discussion of the kit

MagMAX Cell-Free DNA (cfDNA) Isolation Kit (Thermo) [77] is a RUO kit that uses magnetic beads to separate cfDNA from 500 μL to 10 mL of plasma. It is compatible with the automated nucleic acid extraction instruments KingFisher Duo Prime and KingFisher Flex magnetic particle processors. The final elution volume is 15μL.

5.8.2 Limitations

During the kit test, we inadvertently spilled one of the reactions thus we have data for only one extraction.

5.8.3 Results

Plasma from Patients with Hepatic Cirrhosis

Qubit Analysis From Qubit analysis, the following concentrations and adjusted concentrations were obtained:

- Sample concentration measured with Qubit: 1.69 ng/μL.
- Sample adjusted concentration measured with Qubit: 8.45 ng/mL.

Tapestation Analysis cfDNA TapeScreen was used to determine cfDNA concentration and size distribution. The following concentrations and adjusted concentrations were obtained:

- Sample concentration measured with TapeStation (range: 50 -700 bp): 1.91 ng/μL.
- Sample adjusted concentration measured with TapeStation (range: 50 -700 bp): 9.55 ng/mL.

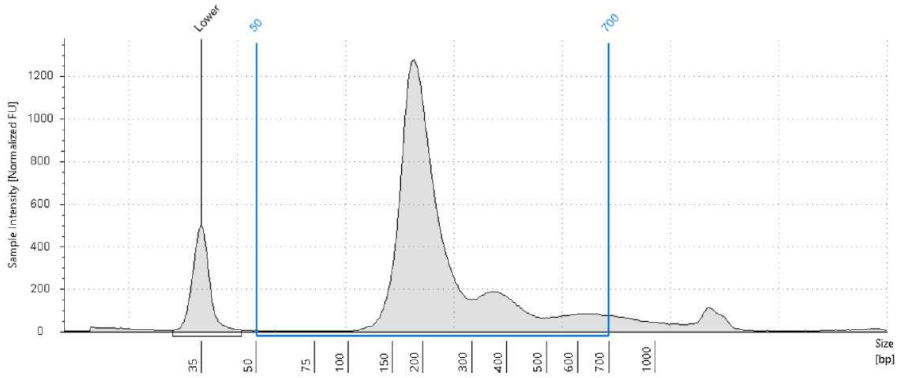

Sample Table

Well	%cfDNA	Conc. [pg/µl]	Sample Description	Alert	Observations
F1	90	2120	MagMax Thermo	⚠	Caution! Expired ScreenTape device

Region Table

From [bp]	To [bp]	Average Size [bp]	Conc. [pg/µl]	Region Molarity [pmol/l]	% of Total	Region Comment	Color
50	700	253	1910	13600	89.77	%cfDNA	

Figure 5.25: Thermo cirrhotic sample analyzed with cfDNA TapeScreen

5.8.4 Discussion of the results

While Thermo did not purify more DNA than the average, its main advantage is the very low elution volume which may help with the following steps of library creation.

Tables summarizing TapeStation and Qubit results Table 5.1 summarizes the results obtained from the Qubit analysis

Table 5.1: Qubit results

Extraction Kit	Patient Status	Concentration ng/µL	Elution Volume µL	Plasma Volume mL	DNA quantity ng	DNA quantity per mL of plasma ng/mL	Adjusted Concentration ng/mL	Qubit Promega's Ratio
CNA	Healthy	0.552	45	3	24.84	8.28	20.45424658	2.470319635
CNA	Healthy	0.448	45	3	20.16	6.72	16.60054795	
Promega	Healthy	0.226	60	3	13.56	4.52	11.16584475	
Promega	Healthy	0.212	60	3	12.72	4.24	10.47415525	
Magen Spin	Healthy	1.03	40	3	41.2	13.73333333	33.92572298	
Magen Spin	Healthy	0.908	40	3	36.32	12.10666667	29.90733638	
Magen Maxi	Healthy	0.242	80	3	19.36	6.453333333	15.94179604	
Mageni Maxi	Healthy	0.252	80	3	20.16	6.72	16.60054795	
Magen Rich Maxi	Healthy	0.298	100	5	29.8	5.96	14.72310502	
Magen Rich Maxi	Healthy	0.29	100	5	29	5.8	14.32785388	
Promega	Cirrhotic	0.546	60	3	32.76	10.92	10.92	
Promega	Cirrhotic	0.536	60	3	32.16	10.72	10.72	
Magen Spin	Cirrhotic	0.966	40	3	38.64	12.88	12.88	
Magen Spin	Cirrhotic	0.916	40	3	36.64	12.21333333	12.21333333	
Magen Maxi	Cirrhotic	0.448	70	3	31.36	10.45333333	10.45333333	
Magen Maxi	Cirrhotic	0.304	70	3	21.28	7.093333333	7.093333333	
Magen Rich Maxi	Cirrhotic	0.356	100	5	35.6	7.12	7.12	
Magen Rich Maxi	Cirrhotic	0.63	100	5	63	12.6	12.6	
Apostle	Cirrhotic	0.256	40	2	10.24	5.12	5.12	
Vazyme	Cirrhotic	0.336	100	2	33.6	16.8	16.8	
Vazyme	Cirrhotic	0.422	100	2	42.2	21.1	21.1	
ThermoFisher	Cirrhotic	1.69	15	3	25.35	8.45	8.45	

Table 5.2 summarizes the results obtained from the TapeStation analysis

Table 5.2: TapeStation Results

Kit Name	Patient health status	TapeScreen used	Plasma Volume mL	Elution Volume µL	cfDNA concentration ng/µL	cfDNA quantity ng	cfDNA Concentration per mL of Plasma ng/mL	Adjusted Concentration ng/mL	Promega Ratio Cirrhosis/Healthy
CNA	Healthy	D1000 HS	3	45	0.209	9.405	3.135	Not computable	2.690248566
CNA	Healthy	D1000 HS	3	45	0.252	11.34	3.78	Not computable	
Promega	Healthy	D1000 HS	3	60	0.299	17.94	5.98	Not computable	
Promega	Healthy	D1000 HS	3	60	0.237	14.22	4.74	Not computable	
CNA	Healthy	cfDNA	3	45	0.219	9.855	3.285	8.837466539	
CNA	Healthy	cfDNA	3	45	0.249	11.205	3.735	10.04807839	
Promega	Healthy	cfDNA	3	60	0.266	15.96	5.32	14.31212237	
Promega	Healthy	cfDNA	3	60	0.257	15.42	5.14	13.82787763	
Magen Spin	Healthy	cfDNA	3	40	0.363	14.52	4.84	13.02080306	
Magen Spin	Healthy	cfDNA	3	40	0.262	10.48	3.493333333	9.39793499	
Magen Maxi	Healthy	cfDNA	3	80	0.151	12.08	4.026666667	10.83273423	
Magen Rich Maxi	Healthy	cfDNA	5	100	0.143	14.3	2.86	7.694110899	
Magen Rich Maxi	Healthy	cfDNA	5	100	0.153	15.3	3.06	8.232160612	
Promega	Cirrhosis	cfDNA	3	60	0.71	42.6	14.2	14.2	
Promega	Cirrhosis	cfDNA	3	60	0.697	41.82	13.94	13.94	
Magen Spin	Cirrhosis	cfDNA	3	40	1.02	40.8	13.6	13.6	
Magen Spin	Cirrhosis	cfDNA	3	40	1	40	13.33333333	13.33333333	
Magen Maxi	Cirrhosis	cfDNA	3	70	0.582	40.74	13.58	13.58	
Magen Maxi	Cirrhosis	cfDNA	3	70	0.451	31.57	10.52333333	10.52333333	
Magen Rich Maxi	Cirrhosis	cfDNA	5	100	0.883	88.3	17.66	17.66	
Magen Rich Maxi	Cirrhosis	cfDNA	5	100	0.729	72.9	14.58	14.58	
Apostle	Cirrhosis	cfDNA	2	40	0.247	9.88	4.94	4.94	
Vazyme	Cirrhosis	cfDNA	2	100	0.286	28.6	14.3	14.3	
Vazyme	Cirrhosis	cfDNA	2	100	0.279	27.9	13.95	13.95	
ThermoFisher	Cirrhosis	cfDNA	3	15	1.91	28.65	9.55	9.55	

6

Discussion of the results of cfDNA extraction kit results

In Figure 6.1, the cfDNA quantity per mL of plasma obtained with TapeStation between patients with hepatic cirrhosis and healthy ones are compared (Magen Maxi results in plasma from healthy patients have been duplicated to be able to confront them visually against the results of plasma from patients with hepatic cirrhosis, but they were not used in the calculation), it can be observed that on average the plasma from patients with hepatic cirrhosis has a higher concentration compared to that from healthy patients, as expected from the literature. Performing the Shapiro-Wilk test on the kits that extracted cfDNA from patients with hepatic cirrhosis, it is observed that the data are not distributed according to the normal distribution (Shapiro-Wilk test statistic: 0.8359487056732178 P-value: 0.024727612733840942). I have therefore performed the non-parametric Mann-Whitney U test, which showed that the average concentration per mL of patients with hepatic cirrhosis is significantly different from that of healthy patients (Mann-Whitney U test statistic: 56.0 P-value: 0.0001554001554001554), being 13.93 ng/mL greater than 4.11 ng/mL, therefore it is significantly higher.

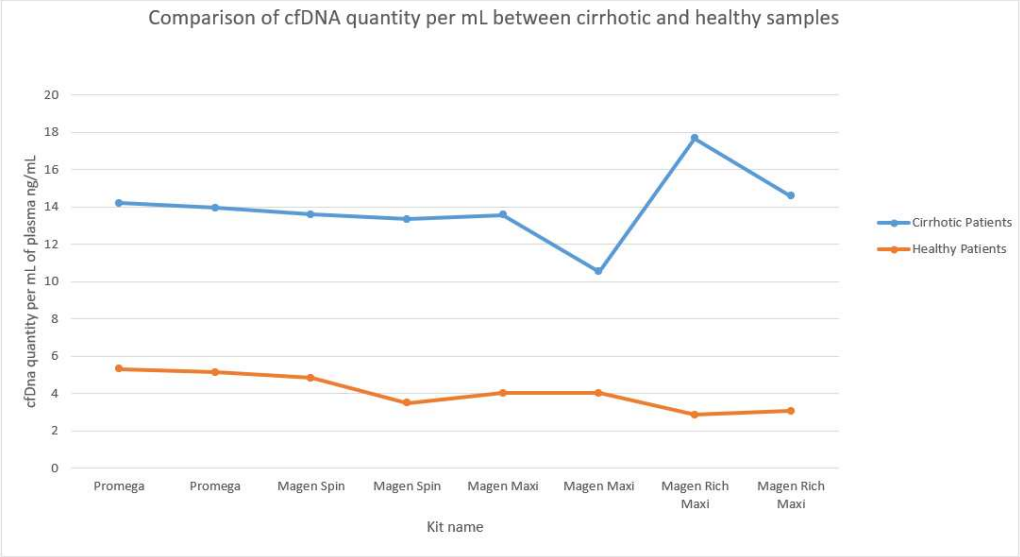

Figure 6.1: Comparison between the TapeStation results of plasma from healthy patients and patients with hepatic cirrhosis using cfDNA TapeScreen

It was not possible to perform this analysis with the data obtained from the Qubit analysis, as for the healthy patients only the Magen Rich Maxi kit had a reliable result. Both CNA and Magen Spin use carrier RNA, which alters concentration analyses with the Qubit. Additionally, both Magen Spin and Magen Maxi encountered issues in extracting cfDNA from healthy patients.

In figure 6.2, there is a comparison between the results obtained using the cfDNA TapeScreen and the D1000 HS TapeScreen, as we can see the results for the base pair range of 50 - 700 are similar, in fact, the Mann-Whitney U test proves that there is no statistical difference between the averages of the two populations (Mann-Whitney U test: 8.0 P-value: 0.5571428571428572). Probably both kits can be used to evaluate cfDNA concentration giving then the same results, but D1000 HS TapeScreen allows a better assessment of gDNA contamination.

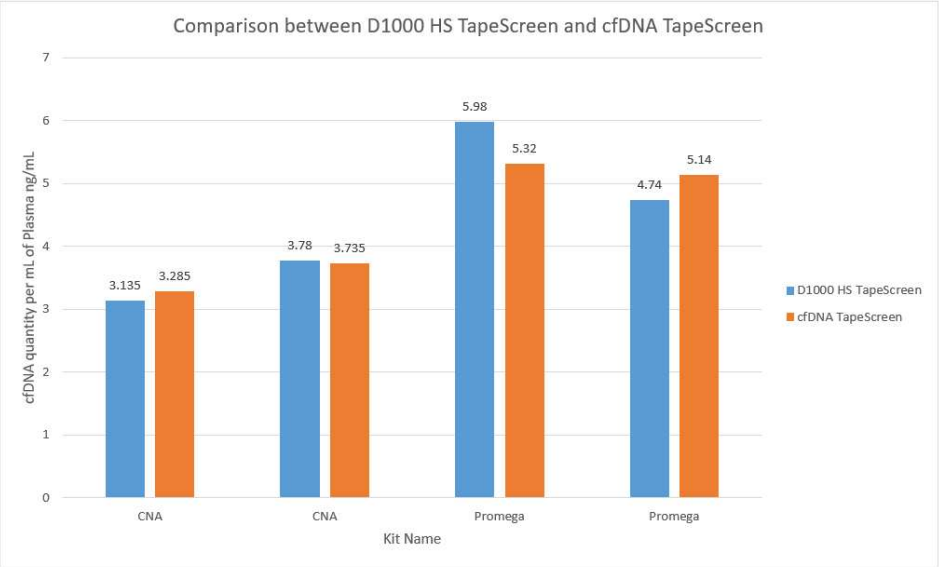

Figure 6.2: Comparison between the TapeStation results of plasma from healthy patients analyzed with D1000 HS TapeScreen and cfDNA TapeScreen

Figure 6.3 (TapeStation) and figure 6.4 (Qubit) represent the adjusted cfDNA quantity per volume of extracted plasma (ng/mL). Healthy patients were normalized based on the ratio of cfDNA extracted from cirrhotic liver patients to the cfDNA extracted from healthy patients, both using the Promega kit. Magen Spin and Magen Maxi kits used in healthy patients have not been included in the analysis due to potentially altered results from incorrect extraction. However, the Magen Rich Maxi kit used in healthy patients was included. In figure6.4 the kits using carrier RNA have been included.

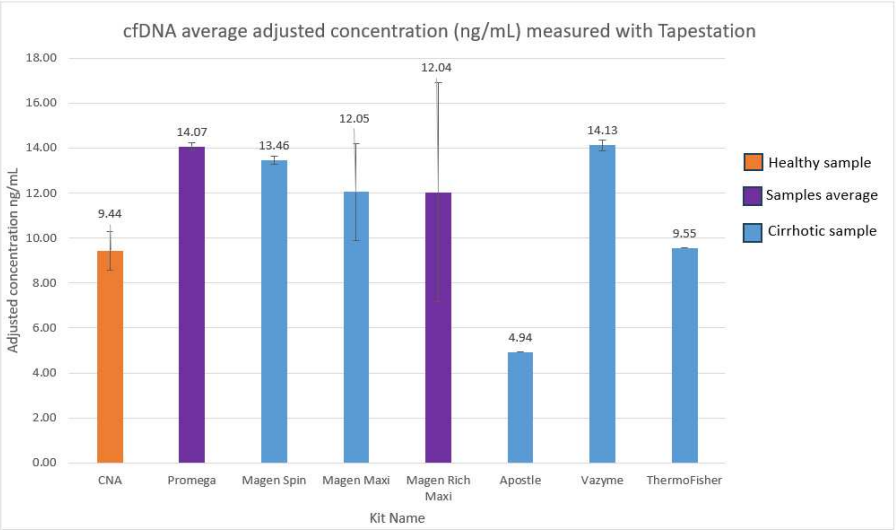

Figure 6.3: Samples adjusted concentration averages obtained from TapeStation analysis using cfDNA TapeScreen

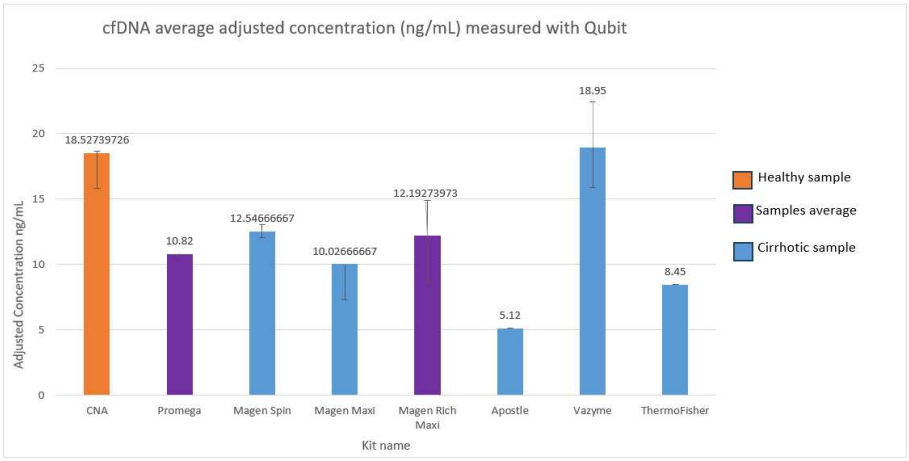

Figure 6.4: Samples adjusted concentration averages obtained from Qubit analysis including kits using carrier RNA

Figure 6.3 shows that the Vazyme kit extracted the highest amount of cfDNA per mL of plasma, followed by Promega. Using the bootstrap method, I determined that the extraction efficiency means for Vazyme and Promega kits are significantly higher than the population mean. This indicates that these kits have greater extraction efficiency per mL of plasma compared to the other kits(Adjusted Vazyme concentration: 14.125 ng/mL, Confidence level = 0.95; Adjusted Promega concentration: 14.07 ng/mL, Confidence level = 0.95). The third kit with a higher concentration, Magen Spin (concentration = 13.46 ng/mL, Confidence level =0.95), was not significantly superior to the population mean. In figure 6.4 (Qubit), it is observed

that the kits that extracted the highest amount of DNA per mL of plasma are the Vazyme kit (18.95 ng/mL) and the CNA kit (18.53 ng/mL). Using the bootstrap method, I determined that the extraction efficiency means for the Vazyme and CNA kits are significantly higher than the population mean. This indicates that these kits have greater extraction efficiency per mL of plasma compared to the other kits(Adjusted Vazyme concentration: 18.95 ng/mL, Confidence level = 0.95; Adjusted CNA concentration: 18.53 ng/mL, Confidence level = 0.95). The third kit with the highest concentration, Magen Spin (12.55 ng/mL), was not statistically significantly superior to the population mean, and the same applies to Promega (10.82 ng/mL).

From these results, it is evident that the Vazyme kit extracted the highest concentration of cfDNA per mL of plasma. Not only did it extract a high DNA concentration, as seen in the Qubit analysis, but it also favored the preferential extraction of cfDNA within the 50 700 bp size range, as observed through TapeStation results.

Promega kit ranks second to the Vazyme kit for cfDNA extraction, as it preferentially extracted cfDNA (50 700 bp) over larger DNA sizes. This preference is evident from the comparison between the Qubit and Tapestation analyses, where it appears to have extracted a greater quantity of cfDNA.

CNA kit extracted the second-highest amount of cfDNA according to the Qubit analysis. However, this kit uses carrier RNA, which can alter Qubit analysis results by increasing the measured concentration. For this reason, I consider the TapeStation analysis more reliable than the Qubit, and thus I believe that CNA did not significantly extract a greater amount of cfDNA compared to the other kits.

Figure 6.5 shows the adjusted concentrations analyzed with Qubit excluding the kits that used carrier RNA and those that had technical problems, it shows that only the Vazyme kit extracted a concentration of cfDNA above the kit average (Average Vazyme concentration = 18.95 ng/mL, Confidence level = 0.95).

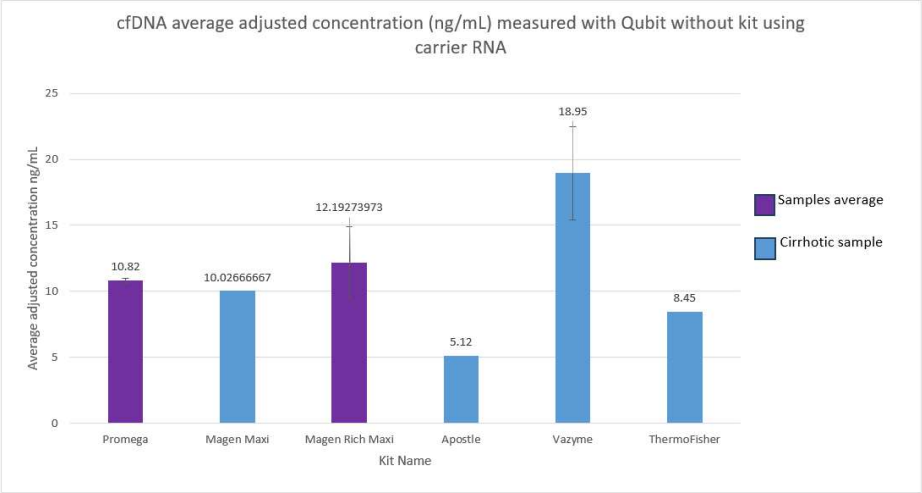

Figure 6.5: Samples adjusted concentration averages obtained from Qubit analysis

Based on these results, it appears that the Vazyme kit has the highest extraction efficiency. Although it can only extract 2 mL of cfDNA, a second extraction with 2 mL of plasma (totaling 4 mL) would yield on average almost 50 ng of cfDNA. This quantity is sufficiently abundant to construct a sequencing library, where there is a high likelihood of detecting low-represented or low-VAF tumor variants.

7

Conclusions and Perspectives

The development of a new medical device based on Next Generation Sequencing (NGS) for determining Homologous Recombination Deficiency in ovarian tumors represents a significant advancement in personalized medicine, as it will allow to determine the HRD status of the patient at a cheaper cost. During my internship at AB ANALITICA S.r.l., I contributed to an extensive bibliographic research and experimental activities to create a diagnostic kit for HRD. This kit utilizes NGS analysis of tumor tissue, focusing on the BRCA1 and BRCA2 genes, combined with shallow Whole Genome Sequencing to calculate the HRD score.

The HRD diagnostic kit for ovarian tumors will empower laboratories to perform comprehensive analyses in-house, from DNA extraction to result interpretation. Overall the results indicate the promising role of cell-free DNA analysis for early hepatocarcinoma diagnosis, which could also be applied to non-invasive HRD diagnosis and PARPi therapy monitoring.

Future research and development in this area will improve cancer diagnostics and treatment personalization. Several key areas for further exploration include:

- Enhanced Sensitivity and Specificity of HRD Detection: Improving the algorithms and bioinformatics pipelines used for HRD status determination will improve the accuracy and reliability of diagnoses. One promising open-source algorithm for HRD detection from sWGS is shallowHRD and its capability to detect HRD will be explored.

- Expansion to Other Cancers: While this thesis focuses on ovarian cancer, the principles, and technologies could be extended to other HRD-positive cancers such as breast, pancreatic, and prostate cancers. Expanding the application of HRD diagnostic kits to these cancers is also a valuable research topic.

- Non-Invasive Diagnostic Methods: The potential of cfDNA analysis for HRD diagnosis where biopsies are not feasible remains an open research direction. Further optimizing cfDNA extraction, preservation, and analysis are crucial for developing reliable and non-invasive diagnostic methods.
- Therapy Monitoring and Resistance Detection: Using cfDNA analysis to monitor tumor response to PARP inhibitors and detect emerging resistance mutations offers a real-time approach to treatment management. Developing protocols for regular cfDNA monitoring could enhance patient outcomes by allowing timely adjustments to therapeutic strategies.

To conclude, even if the DECIDER project is still in development, it holds the potential to substantially help patients with HRD-positive cancer via fast, efficient, and cheap detection kits.

References

[1] Claudia Admoun and Harvey N. Mayrovitz. "The Etiology of Breast Cancer". In: *Breast Cancer*. Exon Publications, Aug. 2022, pp. 21–30. ISBN: 9780645332032. DOI: 10.36255/exon-publications-breast-cancer-etiology. URL: http://dx.doi.org/10.36255/exon-publications-breast-cancer-etiology.

[2] Agilent. *4150 TapeStation System*. Accessed on 09/04/2026. URL: https://shorturl.at/9UFJi.

[3] Agilent. *Detection of Contaminating High Molecular Weight DNA with the Cell-Free DNA ScreenTape Assay*. Accessed 28/05/2024. URL: https://www.agilent.com/cs/library/technicaloverviews/public/technical_overview_contaminating_hmw_dna_cell_free_dna_screentape_5994-6545en_agilent.pdf.

[4] Agilent. *Quality Control of Cell-free DNA Samples Analyzed with Next-Generation Sequencing*. Accessed on 28/05/2024. URL: https://www.agilent.com/cs/library/applications/application-QC-cell-free-DNA-NGS-5994-2284en-agilent.pdf.

[5] Fadi M. Alkabban and Troy Ferguson. "Breast Cancer". In: (2022).

[6] Marianna Alunni-Fabbroni et al. "Circulating Cell-Free DNA Combined to Magnetic Resonance Imaging for Early Detection of HCC in Patients with Liver Cirrhosis". In: *Cancers* 13.3 (Jan. 2021), p. 521. ISSN: 2072-6694. DOI: 10.3390/cancers13030521. URL: http://dx.doi.org/10.3390/cancers13030521.

[7] AmoyDx. *AmoyDxő HRD Focus Panel*. Accessed on 20/05/2024. URL: https://www.amoydiagnostics.com/products/amoydx-hrd-focus-panel.

[8] Taruna Arora, Sanjana Mullangi, and Manidhar Reddy Lekkala. "Ovarian Cancer". In: (2023).

[9] Shoumei Bai et al. "Targeting Therapeutic Resistance and Multinucleate Giant Cells in CCNE1-Amplified HR-Proficient Ovarian Cancer". In: *Molecular Cancer Therapeutics* 21.9 (June 2022), pp. 1473–1484. ISSN: 1538-8514. DOI: 10.1158/1535-7163.mct-21-0873. URL: http://dx.doi.org/10.1158/1535-7163.MCT-21-0873.

[10] Catalin Barbacioru et al. "Detection of homologous recombination deficiency (HRD) using a novel genomic and epigenomic liquid biopsy assay in patients with breast cancer." In: *Journal of Clinical Oncology* 41.16$_{s}uppl$ (June 2023), pp. 556–556. ISSN: 1527-7755. DOI: 10.1200/jco.2023.41.16_suppl.556. URL: http://dx.doi.org/10.1200/JCO.2023.41.16_suppl.556.

[11] Arya Bhushan, Andrea Gonsalves, and Jyothi U. Menon. "Current State of Breast Cancer Diagnosis, Treatment, and Theranostics". In: *Pharmaceutics* 13.5 (May 2021), p. 723. ISSN: 1999-4923. DOI: 10.3390/pharmaceutics13050723. URL: http://dx.doi.org/10.3390/pharmaceutics13050723.

[12] Elodie Bohers, Pierre-Julien Viailly, and Fabrice Jardin. "cfDNA Sequencing: Technological Approaches and Bioinformatic Issues". In: *Pharmaceuticals* 14.6 (June 2021), p. 596. ISSN: 1424-8247. DOI: 10.3390/ph14060596. URL: http://dx.doi.org/10.3390/ph14060596.

[13] Pieter A. Boonstra et al. "Clinical utility of circulating tumor DNA as a response and follow-up marker in cancer therapy". In: *Cancer and Metastasis Reviews* 39.3 (May 2020), pp. 999–1013. ISSN: 1573-7233. DOI: 10.1007/s10555-020-09876-9. URL: http://dx.doi.org/10.1007/s10555-020-09876-9.

[14] Timothy J. Brown and Kim A. Reiss. "PARP Inhibitors in Pancreatic Cancer". In: *The Cancer Journal* 27.6 (Nov. 2021), pp. 465–475. ISSN: 1528-9117. DOI: 10.1097/ppo.0000000000000554. URL: http://dx.doi.org/10.1097/PPO.0000000000000554.

[15] Petra ter Brugge et al. "Homologous recombination deficiency derived from whole-genome sequencing predicts platinum response in triple-negative breast cancers". In: *Nature Communications* 14.1 (Apr. 2023). ISSN: 2041-1723. DOI: 10.1038/s41467-023-37537-2. URL: http://dx.doi.org/10.1038/s41467-023-37537-2.

[16] Raffaella Casolino et al. "Germline Aberrations in Pancreatic Cancer: Implications for Clinical Care". In: *Cancers* 14.13 (June 2022), p. 3239. ISSN: 2072-6694. DOI: 10.3390/cancers14133239. URL: http://dx.doi.org/10.3390/cancers14133239.

[17] Raffaella Casolino et al. "Homologous Recombination Deficiency in Pancreatic Cancer: A Systematic Review and Prevalence Meta-Analysis". In: *Journal of Clinical Oncology* 39.23 (Aug. 2021), pp. 2617–2631. ISSN: 1527-7755. DOI: 10.1200/jco.20.03238. URL: http://dx.doi.org/10.1200/JCO.20.03238.

[18] Chung Ying Chan, Kel Vin Tan, and Bart Cornelissen. "PARP Inhibitors in Cancer Diagnosis and Therapy". In: *Clinical Cancer Research* 27.6 (Oct. 2020), pp. 1585–1594. ISSN: 1557-3265. DOI: 10.1158/1078-0432.ccr-20-2766. URL: http://dx.doi.org/10.1158/1078-0432.CCR-20-2766.

[19] Ying-Cheng Chiang, Po-Han Lin, and Wen-Fang Cheng. "Homologous Recombination Deficiency Assays in Epithelial Ovarian Cancer: Current Status and Future Direction". In: *Frontiers in Oncology* 11 (Oct. 2021). ISSN: 2234-943X. DOI: 10.3389/fonc.2021.675972. URL: http://dx.doi.org/10.3389/fonc.2021.675972.

[20] Guardant Complete. *Guardant360ő CDx*. Accessed on 08/06/2024. URL: https://www.guardantcomplete.com/products/guardant360-cdx.

[21] T. Conroy et al. "Pancreatic cancer: ESMO Clinical Practice Guideline for diagnosis, treatment and follow-up". In: *Annals of Oncology* 34.11 (Nov. 2023), pp. 987–1002. ISSN: 0923-7534. DOI: 10.1016/j.annonc.2023.08.009. URL: http://dx.doi.org/10.1016/j.annonc.2023.08.009.

[22] Beckman Coulter. *Apostle MiniMax High Efficiency Isolation Kit*. Accessed on 03/06/2024. URL: https://www.beckman.it/reagents/genomic/dna-isolation/from-plasma/c40603.

[23] Nicola J. Curtin and Csaba Szabo. "Poly(ADP-ribose) polymerase inhibition: past, present and future". In: *Nature Reviews Drug Discovery* 19.10 (Sept. 2020), pp. 711–736. ISSN: 1474-1784. DOI: 10.1038/s41573-020-0076-6. URL: http://dx.doi.org/10.1038/s41573-020-0076-6.

[24] *DECIDER*. Accessed on 20/05. URL: https://www.deciderproject.eu/.

[25] Kenneth D. Doig, Andrew P. Fellowes, and Stephen B. Fox. "Homologous Recombination Repair Deficiency: An Overview for Pathologists". In: *Modern Pathology* 36.3 (Mar. 2023), p. 100049. ISSN: 0893-3952. DOI: 10.1016/j.modpat.2022.100049. URL: http://dx.doi.org/10.1016/j.modpat.2022.100049.

[26] Alexandre Eeckhoutte et al. "ShallowHRD: detection of homologous recombination deficiency from shallow whole genome sequencing". In: *Bioinformatics* 36.12 (Apr. 2020). Ed. by Inanc Birol, pp. 3888–3889. ISSN: 1367-4811. DOI: 10.1093/bioinformatics/btaa261. URL: http://dx.doi.org/10.1093/bioinformatics/btaa261.

[27] Amira Elbakry and Markus Löbrich. "Homologous Recombination Subpathways: A Tangle to Resolve". In: *Frontiers in Genetics* 12 (Aug. 2021). ISSN: 1664-8021. DOI: 10.3389/fgene.2021.723847. URL: http://dx.doi.org/10.3389/fgene.2021.723847.

[28] FoundationMedicine. *FoundationOne Liquid CDx*. Accessed on 17/05/2024. URL: https://www.foundationmedicine.it/our-services/liquid.html.

[29] Amélie Fradet-Turcotte et al. "BRCA2 functions: from DNA repair to replication fork stabilization". In: *Endocrine-Related Cancer* 23.10 (Oct. 2016), T1–T17. ISSN: 1479-6821. DOI: 10.1530/erc-16-0297. URL: http://dx.doi.org/10.1530/ERC-16-0297.

[30] Xiaoyu Fu et al. "BRCA1 and Breast Cancer: Molecular Mechanisms and Therapeutic Strategies". In: *Frontiers in Cell and Developmental Biology* 10 (Mar. 2022). ISSN: 2296-634X. DOI: 10.3389/fcell.2022.813457. URL: http://dx.doi.org/10.3389/fcell.2022.813457.

[31] Caterina Fumagalli et al. "In-house testing for homologous recombination repair deficiency (HRD) testing in ovarian carcinoma: a feasibility study comparing AmoyDx HRD Focus panel with Myriad myChoiceCDx assay". In: *Pathologica* 114.4 (Sept. 2022), pp. 288–294. ISSN: 1591-951X. DOI: 10.32074/1591-951x-791. URL: http://dx.doi.org/10.32074/1591-951X-791.

[32] A. Gennari et al. "ESMO Clinical Practice Guideline for the diagnosis, staging and treatment of patients with metastatic breast cancer". In: *Annals of Oncology* 32.12 (Dec. 2021), pp. 1475–1495. ISSN: 0923-7534.

DOI: 10.1016/j.annonc.2021.09.019. URL: http://dx.doi.org/10.1016/j.annonc.2021.09.019.

[33] Teresa Gerber et al. "Assessment of Pre-Analytical Sample Handling Conditions for Comprehensive Liquid Biopsy Analysis". In: *The Journal of Molecular Diagnostics* 22.8 (Aug. 2020), pp. 1070–1086. ISSN: 1525-1578. DOI: 10.1016/j.jmoldx.2020.05.006. URL: http://dx.doi.org/10.1016/j.jmoldx.2020.05.006.

[34] Elena Giudice et al. "PARP Inhibitors Resistance: Mechanisms and Perspectives". In: *Cancers* 14.6 (Mar. 2022), p. 1420. ISSN: 2072-6694. DOI: 10.3390/cancers14061420. URL: http://dx.doi.org/10.3390/cancers14061420.

[35] Ewa Gogola et al. "Selective Loss of PARG Restores PARylation and Counteracts PARP Inhibitor-Mediated Synthetic Lethality". In: *Cancer Cell* 33.6 (June 2018), 1078–1093.e12. ISSN: 1535-6108. DOI: 10.1016/j.ccell.2018.05.008. URL: http://dx.doi.org/10.1016/j.ccell.2018.05.008.

[36] A. González-Martín et al. "Newly diagnosed and relapsed epithelial ovarian cancer: ESMO Clinical Practice Guideline for diagnosis, treatment and follow-up". In: *Annals of Oncology* 34.10 (Oct. 2023), pp. 833–848. ISSN: 0923-7534. DOI: 10.1016/j.annonc.2023.07.011. URL: http://dx.doi.org/10.1016/j.annonc.2023.07.011.

[37] Ielizaveta Gorodetska, Iryna Kozeretska, and Anna Dubrovska. "BRCA Genes: The Role in Genome Stability, Cancer Stemness and Therapy Resistance". In: *Journal of Cancer* 10.9 (2019), pp. 2109–2127. ISSN: 1837-9664. DOI: 10.7150/jca.30410. URL: http://dx.doi.org/10.7150/jca.30410.

[38] Lena Haeberle and Irene Esposito. "Pathology of pancreatic cancer". In: *Translational Gastroenterology and Hepatology* 4 (June 2019), pp. 50–50. ISSN: 2415-1289. DOI: 10.21037/tgh.2019.06.02. URL: http://dx.doi.org/10.21037/tgh.2019.06.02.

[39] Catherine Handy et al. "Prevalence of homologous recombination deficiency (HRD) mutations in localized prostate cancer according to Gleason grade: Implications for neoadjuvant clinical trial design." In: *Journal of Clinical Oncology* 36.15_{suppl} (May 2018), pp. 5062–5062. ISSN: 1527-7755. DOI: 10.1200/jco.2018.36.15_suppl.5062. URL: http://dx.doi.org/10.1200/JCO.2018.36.15_suppl.5062.

[40] Tao Huang. "Copy Number Variations in Tumors". In: *Reference Module in Biomedical Sciences*. Elsevier, 2018. DOI: 10.1016/b978-0-12-801238-3.65047-x. URL: http://dx.doi.org/10.1016/B978-0-12-801238-3.65047-X.

[41] Rachel M. Hurley et al. "53BP1 as a potential predictor of response in PARP inhibitor-treated homologous recombination-deficient ovarian cancer". In: *Gynecologic Oncology* 153.1 (Apr. 2019), pp. 127–134. ISSN: 0090-8258. DOI: 10.1016/j.ygyno.2019.01.015. URL: http://dx.doi.org/10.1016/j.ygyno.2019.01.015.

[42] Marianna Jagelkova et al. "Comparison of Somatic Mutation Profiles Between Formalin-Fixed Paraffin Embedded Tissues and Plasma Cell-Free DNA from Ovarian Cancer Patients Before and After Surgery". In: *BioResearch Open Access* 9.1 (Mar. 2020), pp. 73–79. ISSN: 2164-7860. DOI: 10.1089/biores.2019.0031. URL: http://dx.doi.org/10.1089/biores.2019.0031.

[43] Maria Kfoury et al. "Circulating Tumor DNA from Ascites as an alternative to tumor sampling for genomic profiling in ovarian cancer patients". In: *Biomarker Research* 11.1 (Oct. 2023). ISSN: 2050-7771. DOI: 10.1186/s40364-023-00533-1. URL: http://dx.doi.org/10.1186/s40364-023-00533-1.

[44] Gene Koh et al. "Mutational signatures: emerging concepts, caveats and clinical applications". In: *Nature Reviews Cancer* 21.10 (July 2021), pp. 619–637. ISSN: 1474-1768. DOI: 10.1038/s41568-021-00377-7. URL: http://dx.doi.org/10.1038/s41568-021-00377-7.

[45] Alessandro Lavoro et al. "Identification of the most common BRCA alterations through analysis of germline mutation databases: Is droplet digital PCR an additional strategy for the assessment of such alterations in breast and ovarian cancer families?" In: *International Journal of Oncology* 60.5 (Apr. 2022). ISSN: 1791-2423. DOI: 10.3892/ijo.2022.5349. URL: http://dx.doi.org/10.3892/ijo.2022.5349.

[46] Paul van der Leest et al. "Comparison of Circulating Cell-Free DNA Extraction Methods for Downstream Analysis in Cancer Patients". In: *Cancers* 12.5 (May 2020), p. 1222. ISSN: 2072-6694. DOI: 10.3390/cancers12051222. URL: http://dx.doi.org/10.3390/cancers12051222.

[47] Xuan Li and Wolf-Dietrich Heyer. "Homologous recombination in DNA repair and DNA damage tolerance". In: *Cell Research* 18.1 (Jan. 2008), pp. 99–113. ISSN: 1748-7838. DOI: 10.1038/cr.2008.1. URL: http://dx.doi.org/10.1038/cr.2008.1.

[48] Yun Li et al. "Recent advances in therapeutic strategies for triple-negative breast cancer". In: *Journal of Hematology amp; Oncology* 15.1 (Aug. 2022). ISSN: 1756-8722. DOI: 10.1186/s13045-022-01341-0. URL: http://dx.doi.org/10.1186/s13045-022-01341-0.

[49] Keng Lim Ng. "The Etiology of Prostate Cancer". In: *Prostate Cancer*. Exon Publications, May 2021, pp. 17–28. ISBN: 9780645001754. DOI: 10.36255/exonpublications.prostatecancer.etiology.2021. URL: http://dx.doi.org/10.36255/exonpublications.prostatecancer.etiology.2021.

[50] Yang Liu et al. "Homologous recombination deficiency prediction using low-pass whole genome sequencing in breast cancer". In: *Cancer Genetics* 272273 (Apr. 2023), pp. 35–40. ISSN: 2210-7762. DOI: 10.1016/j.cancergen.2023.02.001. URL: http://dx.doi.org/10.1016/j.cancergen.2023.02.001.

[51] Zhongzhen Liu et al. "Evaluation of five cell-free DNA isolation kits for plasma". In: (July 2019). DOI: 10.1101/715821. URL: http://dx.doi.org/10.1101/715821.

[52] Sergiusz ukasiewicz et al. "Breast CancerEpidemiology, Risk Factors, Classification, Prognostic Markers, and Current Treatment StrategiesAn Updated Review". In: *Cancers* 13.17 (Aug. 2021), p. 4287. ISSN: 2072-6694. DOI: 10.3390/cancers13174287. URL: http://dx.doi.org/10.3390/cancers13174287.

[53] H. Ma et al. "53BP1 Deletion Induced Treatment Resistance in Neoadjuvant Chemoradiotherapy Rectal Patients by Inhibiting Immune Function". In: *International Journal of Radiation Oncology*Biology*Physics* 102.3 (Nov. 2018), e12. ISSN: 0360-3016. DOI: 10.1016/j.ijrobp.2018.07.219. URL: http://dx.doi.org/10.1016/j.ijrobp.2018.07.219.

[54] Kendra K. Maass et al. "From Sampling to Sequencing: A Liquid Biopsy Pre-Analytic Workflow to Maximize Multi-Layer Genomic Information from a Single Tube". In: *Cancers* 13.12 (June 2021), p. 3002. ISSN: 2072-6694. DOI: 10.3390/cancers13123002. URL: http://dx.doi.org/10.3390/cancers13123002.

[55] Magen. *HiPure Circulating DNA Midi Spin Kit D (Spin Protocol)*. Accessed on 17/05/2024. URL: https://www.magen-tec.com/products/info.aspx?lcid=35&itemid=73.

[56] Magen. *MagPure Circulating DNA Maxi Kit*. Accessed on 03/06/2024. URL: https://www.magen-tec.com/products/info.aspx?lcid=35&itemid=75.

[57] Magen. *MagPure Circulating DNA Rich Maxi Kit*. Accessed on 03/06/2024. Year Published. URL: https://www.magen-tec.com/products/info.aspx?lcid=35&itemid=76.

[58] Alessandro Mangogna et al. "Homologous Recombination Deficiency in Ovarian Cancer: from the Biological Rationale to Current Diagnostic Approaches". In: *Journal of Personalized Medicine* 13.2 (Feb. 2023), p. 284. ISSN: 2075-4426. DOI: 10.3390/jpm13020284. URL: http://dx.doi.org/10.3390/jpm13020284.

[59] Carlotta Mazzitelli et al. "Liquid Biopsy in the Management of Breast Cancer Patients: Where Are We Now and Where Are We Going". In: *Diagnostics* 13.7 (Mar. 2023), p. 1241. ISSN: 2075-4418. DOI: 10.3390/diagnostics13071241. URL: http://dx.doi.org/10.3390/diagnostics13071241.

[60] Romain Meddeb, Ekaterina Pisareva, and Alain R Thierry. "Guidelines for the Preanalytical Conditions for Analyzing Circulating Cell-Free DNA". In: *Clinical Chemistry* 65.5 (May 2019), pp. 623–633. ISSN: 1530-8561. DOI: 10.1373/clinchem.2018.298323. URL: http://dx.doi.org/10.1373/clinchem.2018.298323.

[61] Foundation Medicine. *FoundationOne CDx*. Accessed on 17/05/2024. URL: https://www.foundationmedicine.it/our-services/cdx.html.

[62] R.E. Miller et al. "ESMO recommendations on predictive biomarker testing for homologous recombination deficiency and PARP inhibitor benefit in ovarian cancer". In: *Annals of Oncology* 31.12 (Dec. 2020), pp. 1606–1622. ISSN: 0923-7534. DOI: 10.1016/j.annonc.2020.08.2102. URL: http://dx.doi.org/10.1016/j.annonc.2020.08.2102.

[63] Rowan E Miller et al. "Ovarian Cancer Therapy: Homologous Recombination Deficiency as a Predictive Biomarker of Response to PARP Inhibitors". In: *OncoTargets and Therapy* Volume 15 (Oct. 2022),

pp. 1105–1117. ISSN: 1178-6930. DOI: 10.2147/ott.s272199. URL: http://dx.doi.org/10.2147/OTT.S272199.

[64] Julio Morales et al. "Review of Poly (ADP-ribose) Polymerase (PARP) Mechanisms of Action and Rationale for Targeting in Cancer and Other Diseases". In: *Critical Reviews in Eukaryotic Gene Expression* 24.1 (2014), pp. 15–28. ISSN: 1045-4403. DOI: 10.1615/critreveukaryotgeneexpr.2013006875. URL: http://dx.doi.org/10.1615/critreveukaryotgeneexpr.2013006875.

[65] Myriad. *Myriad MyChoice*. Accessed on 17/05/2024. URL: https://myriad.com/genetic-tests/mychoicecdx-tumor-test/.

[66] *ONCOFLUID*. Accessed on 20/05. URL: https://www.abanalitica.com/oncofluid/.

[67] Wungki Park and Akhil and Chawla. "Pancreatic Cancer: A Review". In: *JAMA* 326.9 (). ISSN: 0098-7484. DOI: 10.1001/jama.2021.13027. URL: http://dx.doi.org/10.1001/jama.2021.13027.

[68] Tanja Pejovic, Katherine Fitch, and Gordon Mills. "Ovarian cancer recurrence: is the definition of platinum resistance modified by PARP inhibitors and other intervening treatments?" In: *Cancer Drug Resistance* 5.2 (2022), pp. 451–458. ISSN: 2578-532X. DOI: 10.20517/cdr.2021.138. URL: http://dx.doi.org/10.20517/cdr.2021.138.

[69] Eleni Polatoglou et al. "Isolation and Quantification of Plasma Cell-Free DNA Using Different Manual and Automated Methods". In: *Diagnostics* 12.10 (Oct. 2022), p. 2550. ISSN: 2075-4418. DOI: 10.3390/diagnostics12102550. URL: http://dx.doi.org/10.3390/diagnostics12102550.

[70] Promega. *Maxwellő RSC ccfDNA Plasma Kit*. Accessed on 17/05/2024. URL: https://ita.promega.com/resources/protocols/technical-manuals/500/maxwell-rsc-ccfdna-lv-plasma-kit-protocol/.

[71] Eric Pujade-Lauraine et al. "Homologous Recombination Repair Gene Mutations to Predict Olaparib Plus Bevacizumab Efficacy in the First-Line Ovarian Cancer PAOLA-1/ENGOT-ov25 Trial". In: *JCO Precision Oncology* 7 (Jan. 2023). ISSN: 2473-4284. DOI: 10.1200/po.22.00258. URL: http://dx.doi.org/10.1200/PO.22.00258.

[72] Qiagen. *QIAamp Circulating Nucleic Acid Kit*. Accessed on 17/05/2024. URL: https://www.qiagen.com/us/products/discovery-and-translational-research/dna-rna-purification/dna-purification/cell-free-dna/qiaamp-circulating-nucleic-acid-kit.

[73] Qiagen. *QIAcube Connect*. Accessed on 08/06/2024. URL: https://www.qiagen.com/us/products/discovery-and-translational-research/dna-rna-purification/instruments-equipment/qiacube-connect.

[74] I. Ray-Coquard et al. "Olaparib plus bevacizumab first-line maintenance in ovarian cancer: final overall survival results from the PAOLA-1/ENGOT-ov25 trial". In: *Annals of Oncology* 34.8 (Aug. 2023), pp. 681–692. ISSN: 0923-7534. DOI: 10.1016/j.annonc.2023.05.005. URL: http://dx.doi.org/10.1016/j.annonc.2023.05.005.

[75] Florian Scherer. "Capturing Tumor Heterogeneity and Clonal Evolution by Circulating Tumor DNA Profiling". In: *Recent Results in Cancer Research*. Springer International Publishing, Oct. 2019, pp. 213–230. ISBN: 9783030264390. DOI: 10.1007/978-3-030-26439-0_11. URL: http://dx.doi.org/10.1007/978-3-030-26439-0_11.

[76] Thermo Fisher Scientific. *HRD Evaluation and Scoring using OncoScan CNV Assay, a whole-genome microarray research solution*. Accessed on 10/06/2024. 2024. URL: https://shorturl.at/P7aFt.

[77] Thermo Fisher Scientific. *MagMAX Cell-Free DNA Isolation Kit*. Accessed on 03/06/2024. URL: MagMAX%E2%84%A2%20Cell-Free%20DNA%20Isolation%20Kit.

[78] ThermoFisher Scientific. *Qubit 3 Fluorometer manual*. Accessed on 09/06/2024. URL: https://tools.thermofisher.com/content/sfs/manuals/qubit_3_fluorometer_man.pdf.

[79] Mamello Sekhoacha et al. "Prostate Cancer Review: Genetics, Diagnosis, Treatment Options, and Alternative Approaches". In: *Molecules* 27.17 (Sept. 2022), p. 5730. ISSN: 1420-3049. DOI: 10.3390/molecules27175730. URL: http://dx.doi.org/10.3390/molecules27175730.

[80] SeqOne. *SeqOne HRD*. Accessed on 08/06/2024. URL: https://seqone.com/hrd/.

[81] Changxia Shao et al. "A comprehensive literature review and meta-analysis of the prevalence of pancancer <scp>BRCA</scp> mutations, homologous recombination repair gene mutations, and homologous recombination deficiencies". In: *Environmental and Molecular Mutagenesis* 63.6 (July 2022), pp. 308–316. ISSN: 1098-2280. DOI: 10.1002/em.22505. URL: http://dx.doi.org/10.1002/em.22505.

[82] Zhiwen Shi et al. "Genomic and molecular landscape of homologous recombination deficiency across multiple cancer types". In: *Scientific Reports* 13.1 (June 2023). ISSN: 2045-2322. DOI: 10.1038/s41598-023-35092-w. URL: http://dx.doi.org/10.1038/s41598-023-35092-w.

[83] Ping Song et al. "Limitations and opportunities of technologies for the analysis of cell-free DNA in cancer diagnostics". In: *Nature Biomedical Engineering* 6.3 (Jan. 2022), pp. 232–245. ISSN: 2157-846X. DOI: 10.1038/s41551-021-00837-3. URL: http://dx.doi.org/10.1038/s41551-021-00837-3.

[84] Laure Sorber et al. "Specialized Blood Collection Tubes for Liquid Biopsy: Improving the Pre-analytical Conditions". In: *Molecular Diagnosis amp; Therapy* 24.1 (Dec. 2019), pp. 113–124. ISSN: 1179-2000. DOI: 10.1007/s40291-019-00442-w. URL: http://dx.doi.org/10.1007/s40291-019-00442-w.

[85] Christoph Springfeld et al. "Neoadjuvant therapy for pancreatic cancer". In: *Nature Reviews Clinical Oncology* 20.5 (Mar. 2023), pp. 318–337. ISSN: 1759-4782. DOI: 10.1038/s41571-023-00746-1. URL: http://dx.doi.org/10.1038/s41571-023-00746-1.

[86] Caitlin M. Stewart and Dana W.Y. Tsui. "Circulating cell-free DNA for non-invasive cancer management". In: *Cancer Genetics* 228229 (Dec. 2018), pp. 169–179. ISSN: 2210-7762. DOI: 10.1016/j.cancergen.2018.02.005. URL: http://dx.doi.org/10.1016/j.cancergen.2018.02.005.

[87] Mark D Stewart et al. "Homologous Recombination Deficiency: Concepts, Definitions, and Assays". In: *The Oncologist* 27.3 (Jan. 2022), pp. 167–174. ISSN: 1549-490X. DOI: 10.1093/oncolo/oyab053. URL: http://dx.doi.org/10.1093/oncolo/oyab053.

[88] Benjamin M. Stinson and Joseph J. Loparo. "Repair of DNA Double-Strand Breaks by the Nonhomologous End Joining Pathway". In: *Annual Review of Biochemistry* 90.1 (June 2021), pp. 137–164. ISSN: 1545-4509. DOI: 10.1146/annurev-biochem-080320-110356. URL: http://dx.doi.org/10.1146/annurev-biochem-080320-110356.

[89] Anna Streubel et al. "Comparison of different semi-automated cfDNA extraction methods in combination with UMI-based targeted sequencing". In: *Oncotarget* 10.55 (Oct. 2019), pp. 5690–5702. ISSN: 1949-2553. DOI: 10.18632/oncotarget.27183. URL: http://dx.doi.org/10.18632/oncotarget.27183.

[90] Valéria Tavares et al. "Paradigm Shift: A Comprehensive Review of Ovarian Cancer Management in an Era of Advancements". In: *International Journal of Molecular Sciences* 25.3 (Feb. 2024), p. 1845. ISSN: 1422-0067. DOI: 10.3390/ijms25031845. URL: http://dx.doi.org/10.3390/ijms25031845.

[91] Tempus. *Tempus xF/xF+ Liquid Biopsy*. Accessed on 08/06/2024. URL: https://www.tempus.com/oncology/genomic-profiling/xf/.

[92] "The role of homologous recombination deficiency testing in ovarian cancer and its clinical implications: do we need it". In: (June 2021). DOI: 10.1016/j.esmoop.2021.100144.

[93] Vazyme. *VAHTS Serum/Plasma Circulating DNA Kit*. Accessed on 03/06/2024. URL: https://www.vazymeglobal.com/product-center/cell-free-dna-extraction/vahts-serum-plasma-circulating-dna-kit.

[94] Svenja Wagener-Ryczek, Sabine Merkelbach-Bruse, and Janna Siemanowski. "Biomarkers for Homologous Recombination Deficiency in Cancer". In: *Journal of Personalized Medicine* 11.7 (June 2021), p. 612. ISSN: 2075-4426. DOI: 10.3390/jpm11070612. URL: http://dx.doi.org/10.3390/jpm11070612.

[95] William Douglass Wright, Shanaya Shital Shah, and Wolf-Dietrich Heyer. "Homologous recombination and the repair of DNA double-strand breaks". In: *Journal of Biological Chemistry* 293.27 (July 2018), pp. 10524–10535. ISSN: 0021-9258. DOI: 10.1074/jbc.tm118.000372. URL: http://dx.doi.org/10.1074/jbc.TM118.000372.

[96] Yongsong Wu et al. "Clinical application of PARP inhibitors in ovarian cancer: from molecular mechanisms to the current status". In: *Journal of Ovarian Research* 16.1 (Jan. 2023). ISSN: 1757-2215. DOI: 10.1186/s13048-023-01094-5. URL: http://dx.doi.org/10.1186/s13048-023-01094-5.

[97] Chunbao Xie et al. "BRCA2 gene mutation in cancer". In: *Medicine* 101.45 (Nov. 2022), e31705. ISSN: 1536-5964. DOI: 10.1097/md.0000000000031705. URL: http://dx.doi.org/10.1097/MD.0000000000031705.

[98] Yan-yan Yan et al. "Cell-Free DNA: Hope and Potential Application in Cancer". In: *Frontiers in Cell and Developmental Biology* 9 (Feb. 2021). ISSN: 2296-634X. DOI: 10.3389/fcell.2021.639233. URL: http://dx.doi.org/10.3389/fcell.2021.639233.

[99] Ken-ichi Yoshioka et al. "Genomic Instability and Cancer Risk Associated with Erroneous DNA Repair". In: *International Journal of Molecular Sciences* 22.22 (Nov. 2021), p. 12254. ISSN: 1422-0067. DOI: 10.3390/ijms222212254. URL: http://dx.doi.org/10.3390/ijms222212254.

[100] Huimei Zhou et al. "Can circulating cell free DNA be a promising marker in ovarian cancer? a genome-scale profiling study in a single institution". In: *Journal of Ovarian Research* 16.1 (Jan. 2023). ISSN: 1757-2215. DOI: 10.1186/s13048-022-01068-z. URL: http://dx.doi.org/10.1186/s13048-022-01068-z.

Acknowledgments

Ringrazio specialmente la mia famiglia: mio Papà Fabio, mia Mamma Mariangela e in particolarmodo mio Fratello Emanuele, che mi ha molto aiutato in tutta la mia vita e che è un amico su cui posso sempre contare. Ringrazio tutti i miei amici per essere le persone con cui mi posso sempre confidare e passare bei momenti assieme. Ringrazio AB ANALITICA S.R.L. in particolare il Dottor Dino Paladin per avermi permesso di poter compiere questa bellissima esperienza che è stato il tirocinio presso AB ANALITICA, il Dottor Diego Boscarino il quale mi ha seguito molto vicino, che ha partecipato attivamente alla mia formazione tecnico-scientifica e che mi ha permesso di partecipare ad altri progetti dell'azienda, ringrazio il mio collega Dottor Davide Viotto che mi ha seguito durante questo mio percorso e ringrazio la mia collega Dottoressa Marah Amer per avermi aiutato nel progetto ONCOFLUID e nel testing dei kit commerciali. Ringrazio il mio Relatore, il Professor Stefano Cagnin, per avermi permesso di compiere il tirocinio ad AB ANALITICA. Ringrazio Clarissa per essermi sempre stata vicina, anche in questo periodo complicato dovuto alla mia tesi. Ringrazio i miei nonni, parenti e cugini per tutto l'affetto e sostegno che mi hanno dato, in particolarmodo mia Nonna Elisena, mio Nonno Valentino e mio Cugino Simone. Ringrazio infine il mio cane Dylan che è mi è un amico su cui posso sempre contare per avere un po' di compagnia.